UNIVERSITY OF THESSALY

SCHOOL OF ENGINEERING

DEPARTMENT OF MECHANICAL ENGINEERING

Diploma Thesis

ΒΕΛΤΙΣΤΟΠΟΙΗΣΗ ΣΥΝΘΗΚΩΝ ΚΟΠΗΣ ΧΑΛΥΒΑ ARMOX 500, ΜΕ LASER ΔΙΟΞΕΙΔΙΟΥ ΤΟΥ ΑΝΘΡΑΚΑ

CO2 LASER CUTTING CONDITIONS OPTIMIZATION FOR ARMOX 500 STEEL

by

KARDARAS FOTIOS

Supervisor

ANNA ZERVAKI

Submitted for the Partial Fulfillment

of the requirements for the degree of

Diploma in Mechanical Engineering

2016

Certified by the member of the thesis committee:

First examiner (Supervisor)	Dr. Anna Zervaki Lab Teaching Staff, Department of Mechanical Engineering, University of Thessaly
Second examiner	Dr. Gregory Haidemenopoulos Professor, Department of Mechanical Engineering, University of Thessaly
Third examiner	Dr. Nikolaos Andritsos Professor, Department of Mechanical Engineering, University of Thessaly

AKNOWLEDGMENTS

This project is accomplished in the scope of partial fulfillment of the requirement for the degree of the Diploma in Mechanical Engineering at University of Thessaly.

For the completion of this Thesis, I would like to thank my thesis supervisor, Dr. Anna Zervaki whose expertise, valuable suggestions, comments, guidance and patience added considerably to my knowledge and for the tremendous support over this semester.

Furthermore, very special thanks go to professors Gregory Haidemenopoulos and Andritsos Nikolaos for accepting to be the examiners of this work.

I would also like to express my very great appreciation to Lazarou Bros Sheet Metal Works, for providing the CO2 laser machine, and specially to Mr. Lazaros Lazarou for his valuable suggestion, patience and flawless cooperation.

I would also like to thank the Instructor Dr. Eleni Kamoutsi for her help and guidance with the laboratory machinery.

Last but not least, special recognition goes to my family for their continuous support and encouragement during this study.

Kardaras Fotios

ABSTRACT

Advanced high strength steels (AHSS) are widely used for specific military applications. A typical member of this alloy family is the ARMOX 500 steel studied in the frame of this diploma thesis. Main advantages of these steels are their superior mechanical properties, good machinability and high ballistic performance in combination to the low production cost. The ballistic performance depends on parameters like strength, hardness, toughness, microstructure and weldability.

In the process chain of the metallic constructions, the first basic step comprises of the cutting of plates/sheets to the proper shape. The cutting methods employed to that purpose have a significant effect on the quality of the produced parts mainly on the heat affected edges as well as their roughness. The mean roughness values, the microstructure and consequently the properties in the heat affected area play a key role on the next processes either forming or welding.

The CO_2 laser exhibits certain advantages in comparison to the conventional cutting methods, mainly because of the ability to control the laser power density, the small dimensions of the beam (0,2mm diameter spot size in focus) and the small pulse width. Within the frame of this thesis, ARMOX 500 plates of three different thicknesses were subjected to laser cutting. A parametric study of experimental conditions (power, speed and focal point position) was carried out and the specimens were then examined in the Laboratory of Materials. The optimum laser cutting conditions for each thickness were determined in relation to the roughness of the cut surface, the microstructure and microhardness.

The results of the thesis, correlate the cutting parameters with the roughness, the microstructure and the microhardness for the case of the ARMOX 500 steel, demonstrate the advantages of laser cutting, and can be exploited by the end users to determine the optimum cutting parameters for this specific steel. The results are in good agreement with similar works published in the open literature.

ΠΕΡΙΛΗΨΗ

Οι προηγμένοι χάλυβες υψηλής αντοχής με μικρή περιεκτικότητα κραματικών στοιχείων (AHSS) στην οικογένεια των οποίων ανήκει και ο χάλυβας ARMOX 500T - που μελετήθηκε στην παρούσα εργασία- βρίσκουν ευρεία εφαρμογή μεταξύ άλλων και σε εξειδικευμένες στρατιωτικές χρήσεις. Τα κύρια πλεονεκτήματά τους είναι το χαμηλό κόστος παραγωγής σε συνδυασμό με τις εξαιρετικές μηχανικές τους ιδιότητες, την καλή κατεργασιμότητά τους καθώς και την υψηλή τους απόδοση σε βαλλιστικές εφαρμογές. Η απόδοση αυτή εξαρτάται από ιδιότητες όπως η αντοχή, η ολκιμότητα, η σκληρότητα η μικροδομή καθώς και η καλή συμπεριφορά στη συγκόλληση.

Για την παραγωγή σύνθετων κατασκευών από ARMOX 500T η αρχική φάση κάθε κατεργασίας είναι η κοπή των ελασμάτων στα επιθυμητά κάθε φορά σχήματα και διαστάσεις. Οι μέθοδοι κοπής που χρησιμοποιούνται επηρεάζουν σημαντικά την ποιότητα των τμημάτων των ελασμάτων που παράγονται, λόγω τόσο της θερμικής επιρροής στην περιοχή της κοπής όσο και λόγω της τραχύτητας των αντίστοιχων επιφανειών κοπής. Οι μεταβολές στην τραχύτητα, στη μικροδομή και κατά συνέπεια στις ιδιότητες του χάλυβα θα πρέπει να διατηρούνται στη μικρότερη δυνατή έκταση, ώστε το επόμενο στάδιο της κατεργασίας διαμόρφωσης ή συγκόλλησης να επηρεάζεται στο μικρότερο δυνατό βαθμό.

Η κοπή με CO2 laser παρέχει σημαντικά ποιοτικά πλεονεκτήματα έναντι των συμβατικών μεθόδων κυρίως λόγω της δυνατότητας πλήρους ελέγχου της παρεχόμενης πυκνότητας ισχύος κατά την κοπή, των πολύ μικρών διαστάσεων της δέσμης (0,2mm) καθώς και της μικρής διάρκειας παλμού του laser. Στα πλαίσια της παρούσας εργασίας χρησιμοποιήθηκε CO2 laser για την κοπή ελασμάτων ARMOX 500 σε τρία διαφορετικά πάχη. Πραγματοποιήθηκε παραμετρική μελέτη εύρους πειραματικών συνθηκών (ισχύς, ταχύτητα κοπής, θέση σημείου εστίασης) και προσδιορίστηκαν οι βέλτιστες συνθήκες κοπής για κάθε πάχος που μελετήθηκε σε σχέση με την τραχύτητα των επιφανειών κοπής, την μικροδομή και την μικροσκληρότητα.

Τα αποτελέσματα της εργασίας, δείχνουν τα πλεονεκτήματα της μεθόδου όσον αφορά το εύρος της επιρροής των συνθηκών κοπής στο παραγόμενο κάθε φορά αποτέλεσμα, συσχετίζουν τις πειραματικές συνθήκες με τη μικροδομή, τη μικροσκληρότητα και την τραχύτητα, και μπορούν να αξιοποιηθούν από τους τελικούς χρήστες προκειμένου να προσδιοριστούν οι βέλτιστες συνθήκες κοπής για τον χάλυβα ARMOX 500T.

TABLE OF CONTENTS

FIGURE CONTENTS

TABLE CONTENTS

GRAPH CONTENTS

1 INTRODUCTION

Armor steels are very sensitive at high temperatures and temperature changes, which lead to degradation of their mechanical properties. Such conditions are met at secondary processes through a construction, such as welding and thermal cutting. The aim of this thesis was, through experimental procedure, to analyze the effect of the laser cutting method and the affection of the method's different parameters on Armox 500T steel. In the frame of the current work laser cutting was employed for the preparation of selected plates of ARMOX 500 steel before welding. The roughness of the cut surface, the microstructure and microhardness changes on transverse cross sections of the plates were the main subjects of study as well as their dependency on the laser parameters .The purpose was to determine the extent of deterioration at the cutting edge and to define the optimum laser cutting conditions so as to minimize the effect from the cutting process.

Introduction to the thesis structure

The second chapter of this thesis includes a history review of the evolution of steel. The basic characteristics of each generation and the reasons that led the researches to carry on are mentioned. At the second segment, a brief reference at the four primary cutting methods used today is done. The reference focuses on the basic operating principals, the advantages and the disadvantages of each method. Finally a more extended reference on armor steels is included in the third and final segment of this chapter.

The beginning of the third chapter refers to the material's production process, microstructural characteristics, chemical composition and its mechanical properties. This is followed by a step by step illustration of the applied experimental process and the tools that were used.

The fourth chapter contains the experimental results in form of tables and graphs.

The results are discussed at the fifth chapter and the conclusions are developed at the sixth one.

2 LITERATURE REVIEW

2.1 THE EVOLUTION OF STEEL

Traditionally, in most constructions, mild steel and cast iron are widely used as the dominant material. However modern technology and market trends demand products with higher strength and lower weight. The cost is a major factor of any product and also steel's bigger benefit upon other competitive materials such as aluminum alloys, magnesium alloys and fiber-reinforced composites. This in association with the already extensive knowledge and familiarity with manufacturing, processing and forming of steel, intensified the researches to develop advanced high strength steels, instead of substitute steel with other materials.

Steel has evolved over the years from mild steel in early 1900's to high-strength low-alloy (HSLA) steels in the late 1970' and the first generation of advanced high strength steel AHSS in the 1990's. Recent approaches to improve the properties of steel have been based on developing steel microstructures of higher strength in order to reduce component section size and weight. In the last two decades have there are significant improvements in the composition, microstructure, strength, ductility and processing approaches to steel manufacture.

Graph 2.1 provides an overview of the steel categories based on strength and ductility. At the lower end of the strength spectrum are the interstitial (IF) and mild steels. These steels are very soft and formable. In the middle are the conventional grades of HSS that include interstitial-free, high strength (IF-HS), isotropic (IS), bake-hardenable (BH) and high strength, low-alloy (HSLA) steels. These steels have higher strength compared to traditional grades but their ductility is much lower. At the high end are the AHSS that include dual-phase (DP), complex-phase (CP), transformation-included plasticity (TRIP) and martensitic steels (MS). These steels exhibits very high strength and except the MS grade, have good formability. [1]

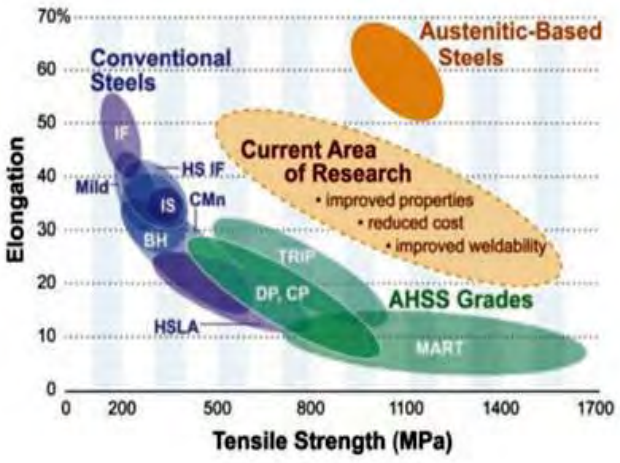

Graph 2.1 - STEEL CATEGORIES BASED ON STRENGTH AND DUCTILITY

2.1.1 HISTORY OF DEVELOPMENT OF AHSS

Early efforts to obtain lighter weight and enhanced strength were aimed at the development of High Strength Low Alloy (HSLA) steel. This kind of conventional High Strength Steel (HSS) has a tensile strength of 250 to 590 MPa. However, the tradeoff between strength and ductility limited the performance and the manufacturability of HSLA steels. To fulfill the requirements for steel with higher strength while retaining its formability, Advanced High Strength Steels (AHSS) were developed during mid - 1990's.

Advanced High Strength Steels, refers to steels with 500 MPa or more tensile strength and complex microstructures such as bainite, martensite and retained austenite. The strengthening mechanisms include solid solution strengthening, precipitation strengthening, grain refinement and phase transformation. There are two generations of AHSS based upon the microstructure of the steels. The first generation of AHSS are ferrite based steels, including dual-phase (DP) steel, martensitic steel (MS), complex-phase (CP) steel and transformation-induced plasticity (TRIP) steel. [2]

The microstructure and tensile strength of these steels are listed in Table 2.1.

Table 2.1 – MICROSTRUCTURE AND TENSILE STRENGHT OF FIRST GENERATION HIGH STRENGHT STEELS [2]

MICROSTRUCTURE AND TENSILE STRENGHT - FIRST GENERATION HIGH STRENGHT STEELS		
1st GEN. AHSS	MICROSTRUCTURE	STRENGHT (MPa)
DUAL-PHASE	Ferrite + martensite	400 to1000
MARTENSITIC	martensite	700 to 1600
COMPLEX PHASE	Ferrite + bainite + pearlite	400 to1000
TRANSFORMATION-INDUCED PLASTICITY	Ferrite + martensite/ bainite +austenite	500 to 1000

Although the strength level for the 1st generation of AHSS was far beyond that of the conventional HSS, the limited formability remained a problem. During the past few years, a second generation of AHSS was developed based upon an austenitic microstructure. Twinning-induced plasticity (TWIP) steel, lightweight steel with induced plasticity (L-IP) and shear band formation-induced plasticity (SIP) steel are different grades in this catalog. A ductile austenite matrix provides better formability to the 2nd generation of AHSS than the 1st generation. However, the high austenite stabilizer content, such as 20 wt. pct. manganese and nickel, limits the use of the 2nd generation of AHSS because of its high cost. [2]

2.1.2 THIRD GENERATION OF AHSS

Despite the growing market for AHSS, the trade-off between the strength and formability of the AHSS remains the limitation for their application. According to Graph2.1, the conventional HSS provides steels with total elongation in the range of 10 to 50 %, but the tensile strength of the steels are all below 800 MPa. Most of the first generation of AHSS have tensile strength larger than the conventional HSS. However, the total elongation of this generation of steels drops to as low as 10 %. when the tensile strength reaches 1000 MPa. Although the second generation of AHSS solved the problem caused by the competition between tensile strength and total elongation according to Graph2.1, the high cost for this solution remains the main obstacle for its broad application. Recently, the need to develop AHSS with a range of properties that give engineers more flexibility in selecting an ideal grade of steel for any given application has raised increasing interest in developing a third generation of AHSS.

The design of the 3rd generation of AHSS is intended to produce steels with a better combination of strength and ductility than the 1st generation of AHSS and at a lower cost than the 2nd generation of AHSS. The mechanical properties of the 3rd generation of AHSS are intended to fall within the gap between the 1st and 2nd generation of AHSS in Graph 2.1.

In order to reduce the cost, lean alloy steel compositions will need to be used in developing the 3rd generation of AHSS. Because microstructure determines the behavior and performance of AHSS steels, the design and control of the microstructure becomes essential for the 3rd generation of AHSS. It is predicted, based on the rule of mixtures, that the properties of the 3rd generation AHSS could be achieved using steels with martensite and austenite microstructures. The data in Table 2.2 show the ultimate tensile strength and true uniform strain for ferrite, austenite and martensite, which indicate the high strength of martensite and the great ductility of austenite.

Table 2.2 – CONSTITUENT PROPERTIES FOR FERRITE, AUSTENITE AND MARTENSITE PHASES [2]

CONSTITUENT PROPERTIES FOR FERRITE, AUSTENITE AND MARTENSITE PHASES		
Constituent Ultimate	Tensile Strength (MPa)	Uniform True Strain
Ferrite	300	0.3
Austenite	640	0.6
Martensite	2000	0.08

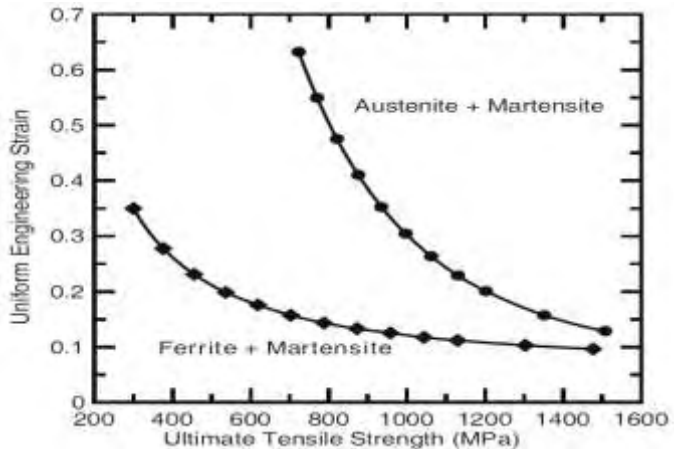

Graph 2.2 PREDICTED STRENGTH/DUCTILITY RELATIONSHIPS FOR TWO HYPOTHETICAL STEEL MICROSTRUCTURES: FERRITE + MARTENSITE (I.E. DP STEEL) AND STABLE AUSTENITE + MARTENSITE [2].

The prediction of strength/ductility relationships for steels with ferrite/martensite and austenite/martensite microstructures is shown in Figure 2.1. Steel with a microstructure containing austenite and martensite has larger strain energy than steel consisting of ferrite and martensite. The volume fraction of austenite has stronger influence on the ductility of the steel than ferrite does. A combination of Graph 1.3 and 2.1 in Graph 1.6 reveals that the prediction on the mechanical properties of steels, with a ferrite/martensite microstructure, fits well with the experimental values. And the mechanical properties required for the 3rd generation of AHSS could be realized by producing AHSS with austenite and martensite microstructure.

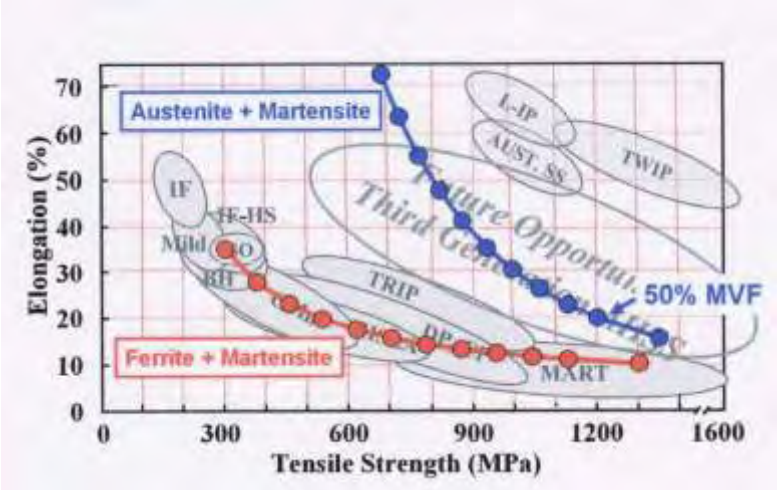

Graph 2.3 – Compination of figures 2.1 and 2.2

The key point for obtaining the 3rd generation AHSS with high tensile strength as well as high ductility is that there is a significant amount of retained austenite in the steels, and the retained austenite can transform to martensite at higher strains, so that the work hardening rate of the steel will increase. Because austenite is not an equilibrium phase in the steel at room temperature, the main challenge of producing the 3rd generation of AHSS lies in the stabilization of a high content of retained austenite in the final structure. [2]

2.1.3 ARMOR STEELS

Suitable material selection is very crucial with respect to reduction in weight of armor and it is essential to determine the material with lowest possible areal density for a defined threat. Many high strength steels, aluminum alloys and titanium alloys are being used as armor. Amongst them AHSS are predominantly used for armor applications owing to their low cost, superior mechanical properties, good machinability and high performance. Ballistic performance of metallic materials depends on parameters like strength, hardness, toughness, microstructure and strain hardening rate, but does not depend on any specific independent parameter. Instead, an optimized value of all the parameters leads to the best ballistic performance and has long been of practical interest in military applications.
Heat treatment is the commonly used process to develop desired properties in steels. Of all the microstructures produced by heat treatment, martensite forms the highest level of strength in steels. However, because of large internal stresses associated with the martensitic transformation, martensite phase is rarely used in an untempered condition. Temperature and time are the two parameters in tempering that play vital roles in determining the mechanical properties of the material. In steels, tempering increases the ductility and toughness, which are essential for enhancing impact energy absorption. However, there is a slight decrease in strength and hardness. [3]

If the steel is exposed to the temperature above 200°C some phase transformations take place in the microstructure and the degradation of mechanical properties needed for the steel usage occurs. These conditions are typical for secondary processing of the steel as are cutting or welding.

There are published several studies about microstructure changes of carbon or low alloyed steels after plasma or laser cutting in scientific literature.

Heat affected zone (HAZ) after the cutting by these processes could be classified to three different areas according that knowledge:

1. Surface area with full recrystallization to the austenite and back to pearlite, bainite or martensite (temperature range from A3 to the solidus). The depth of this area is relatively low (about 50 µm) and depends on chemical composition of steel and parameters of used cutting process as are cutting speed or heat input. If martensitic transformation occurs in the area it may leads to internal stresses generation and consequently to the crack creation.
2. Area with partial recrystallization (temperature range from A1 to A3) where the heating up period is very short and therefore the austenitization is just partial. There is new phase created as a result of partial austenitization beside origin microstructure phases. The amount of new phase decreases in relation to distance from surface. In contrast to full recrystallization area in surface layer, the heating up temperature of this area is not so high and followed cooling is not so rapid. Therefore, the new created phases are more in steady state (bainitic or pearlitic type). The depth of this area is about 500 µm.

3. Transition area between HAZ and core material (heating up below A1) where any essential phase transformation is not present. Processes known from basics of tempering process take place in steels with martensitic structure. Morphology of martensite is changed from tetragonal to cubic tempered martensite, transformation of the residual austenite occurs and cementite and other carbides are created. This area could reach the depth of several millimeters from surface. [4]

In the next paragraphs a review on the main thermal cutting processes is given.

2.2 CUTTING METHODS

2.2.1 Oxy-Fuel Cutting

The process is now about 111-112 years old as it was patented in 1901 by Thomas Fletcher. It is a Thermo-Chemical Process requiring a source of intense heat, referred to as “Preheat”, and pure oxygen.

The process for all thicknesses is the same and that is the material must be “preheated” to a temperature of 870-1000 degrees °C, then the pure Oxygen is discharged into the preheated area and the steel is then oxidized or burned, hence the term “burning”.

Figure 2.1 – OXY FUEL CUTTING

Advantages

- Wide thickness cutting range, from sheet metal to 100 inch thick material
- Quite excellent quality of the final cut surface, with sharp top edge, flat cut surface, and a sharp slag- free lower edge.
- Multiple torches can be used at once, multiplying productivity

Disadvantages

- It is a relatively slow process
- The pure oxygen requirement is of a 99.5% minimum purity. While the source of the Oxygen may be pure, improper connections, bad hoses, or leaks of any sort can allow impurities in the system thereby reducing the cutting speed
- The high purity of the Oxygen presents a very dangerous situation and requires extreme care in the selection of equipment and the design of piping systems for its use
- The basic requirement that the oxide formed must have a lower melting point than the base material to be cut
- Oxy-fuel cutting is ideal for plates thicker than 1 inch, but thin materials are very challenging to flame cut.

Manufacturer recommendation

This process can be applied to high-hardness Armox plate up to 80 mm thickness. It generates a kerf of 2-5 mm and a HAZ which is usually 4-10 mm wide. [5]

2.2.2 Plasma Cutting

Plasma cutting is a process that cuts through electrically conductive materials by means of an accelerated jet of hot plasma. The plasma arc formation begins when a gas such as oxygen, nitrogen, argon, or even shop air is forced through a small nozzle orifice inside the torch. An electric arc generated from the external power supply is then introduced to this high pressured gas flow. The gas stream is heated to such high temperature that it becomes ionized, resulting in what is commonly referred to as a "plasma jet". The ionized gas by definition can then freely exchange electrons between atoms. This electron movement is what allows the gas to carry the cutting amperage. The plasma jet immediately reaches temperatures up to 40,000° F, quickly piercing through the work piece and blowing away the molten material.

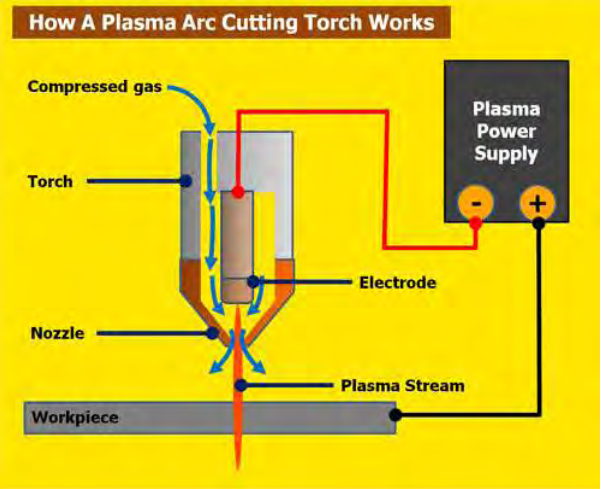

Figure 2.2 – PLASMA NOZZLE

Advantages

- Plasma cutting is the fastest cutting process on carbon steel, aluminum, or stainless steel
- Very good Edge quality from about 1/4 inch up to 1.5 inches thick. Outside of this range the edge smoothness and dross performance may still be quite good
- Can be used for precision cutting on gauge material up to 6" thick stainless steel
- Multiple torches can be used at once, multiplying productivity
- Increased productivity of plasma vs. oxy-fuel will pay for the cost of the system

Disadvantages

- Plasma equipment can be pricy when compared to an oxy-fuel torch
- Sacrificing some edge quality than oxy-fuel cutting
- The additional cost factor usually limits this to two torches at once
- Minimum purity requirements for nitrogen at 99.995% and 99.5 % for oxygen

Manufacturer recommendation

High-hardness Armox plate up to around 25 mm thickness can be cut using this process. It generates a kerf, usually 3-4 mm, and a HAZ up to 5 mm. Plasma cutting can be performed under water, which minimizes the amount of distortion. [5]

2.2.3 Water jet Cutting

At water jet cutting, pressurized water is delivered to a cutting head by high pressure tubing or hose. At the cutting head, the high pressure water is applied to an orifice with a typical diameter ranging from 0.005" to 0.020". The orifice defines and creates the water stream which cuts through the material.

After the water stream exits the orifice, an abrasive, which is usually crushed garnet, can be added to the water stream, allowing to cut hard materials. When cutting hard materials, including steel, stainless steel, aluminum, stone, wood, plastic, glass, etc., it is the abrasive that does the actual cutting using a mechanical sawing type action. When cutting soft materials, such as rubber, leather, cloth, paper, cardboard, insulation, foam, etc., abrasive is not used as the high pressure water stream does the cutting.

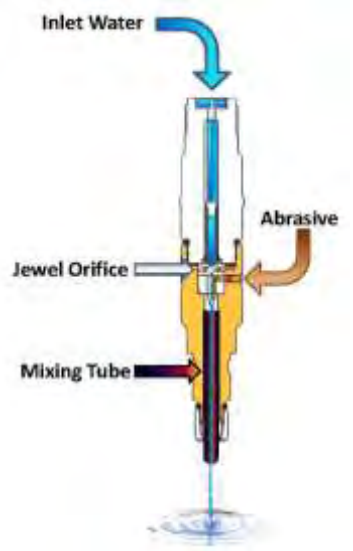

Figure 2.3 – WATER JET NOZZLE

Advantages

- Is the most versatile process. It is able to cut almost any type of material.
- Highest precision cutting on virtually any material.
- It has a narrow kerf width, allowing fine contours to be cut, and producing high tolerance parts
- Leaves a smooth, precision cut surface
- There is no heat distortion
- It has a narrow kerf width, allowing fine contours to be cut, and producing high tolerance parts
- The practical limit on water jet cutting is around 6 to 8 inches
- Multiple heads can be used at once, multiplying productivity

Disadvantages

- It is very slow
- The cost-per-hour to run water jet is much higher, when compared to plasma on most metals, primarily due to the cost of the garnet abrasive
- Up front equipment costs are usually a little higher than plasma, but not as high as laser

Manufacturer recommendation

This process can be applied to the complete range of high-hardness Armox plate, and is recommended as the best method, because the absence of HAZ eliminates the risk of cracking. [5]

2.2.4 LASER

The laser cutting process uses a focused laser beam and an assist gas to a metallic plate with high accuracy and exceptional process reliability. The laser beam is a column of very high intensity light, of a single wavelength, which is generated by a resonator. It is delivered through the cutting nozzle via a system of mirrors, so as to go through the bore of the nozzle and hit the plate. Also compressed gas, such as Oxygen or Nitrogen is flowing through the nozzle.

Focusing of the laser beam takes place in the laser cutting head by a special lens, or by a curved mirror. This results in high power density at the focal point, leading in rapid heating, melting and partial or complete vaporizing of the material. Two laser cutting methods exist:

- Fusion Cutting, or high pressure cutting, where the material is fused by the energy of the laser beam. In this case nitrogen at high pressure (10 to 20 bars), is used to drive out the molten material from the kerf. This cutting method protects the cut edges from oxidation and is mainly used with stainless steels, aluminum and their alloys.
- Oxidation Cutting, or laser torch cutting, in which the material is heated by the laser beam to combustion temperature. In this case oxygen at a medium pressure (0.4 to 5 bar) is used to oxidize the material and to drive the slag out of the kerf. The exothermic reaction of the oxygen with the material supplies a large part of the energy for the cutting process. This cutting method is the quickest and is used for the economical cutting of carbon steels.

There are many parameters that affect cut quality, when all are controlled properly laser cutting is a stable, reliable, and very accurate cutting process. The following points are especially important for achieving good cutting results:

Laser power: The laser power must be adjusted to suit the type and thickness of the work-piece. Laser power is the total energy emitted in the form of laser light per second. The intensity of a laser beam is equal to its power divided by the area over which the power is concentrated. The high intensity causes the material to heat up rapidly so that little time is available for heat to dissipate into the surrounding material. This produces high cutting rates and an excellent quality of cut. A laser's intensity also determines the thickness that can be cut. The thicker the material to be cut, the higher the intensity needed. Higher intensities can be reached by increasing laser power.

Focal length: Optical systems with 5" and 7.5" focal lengths are typically used for cutting. 5" optics are only suitable for thin materials. For thicker materials the 7.5" optics are used. With the 5" optics the kerf is narrower compared to the 7.5" optics, giving a higher energy density for the same laser power. The possible cutting speeds for the 5" optics are therefore slightly higher for the same material thickness and laser power. The 7.5" optics has the advantage of a greater depth of focus, i.e. the maximum cutting thickness is greater. The 7.5" optics can be used universally for a large range of thickness, but they are mainly used for thicker materials. The definition of focal length is shown in figure 2.4.

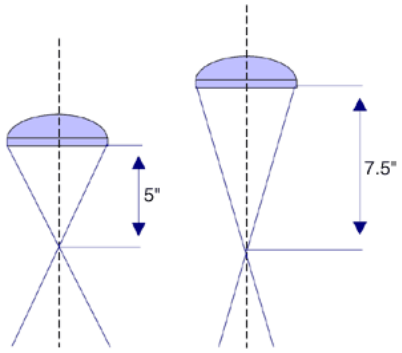

Figure 2.4 – FOCAL LENGHT

Focus position: Exact positioning of the focal point is an important requirement for good cutting results. The focal point can be at, below or above the plate's surface, as shown in figure 2.5.

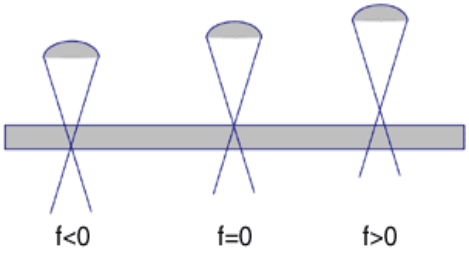

Figure 2.5 – FOCAL POINT

Cutting speed: The cutting speed must be matched to the type and thickness of the work-piece. A speed which is too fast or too slow leads to increased roughness, burr formation and to large drag lines. Cutting speed, though, is determined by the average power level. The higher the average power, the higher the cutting speed.

Type and pressure of cutting gas: The type of material and the requirements of the cutting results determine the cutting gas to be used. The material thickness of the work-piece must be matched to the gas pressure. When thin metallic materials are cut with the torch cutting method a higher gas pressure than thicker materials is appropriate. If the pressure is too low, the fluid slag remains adhered to the base material, forming a permanent burr or closing the kerf again. If the pressure is too high, the lower edges of the cut are burnt out and often make the cut unusable. In contrast, with high pressure cutting thicker work-pieces are cut at higher gas pressure.

Nozzle size and standoff distance: Gas assistance is essential in laser cutting. Therefore, nozzle geometry and standoff distance are important.

Advantages

- High accuracy
- Excellent cut quality
- High processing speed
- Very narrow kerf width
- Very small heat-affected zone compared to other thermal cutting processes
- It is possible to cut complex geometrical shapes, small holes, and beveled parts
- Cutting and marking with the same tool
- Cutting many types of materials
- Very thin oxide layer
- High-pressure laser cutting with nitrogen enables oxide-free cutting
- Edge quality is usually very good, with extremely small serrations and lag lines, very square edges, and little to no dross

Disadvantages

- The laser cutting process is suitable for cutting mild steel from gauge thickness up to about 1.25 inch.
- The speed is limited by the speed of the chemical reaction between Iron and Oxygen.

- Cutting with multiple heads on the same machine is not possible, except for fiber lasers

Manufacturer recommendation

High-hardness Armox plate up to around 20 mm thickness can be cut using this process. It generates a narrow kerf, usually less than 1 mm, and a narrow HAZ, usually less than 3 mm. [5]

Table 2.3 – LIMITATIONS AND RANGES OF CUTTING METHODS

LIMITATIONS AND RANGES OF CUTTING METHODS			
CUTTING METHOD	THICKNESS LIMITATIONS	KERF'S WIDTH	WIDTH OF HAZ
OXY - FUEL	15-60 mm	2-5 mm	4-10 mm
PLASMA	0-15 mm	3-4 mm	up to 5 mm
WATER JET	0-above 60 mm	narrow	absence
LASER	0-25 mm	narrow, usually less than 1mm	narrow, usually less than 3mm

2.3 RESEARCH ON ARMOR STEELS

Many studies have been conducted on the negative effects of secondary thermal processes on the performance of armor steels. These studies are aiming to analyze, find ways to predict and reduce those effects as much as possible.

A study focused on cutting methods on armor steels shows that changes in microstructure, after laser and plasma cutting process reported that a surface layer consisted of martensitic needles is formed after both processes. Also, an area where partial recrystallization is observed, wider at the plasma cutting. Plasma cut also produces HAZ with significantly higher depth, while, white coherent oxide layer and partial saturation by gases (N2, O2) was observed. [4]

Another paper investigates the post welding degradation of the mechanical properties of armor steels, produced either by the quenching and tempering method or by thermomechanical rolling with accelerated cooling. It shows that at the same strength of the steels the microstructure of the heat-affected zone (HAZ) greatly differs for the same welding conditions. Also, it is mentioned that the softened zone of the HAZ in the TMCP steel is wider than in the steel produced by QT. The distribution of microhardness can be seen at graph 2.4. [6]

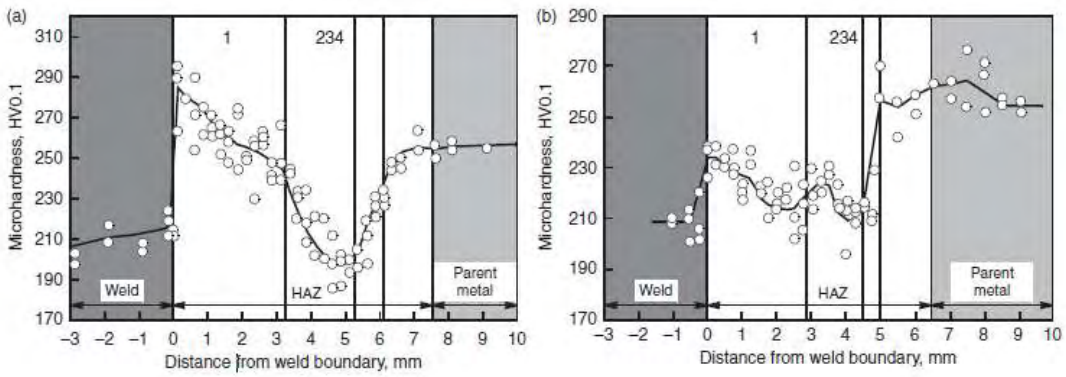

Graph 2.4 – DISTRIBUTION OF THE MICROHARDNESS IN THE CROSS-SECTION OF THE WELDED JOINT AFTER WELDING OF QT a) AND TMCP b) STEELS [6]

In addition a research combining the two above was conducted focused on the degradation of the mechanical properties of armor steels, in HAZ, after cutting with different methods and then welded. Comparisons of the variants between weld and basic materials shows that the yield strength decrease is almost equal in all three methods, plasma, laser and water jet cutting. In addition this is not the case for the tensile strength. The plasma cutting process has such a high effect that it appears even after the welding, causing a reduction of tensile strength 13% and 8% greater than that of laser and water jet respectively, as shown on the graph 2.5. [7]

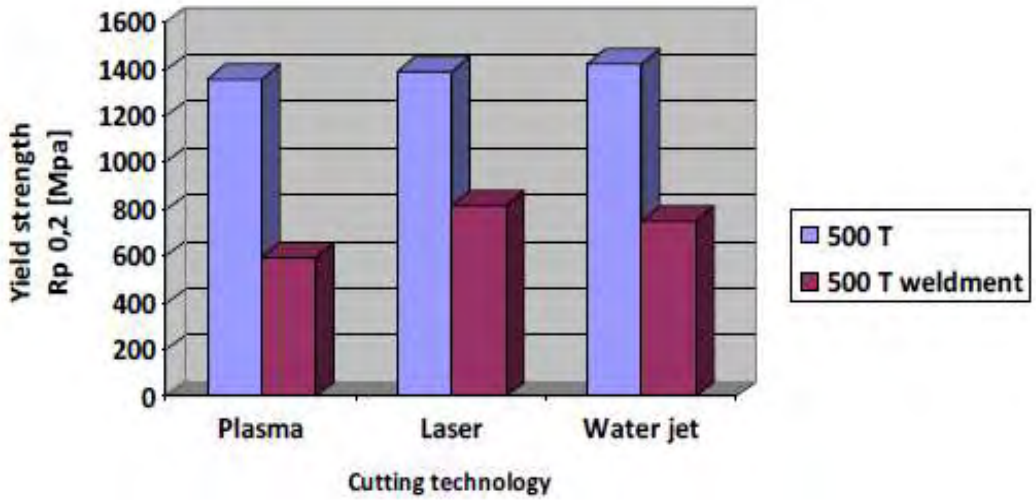

Graph 2.5 – EXPERIMENTAL RESULTS – YIELD STRENGHT OF BASIC AND WELDED MATERIAL [8]

Additional computational researches on changes in mechanical properties of armor steels after over tempering have been done. The purpose of these simulations was to study phase transformations during cooling after over tempering and study the differences between the delivered microstructure state after controlled heat treatment and its state after over tempering. The cooling simulation results show a significant degradation of the mechanical properties (hardness, tensile strength) in

areas where material affected by over tempering. Additional exposure of the material to over tempering temperatures cause continuation of the tempering process and therefore degradation of its mechanical properties. The intensity of degradation rises proportionally with the increase in temperature and the time of exposure. Some of the results are given in table 2.4. [8]

Table 2.4 – ARMOX 500T PROPERTIES CALCULATED BY COOLING SIMULATION [8]

ARMOX 500T properties calculated by simulaton		Starting Temperature		Delivered conditions
		500°C	1000°C	
Critical temperatures [°C]	A_{c3}	786		-
	A_{c1}	707		-
Structural components [%]	Bainite	81	84.5	-
	Martensite	19	15.5	-
Mechanical properties	R_m [MPa]	1335	1312	1750
	$R_{p0.2}$ [MPa]	1070	1049	1250
	HV/HB	441/418	435/413	610/540

At another research, simulations of armor steels were carried out with TTSteel 2.1 software. This software was designated for the determination and calculation of mechanical properties of constructional, micro alloyed and tool steels after their heat treatment. The software creates transformation diagram of simulated steels based on their chemical composition. Then, it calculates cooling curve according the transformation diagram and also input cooling conditions. Next step is the determination of microstructure phases in simulated sample volume based on stated cooling curve. Finally, the mechanical properties are calculated according to microstructure components in every volume element. The results of a simulation on armor steels, show that the degradation of mechanical properties is in range of 20-30% when heated up above the A1 temperature and in range of 14-19% when heated up just below the A1 temperature and then cooled slowly in air of 20°C temperature. Some results are given in tables 2.6 and 2.7. [8] [9]

Table 2.5 – SIMULATION RESULTS FOR ARMOX 500 STEEL HEATED BELOW A1 TEMPERATURE [9]

Conditions	Armox 500T – mechanical properties			
	R_m [MPa]	$R_{p0,2}$ [MPa]	Hardness [HV]	Microstructure
After quenching	1839	1548	559	100% martensite
After cooling on air	1339	1081	412	80% bainite, 20% martensite
Difference [%]	-27 %	-30 %	-26 %	

Table 2.6 – SIMULATION RESULTS FOR ARMOX 500 STEEL HEATED ABOVE A1 TEMPERATURE [9]

Conditions	Armox 500T - mechanical properties		
	R_m [MPa]	$R_{p0,2}$ [MPa]	Hardness [HV]
After quenching	1839	1548	559
After uncontrolled tempering	1516	1247	465
Difference [%]	-18 %	-19 %	-17 %

In the frame of the current work laser cutting was employed for the preparation of selected plates of ARMOX 500 steel before welding. The purpose was to determine the extent of deterioration at the cutting edge and to define the optimum laser cutting conditions so as to minimize the effect from the cutting process.

3 MATERIAL AND EXPERIMENTAL PROCESS

3.1 MATERIAL

ARMOX 500

ARMOX 500 is an armor steel produced by the Swedish company SSAB that belongs at the medium alloy group of steels. In order to reach the required mechanical properties, it undergoes a few important steps through the production process. First step is continuous casting of slabs with using of ore with high chemical purity. The next step is rolling of the slabs at temperature about 1250°C to refine its microstructure – austenitic grains. Then the slabs are solution annealed at temperature about 850°C. The most important are two final steps of quenching and tempering. The slabs are quenched in continuous furnace from the temperature about 1000°C, to harden the steel and finally low tempered at 200°C – 500°C, in order to make the hardened steel tougher . The resulting microstructure from this treatment is fine tempered martensite, combining high strength, high hardness and good toughness. However, ARMOX 500 is very sensitive at high temperatures and temperature changes which lead to degradation of its mechanical properties. Therefore the manufacturer notes out that it is not intended for further heat treatment and should not be heated above 190 °C during secondary processing such as cutting, bending or welding.
Tables 3.1 and 3.2 show in detail the chemical composition and the mechanical properties of Armox 500T respectively, as given by the manufacturer. Also the CCT diagram as given at [8] is included, graph 3.1. [7] [8]

Table 3.1 – CHEMICAL COMPOSITION OF ARMOX 500T [4]

ARMOX 500T

Chemical Composition (ladle analysis)

C [1] (max %)	Si [1] (max %)	Mn [1] (max %)	P (max %)	S (max %)	Cr [1] (max %)	Ni [1] (max %)	Mo [1] (max %)	B [1] (max %)
0.32	0.4	1.2	0.015	0.010	1.01)	1.81)	0.7	0.005

The steel is grain-refined. [1] Intentional alloying elements.

[1] For plate thicknesses >70 mm Cr ≤ 1.5 and Ni ≤3.5

Table 3.2 –MECHANICAL PROPERTIES OF ARMOX 500T [4]

Mechanical Properties

Thickness (mm)	Hardness (HBW)	Charpy-V[1], 10x10 mm test specimen[2] Min.	Yield Strength $R_{p0.2}$ (min MPa)	Tensile Strength R_m (MPa)	Elongation A_5 (min %)	Elongation A_{50} (min %)
3.0- 80.0	480- 540	32 J /-40°C	1250	1450- 1750	8	10

[1] Average of three tests. Transverse to rolling direction. Single value min. 70% of specifi ed average.

[2] For plate thicknesses under 12 mm sub-size Charpy-V specimen are used. The specifi ed minimum value is then proportional to the specimen cross-section.

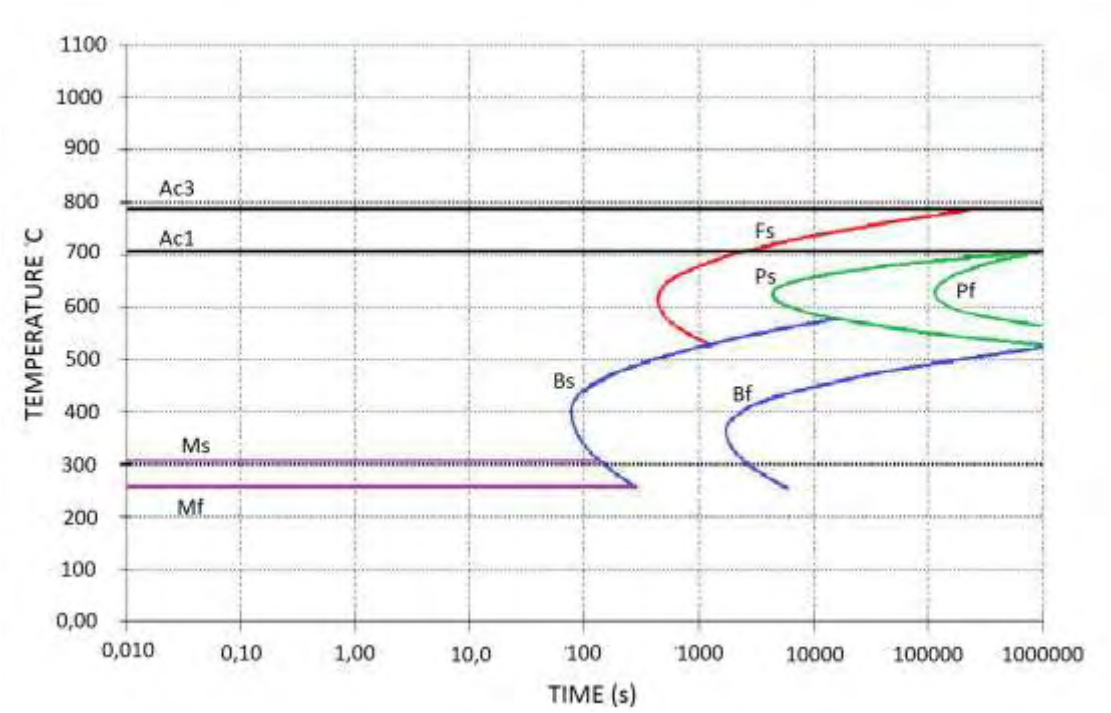

Graph 3.1 - CCT DIAGRAM OF ARMOX 500T [8]

3.2 EXPERIMENTAL PROCEDURE

For the experimental process, a TRUMPF 5kW "TRUMATIC L3050" laser cutting machine (fig.3.1 and 3.2) was used to cut square specimens with sides of 25mm. Three groups of four specimens were produced. Each specimen was coded with the letter A, B or C, depending on its width, continued by the number 1, 2, 3 or 4, depending on the cutting parameters of the laser, as shown in the table 3.3.

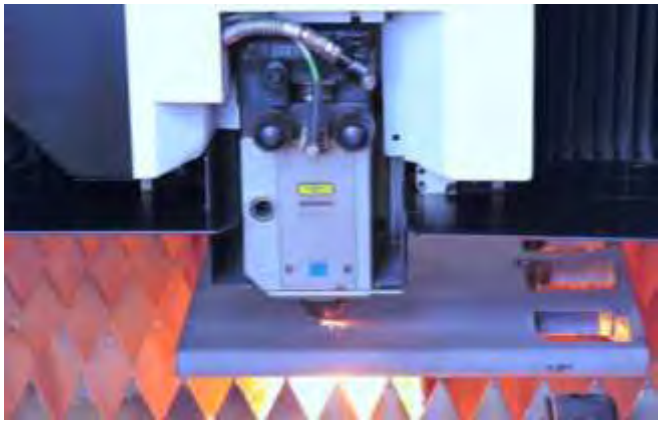

Figure 3.1 – LASER CUTTING HEAD

For each group, a specimen was cut with the initial parameters, the second with the initial parameters but with half the cutting speed, the third with the initial parameters but with the focal point moved lower, 40-45% of the specimens width and the fourth with both the speed lowered and the focal point moved, similar to the two previous.

Table 3.3 – LASER CUTTING PARAMETERS AND HEAT INPUT RATE

CUTTING PARAMETERS & HEAT INPUT RATE												
	GROUP											
	A (ta=5mm)				B (tb=10mm)				C (tc=20mm)			
	SPECIMEN											
PARAMETER	1	2	3	4	1	2	3	4	1	2	3	4
FOCAL LENGTH (in)	7,5	7,5	7,5	7,5	7,5	7,5	7,5	7,5	7,5	7,5	7,5	7,5
NOZZLE (mm)	1	1	1	1	1,2	1,2	1,2	1,2	2	2	2	2
GAS	O2	O2	O2	O2	O2	O2	O2	O2	O2	O2	O2	O2
FOCAL POINT (mm)*	0	0	-2	-2	+0,5	+0,5	-3,5	-3,5	+4,5	+4,5	-4,5	-4,5
LASER POWER (W)	4800	4800	4800	4800	4800	4800	4800	4800	4800	4800	4800	4800
GATING FREQUENCY (Hz)	20.000	20.000	20.000	20.000	20.000	20.000	20.000	20.000	20.000	20.000	20.000	20.000
SPEED (m/min)	3200	1600	3200	1600	1920	960	1920	960	880	440	880	440
NOZZLE STAND OFF (mm)	1,2	1,2	1,2	1,2	1,5	1,5	1,5	1,5	1	1	1	1
GAS PRESSURE (bar)	0,8	0,8	0,8	0,8	0,8	0,8	0,8	0,8	0,6	0,6	0,6	0,6
*The focal point is measured from the plate's top surface and is considered positive when it is above this surface (near the nozzle) and negative when it is below this surface (inside the plate's width)												
HIR (J/mm)	0,09	0,18	0,09	0,18	0,15	0,30	0,15	0,30	0,33	0,65	0,33	0,65

Figure 3.2 – TRUMPF - TRUMATIC L 3050

From these parameters the Heat Input Rate is calculated. Heat Input Rate is the power of the laser beam divided by the cutting speed. The results are shown in the table 3.3.

$$HIR = \frac{LASER\ POWER(W)}{CUTTING\ SPEED(\frac{mm}{s})}\ \ [= \frac{J}{mm}]$$

For each specimen the experimental procedure followed included:

Roughness measurement: Roughness test was performed on the cutting surface, after the cutting process, at 1mm below the upper plate's surface and 1mm above the lower plate's surface with Taylor Hobsons "Surtronic 25" roughness meter, as shown in figures 3.3 and 3.4. The roughness parameter, Ra, is the arithmetic average of the absolute values of the profile height deviations from the mean line.

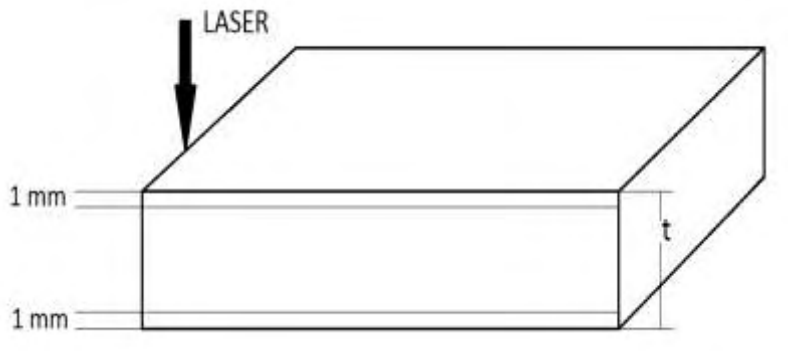

Figure 3.3 – ROUGHNESS MEASURED AREA

Figure 3.4 – ROUGHNESS TESTING

Metallography: Metallographic analysis was performed on transverse cross sections as shown in Fig. 3.5. Specimen's preparation included cutting with Struers ''Accutom 5'', grinding with SiC papers 120, 220, 320, 500, 600, 800, 1000 and 2000 grit, and polishing with diamond paste of 3μm diameter. Etching was performed with Nital 3%. Examination of the metallographic specimens was carried out on an Optical Metallographic Microscope, Leitz ''Aristomet'' at magnifications 100 x –1000 x.

Microhardness Measurements: Microhardness measurements were performed on the cross section of the metallographic specimens at (5~10%)t below the upper plate surface and (5 ~10%)t above the lower plate surface, as shown in figure 3.5. Microhardness tester WOLLPERT 402MVD, was used at a load of 500 gr on Vickers scale.

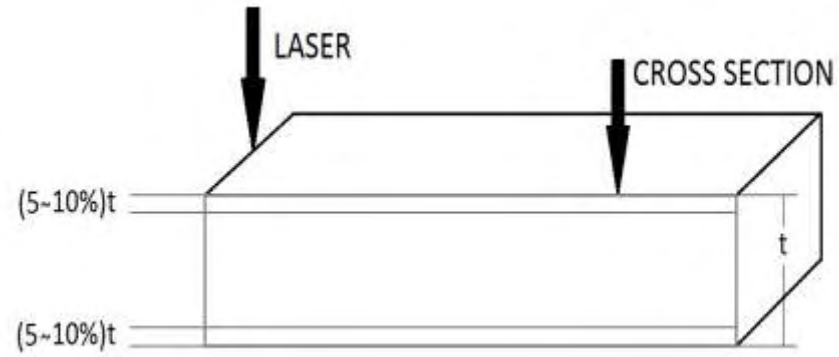

Figure 3.5 - SCHEMATIC REPRESENTATION OF THE METALLOGRAPHIC CROSS SECTION, AND THE POSITION OF THE MICROHARDNESS PROFILES IN RELATION TO PLATE THICKNESS AND THE LASER CUT

4 RESULTS

4.1 ROUGHNESS

Data of the Ra parameter were taken from each region of interest and the average was calculated. Ra roughness parameter is the arithmetic average of the absolute values of the profile height deviations from the mean line. The results are given in the table 4.1.

Table 4.1 – ROUGHNESS TEST MEASUREMENTS

ROUGHNESS TEST								
SAMPLE		Ra(µm)						AVERAGE
A1	TOP	0,9	0,72	0,9	1,1	0,78	0,8	1,04
	BOTTOM	1,28	1,42	1,44	1,38			1,38
A2	TOP	8,42	8,32	9,02				8,59
	BOTTOM	6,66	5,88	6,24				6,26
A3	TOP	1,2	1,22	1,3				1,24
	BOTTOM	1,84	1,46	1,48				1,59
A4	TOP	7,46	7,62	7,82				7,63
	BOTTOM	4,64	5,34	5,28				5,09
B1	TOP	2,68	2,5	2,5	2,32	2,28		2,46
	BOTTOM	1,86	1,52	1,84	1,68	1,8		1,74
B2	TOP	11,6	10,4	12,2	10	11,6		11,16
	BOTTOM	8,8	9,2	5,68	7,08	7,66		7,68
B3	TOP	1,46	1,7	1,42	1,6	1,56		1,55
	BOTTOM	2,88	3,18	3,62	2,64	2,92		3,05
B4	TOP	6,6	6,6	7,2	6,8	7,4		6,92
	BOTTOM	8,6	8,4	8,6	7,8	8,4		8,36
C1	TOP	9,34	9,86	10,1	9,92	9,38		9,72
	BOTTOM	8,2	8	6,8	7,2	6,2		7,28
C2	TOP	OUT OF RANGE						0,00
	BOTTOM	OUT OF RANGE						0,00
C3	TOP	12,8	15,2	15,6	14,6	14,4		14,52
	BOTTOM	10,4	11	9,8	10,6	10,4		10,44
C4	TOP	OUT OF RANGE						0,00
	BOTTOM	OUT OF RANGE						0,00

Graphs 4.1, 4.2 AND 4.3show the effect of cutting parameters on roughness at specimens of the same thickness.

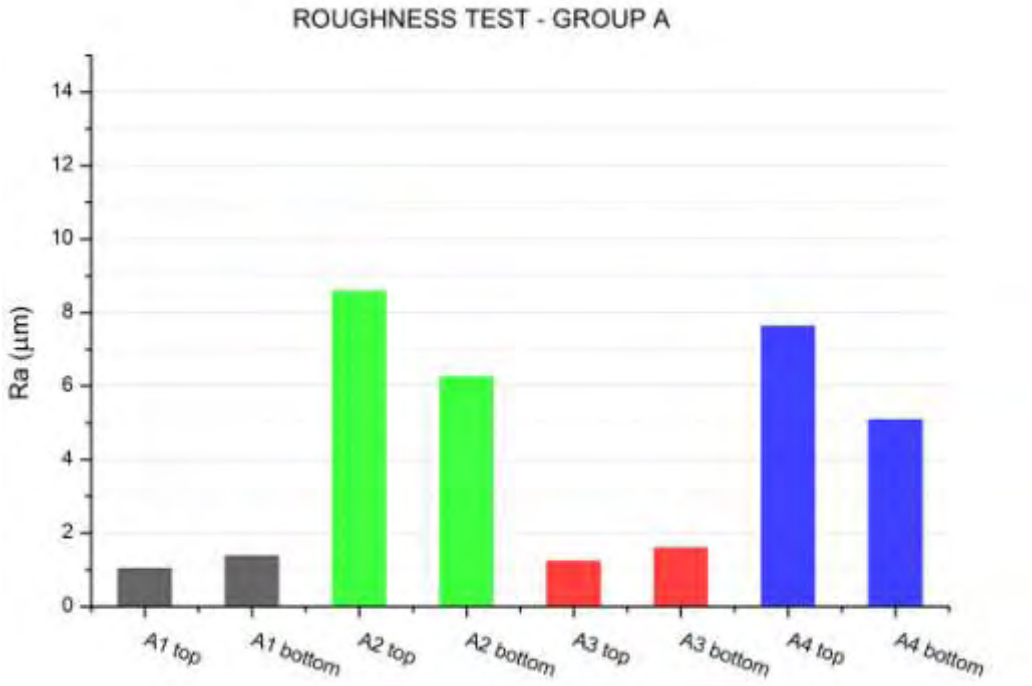

Graph 4.1 – ROUGHNESS OF 5mm SPECIMENS

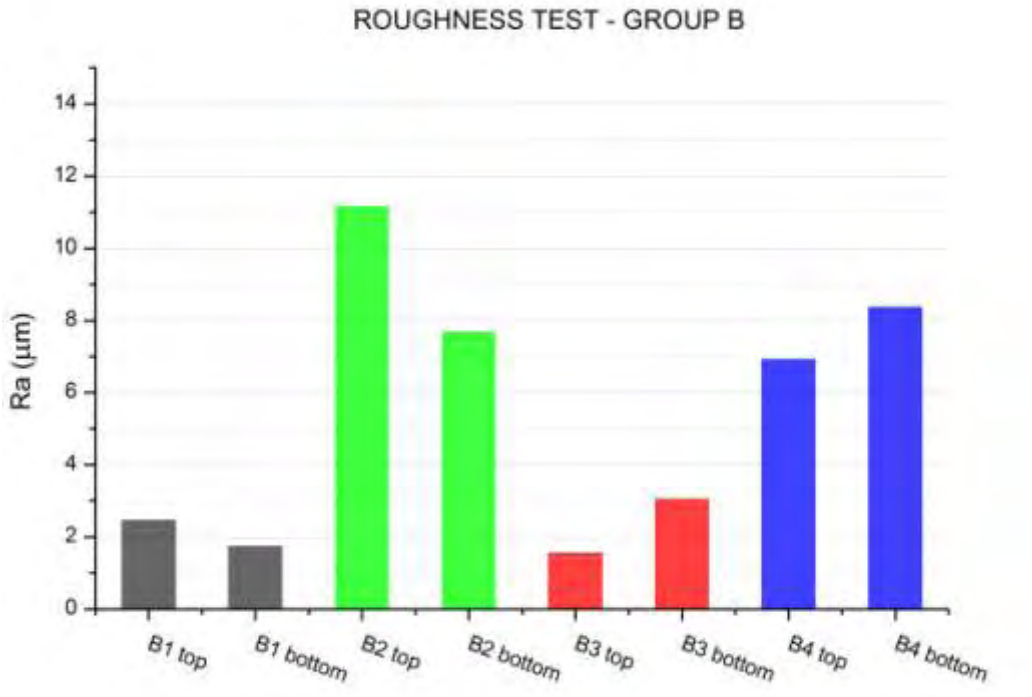

Graph 4.2 – ROUGHNESS OF 10mm SPECIMENS

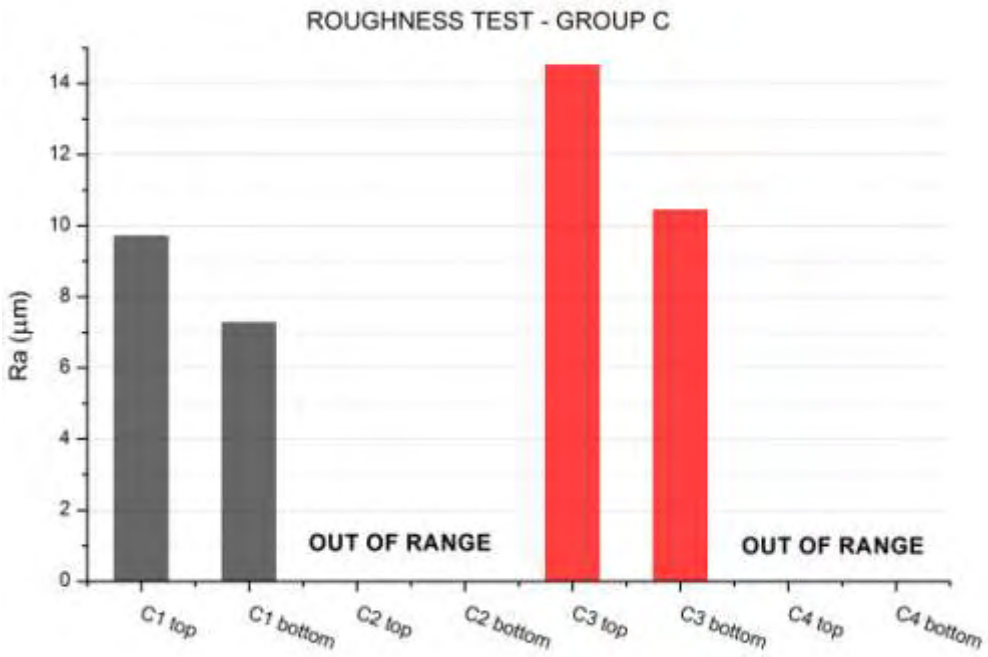

Graph 4.3 – ROUGHNESS OF 20mm SPECIMENS

Graphs 4.4, 4.5, 4.6 and 4.7 show the roughness differences at specimens of different thickness from the same group of cutting parameters.

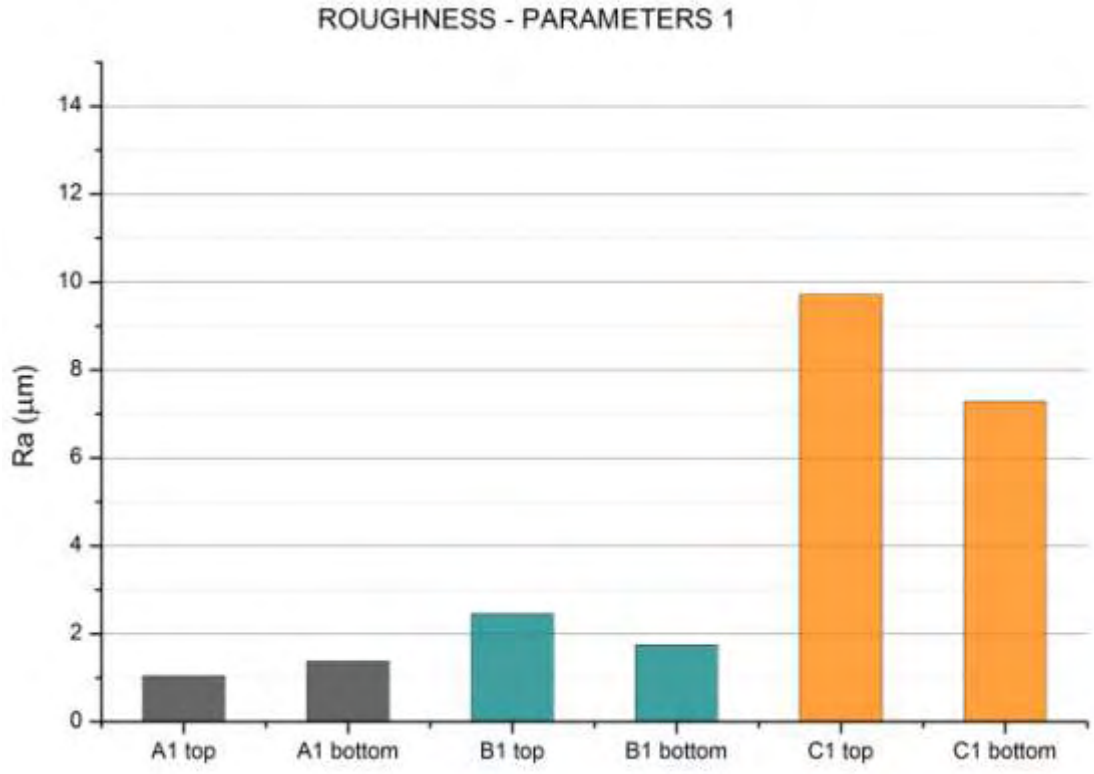

Graph 4.4 – ROUGHNESS OF SPECIMENS CUT WITH PARAMETERS 1

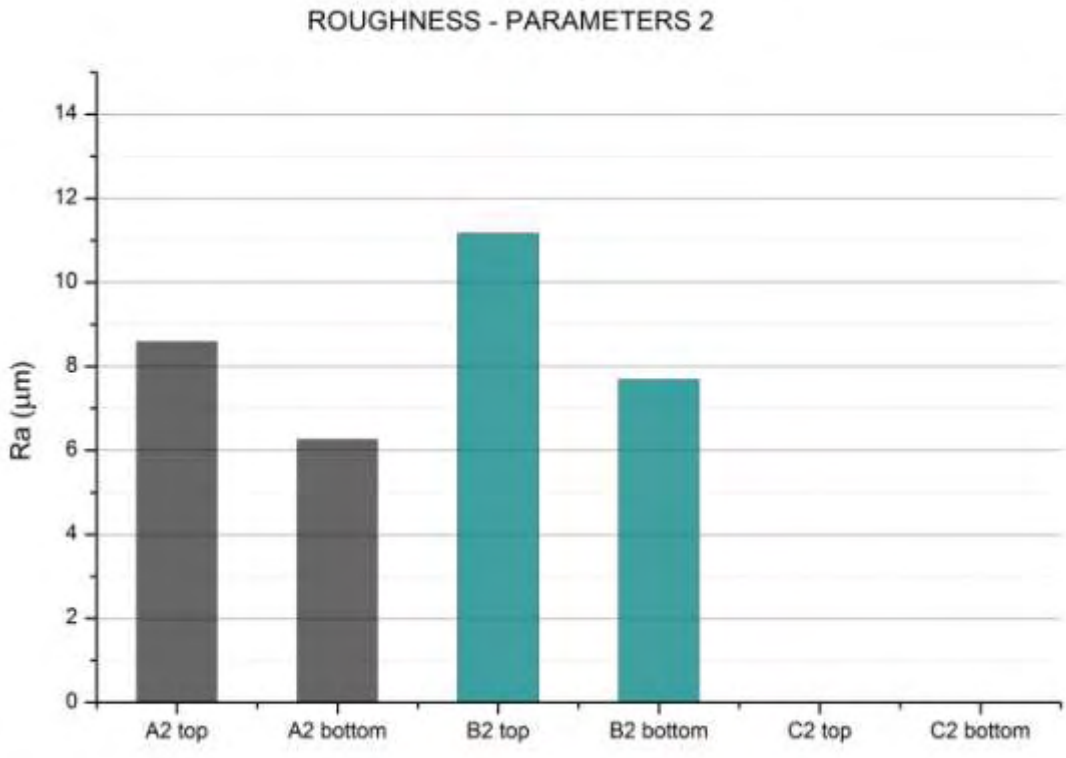

Graph 4.5 – ROUGHNESS OF SPECIMENS CUT WITH PARAMETERS 2

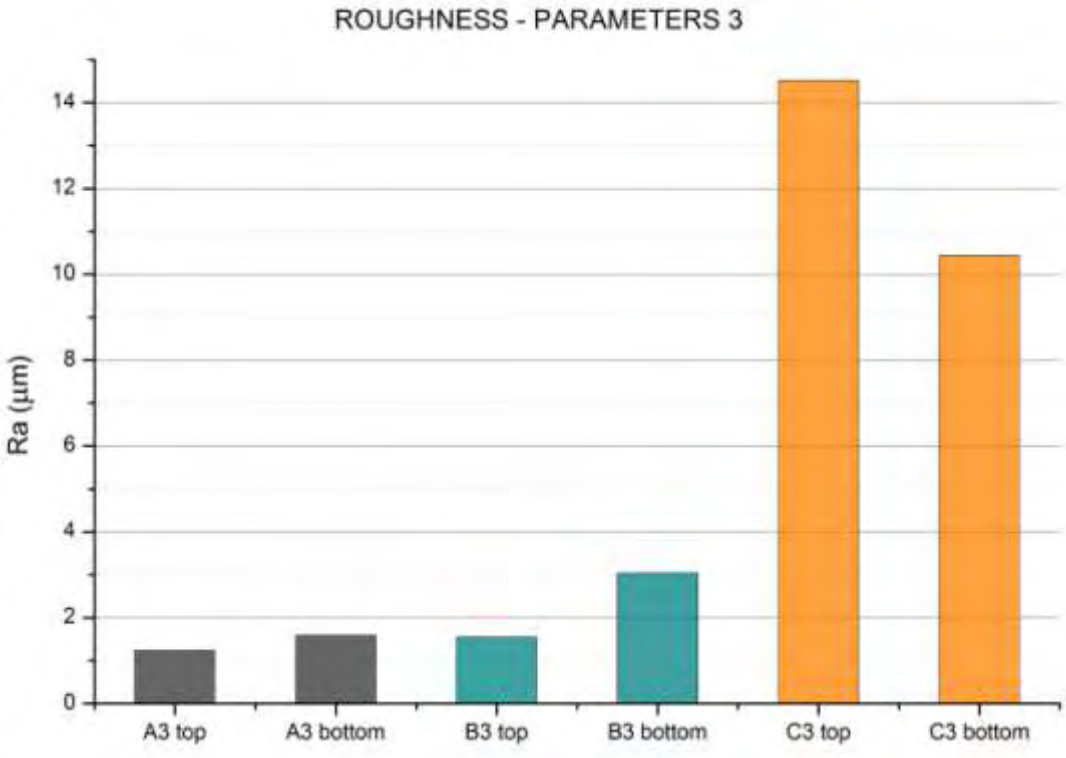

Graph 4.6 – ROUGHNESS OF SPECIMENS CUT WITH PARAMETERS 3

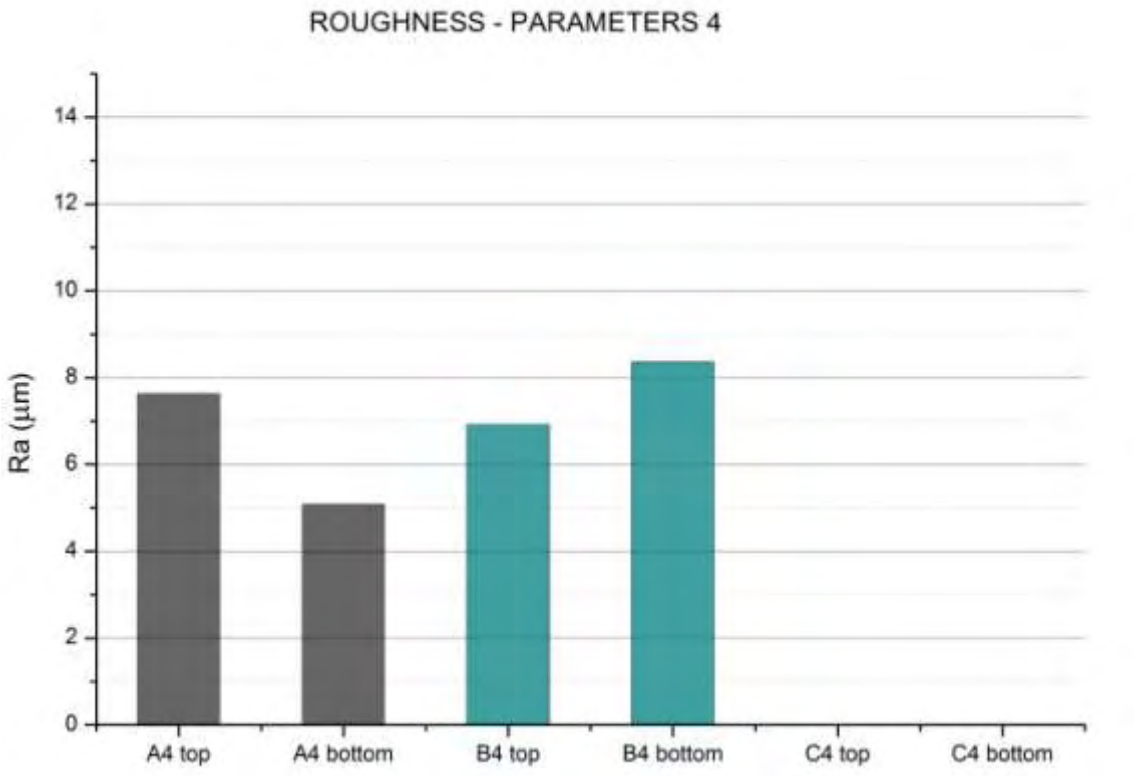

Graph 4.7 – ROUGHNESS OF SPECIMENS CUT WITH PARAMETERS 4

4.2 METALLOGRAPHY

Metallographic analysis was performed on transverse cross sections and was mainly focus on three regions. The first of the base, unaffected, material in the middle of the specimen and the other two at the heat affected zone, near the top and near the bottom, as shown in figure 4.1.

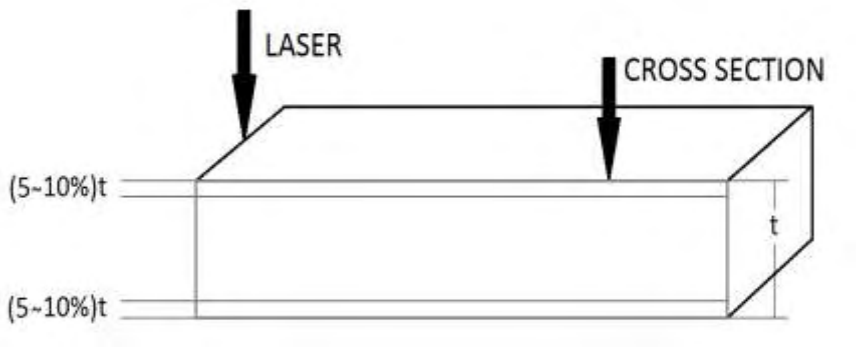

Figure 4.1 - SCHEMATIC REPRESENTATION OF THE METALLOGRAPHIC CROSS SECTION, AND THE POSITION OF THE MICROHARDNESS PROFILES IN RELATION TO PLATE THICKNESS AND THE LASER CUT

4.2.1 GROUP A

Figure 4.1 shows the unaffected material of Group A specimens. The microstructure consists of tempered martensite.

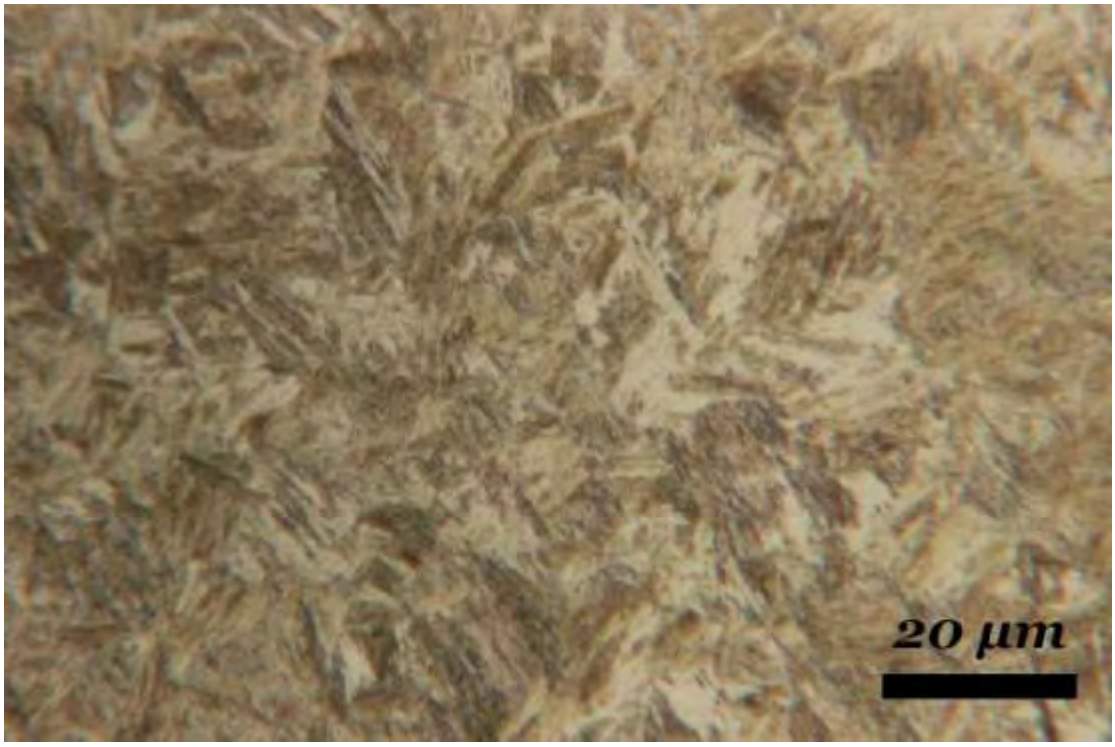

Figure 4.2 (x1000) - A GROUP'S UNAFFECTED MATERIAL, TEMPERED MARTENSITE

SPECIMEN A1

Figures 4.2 and 4.3 show the microstructure of A1 specimen's HAZ near the top and near the bottom respectively. There HAZ appeared narrower at the top of the specimen in comparison to the bottom.

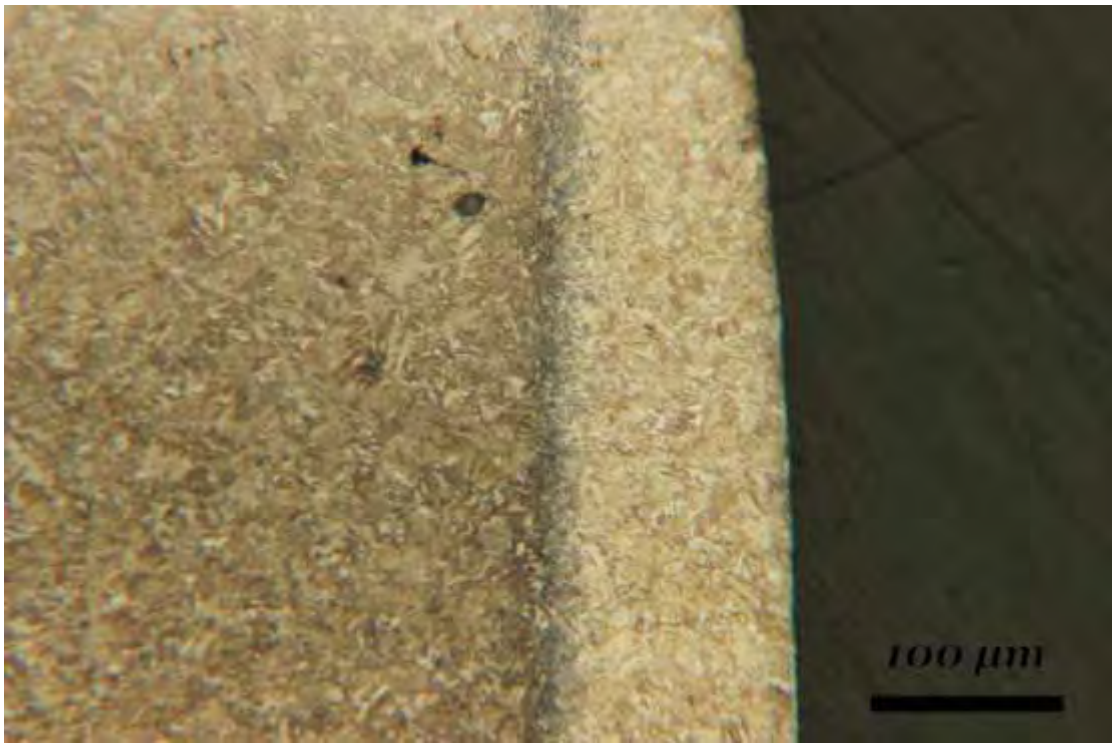

Figure 4.3 (x200) – A1 SPECIMEN'S HAZ, NEAR THE TOP PLATE'S SURFACE

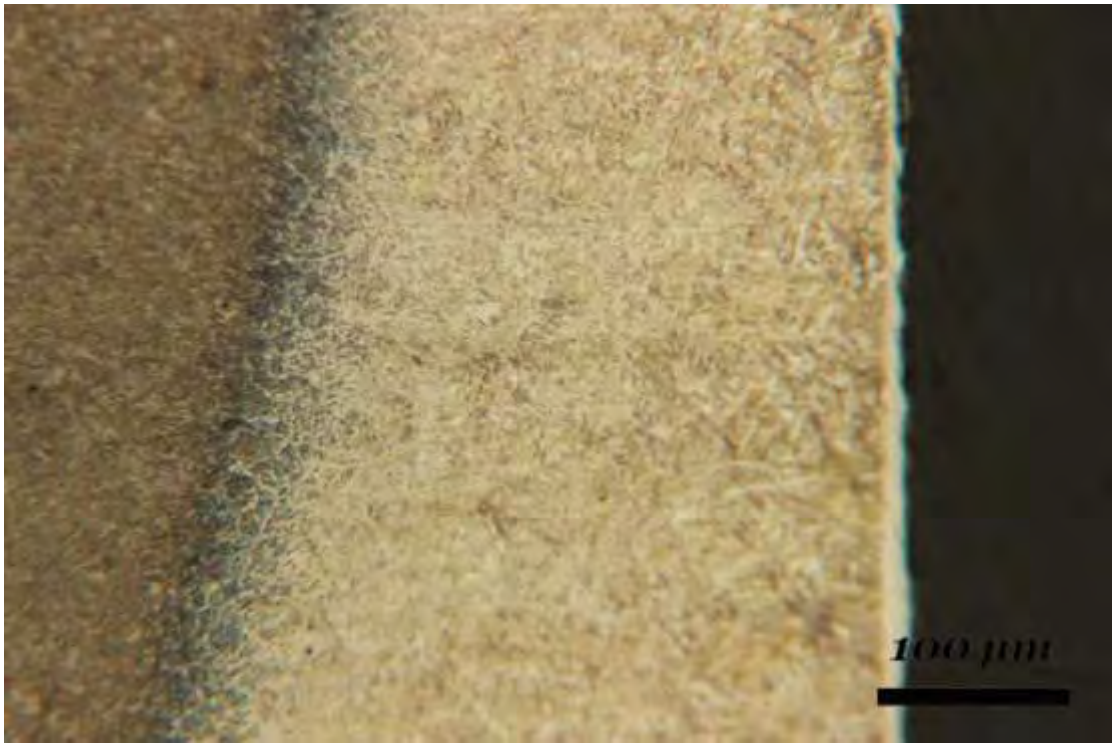

Figure 4.4 (x200) – A1 SPECIMEN'S HAZ, NEAR THE BOTTOM PLATE'S SURFACE

SPECIMEN A2

Figures 4.4 and 4.5 show the microstructure of A2 specimen's HAZ near the top and near the bottom respectively. There HAZ appeared narrower at the top of the specimen in comparison to the bottom.

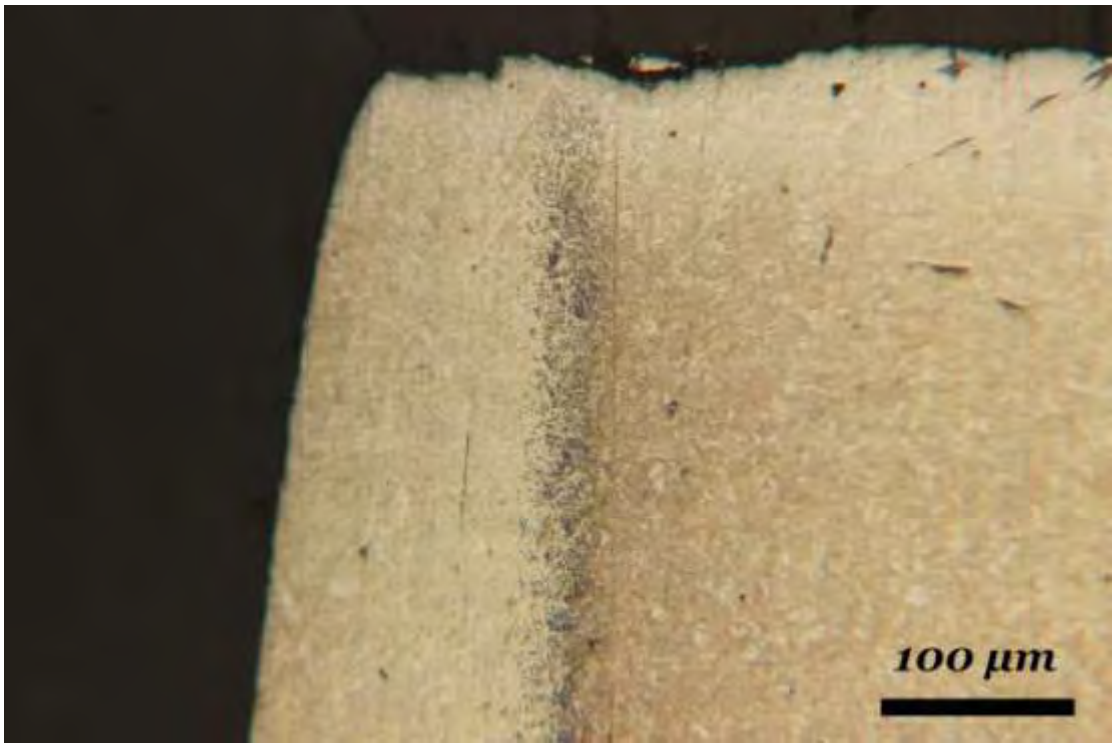

Figure 4.5 (x200) – A2 SPECIMEN'S HAZ, NEAR THE TOP PLATE'S SURFACE

Figure 4.6 (x200) – A2 SPECIMEN'S HAZ, NEAR THE BOTTOM PLATE'S SURFACE

SPECIMEN A3

Figures 4.2 and 4.3 show the microstructure of A3 specimen's HAZ near the top and near the bottom respectively. There HAZ appeared narrower at the top of the specimen in comparison to the bottom.

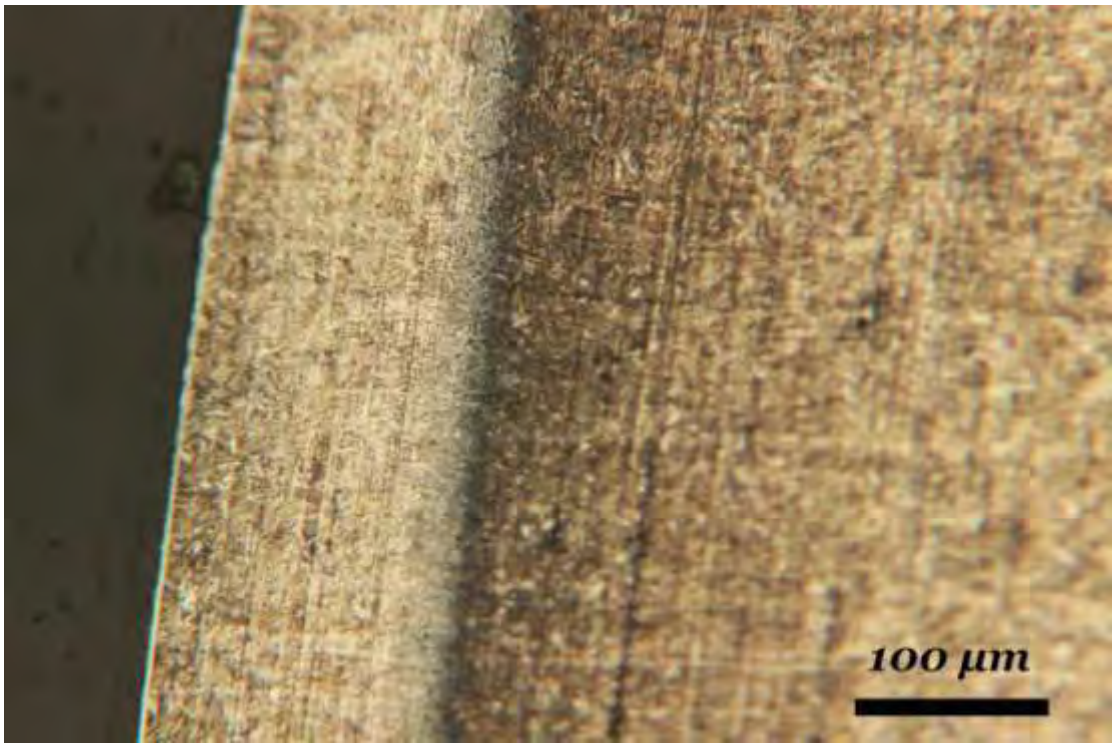

Figure 4.7 (x200) – A3 SPECIMEN'S HAZ, NEAR THE TOP PLATE'S SURFACE

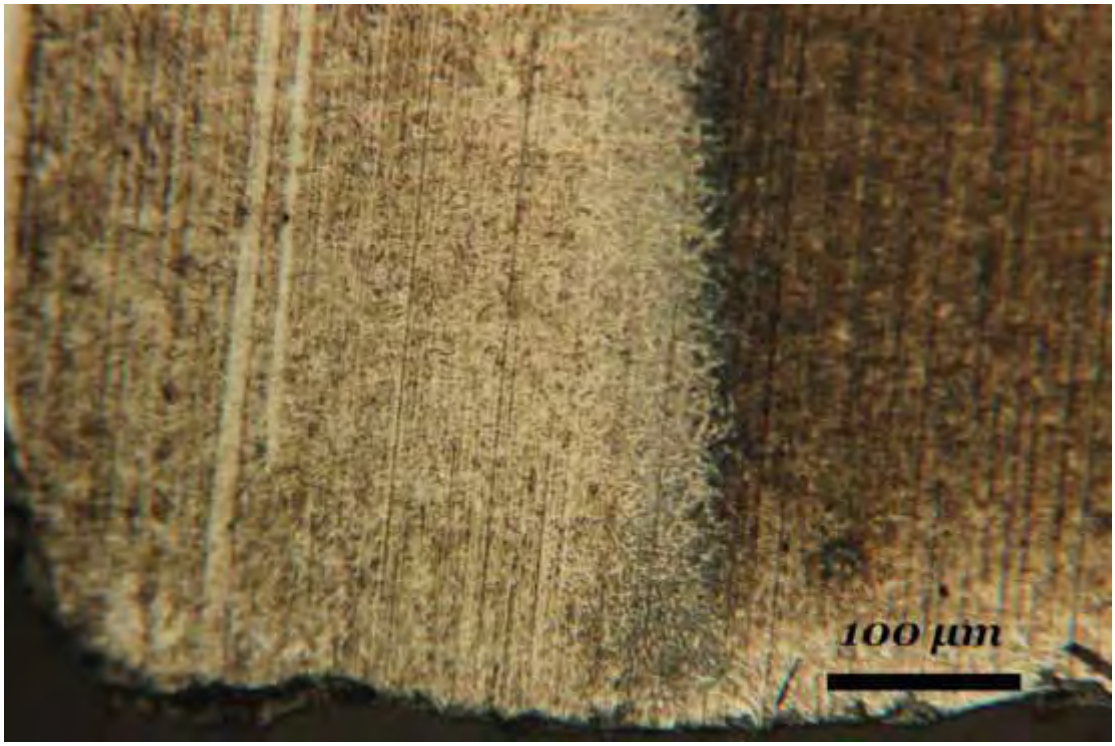

Figure 4.8 (x200) – A3 SPECIMEN'S HAZ, NEAR THE BOTTOM PLATE'S SURFACE

SPECIMEN A4

Figures 4.8 and 4.9 show the microstructure of A4 specimen's HAZ near the top and near the bottom respectively. There HAZ appeared narrower at the top of the specimen in comparison to the bottom.

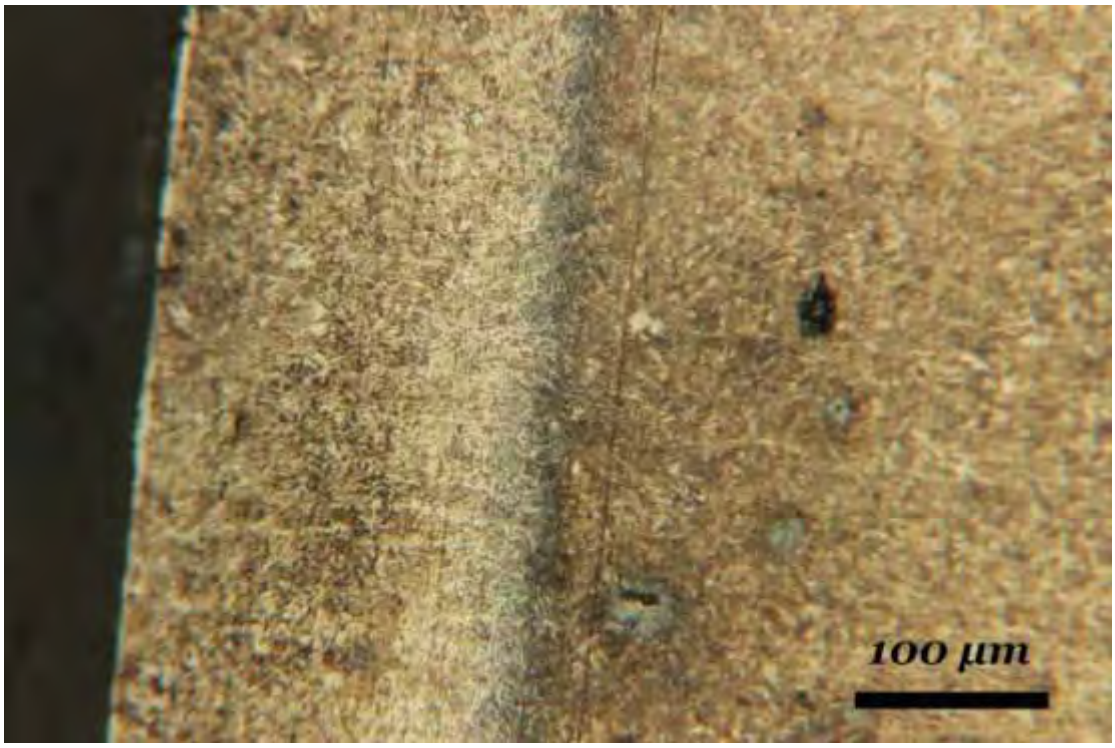

Figure 4.9 (x200) – A4 SPECIMEN'S HAZ, NEAR THE TOP PLATE'S SURFACE

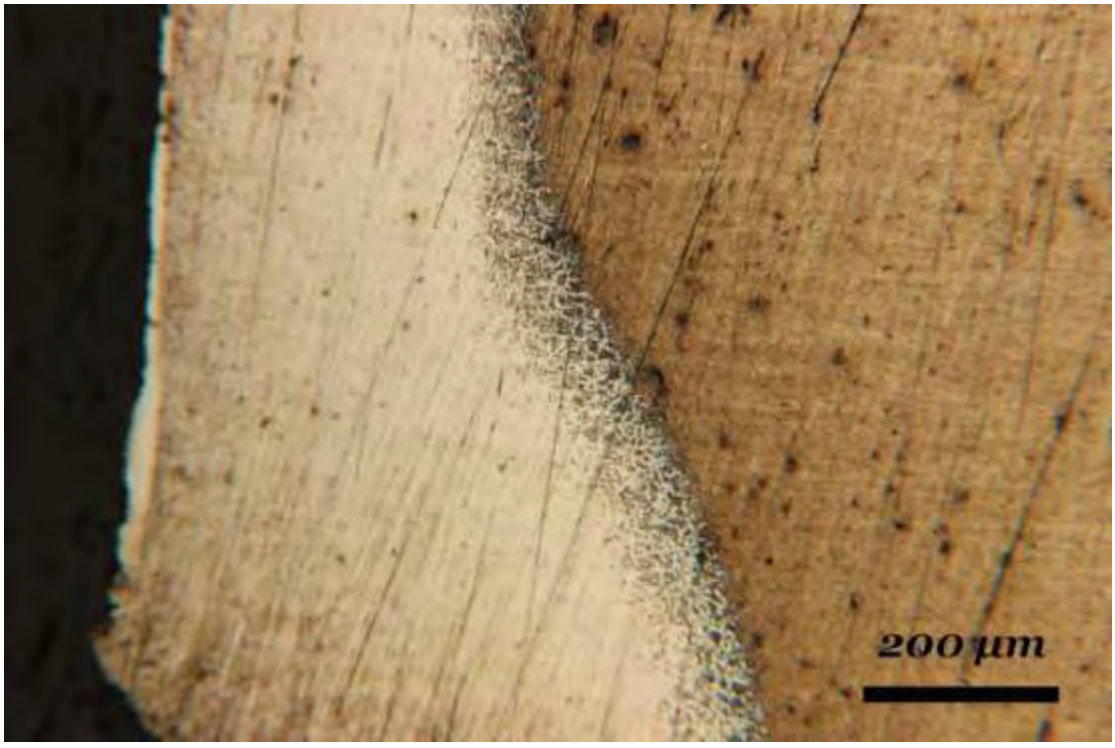

Figure 4.10 (x100) - A2 SPECIMEN'S HAZ, NEAR THE BOTTOM PLATE'S SURFACE

4.2.2 GROUP B

Figure 4.10 shows the unaffected material of Group B specimens. The microstructure consists of tempered martensite.

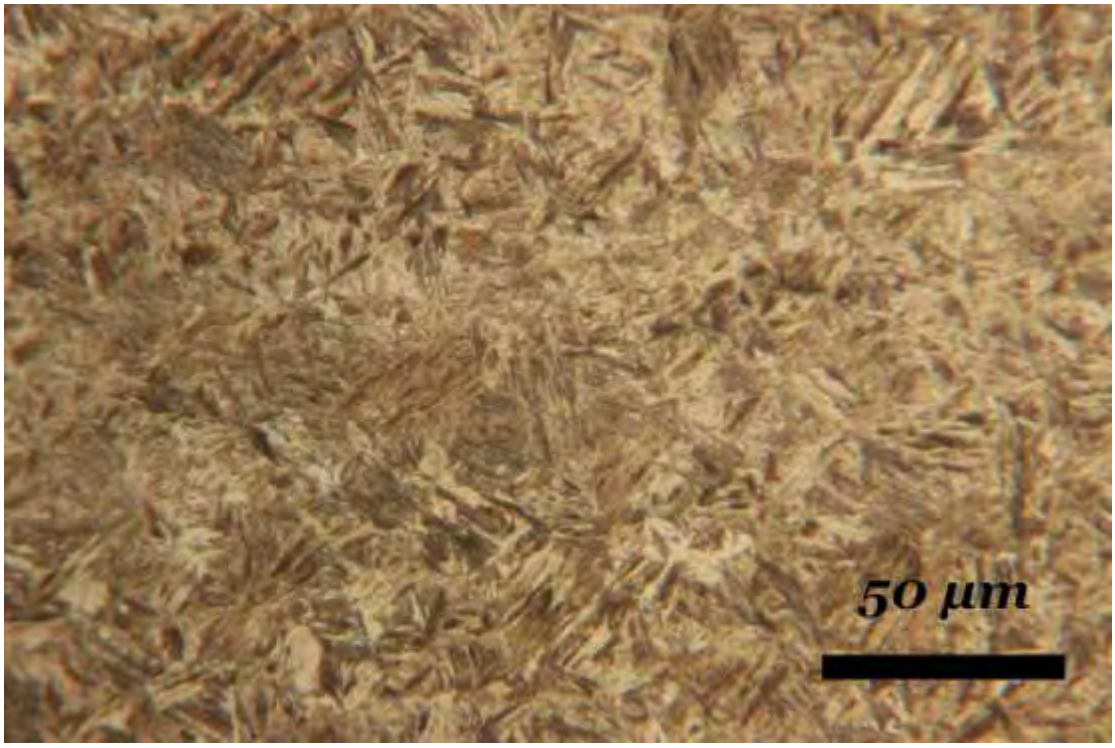

Figure 4.11 (x500) – B GROUP'S UNAFFECTED MATERIAL

SPECIMEN B1

Figures 4.11 and 4.12 show the microstructure of B1 specimen's HAZ near the top and near the bottom respectively. There HAZ appeared narrower at the top of the specimen in comparison to the bottom.

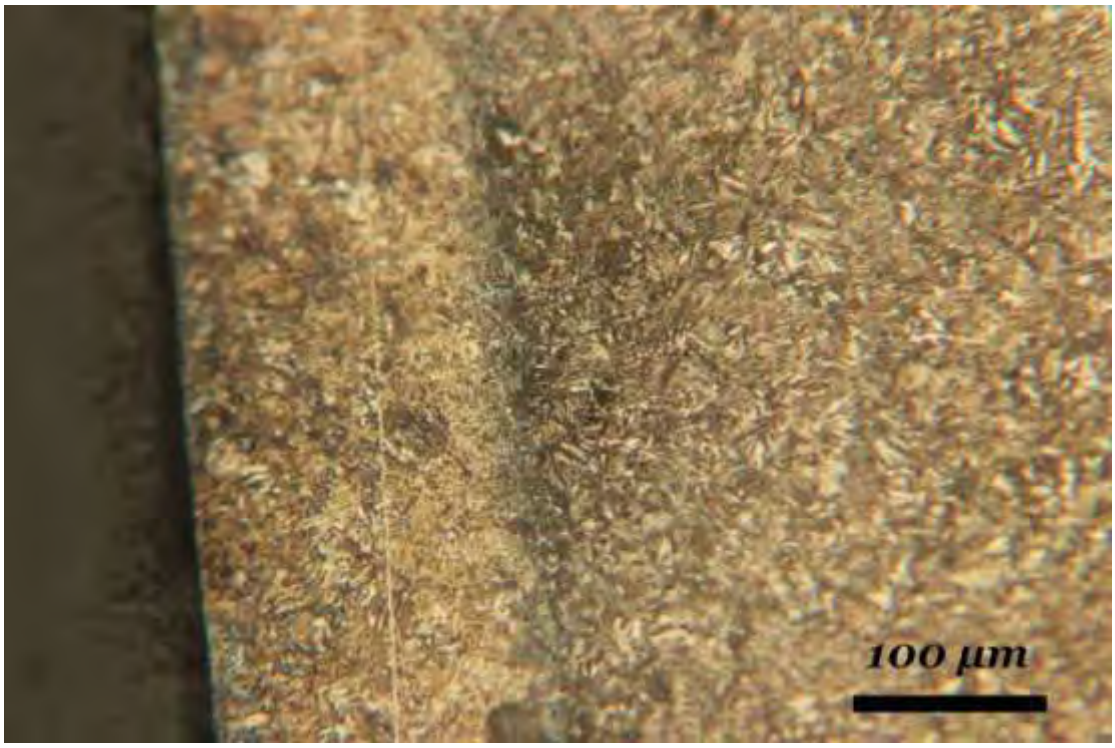

Figure 4.12 (x200) – B1 SPECIMEN'S HAZ, NEAR THE TOP PLATE'S SURFACE

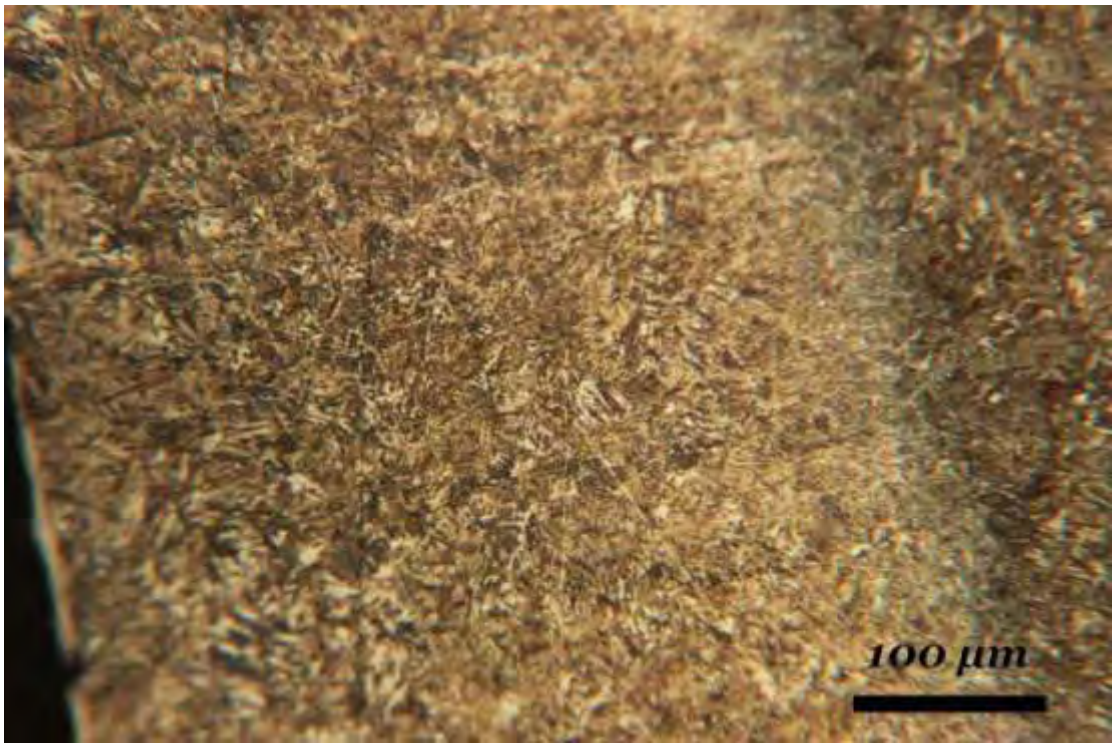

Figure 4.13 (x200) – B1 SPECIMEN'S HAZ, NEAR THE BOTTOM PLATE'S SURFACE

SPECIMEN B2

Figures 4.13 and 4.14 show the microstructure of B2 specimen's HAZ near the top and near the bottom respectively. There HAZ appeared narrower at the top of the specimen in comparison to the bottom.

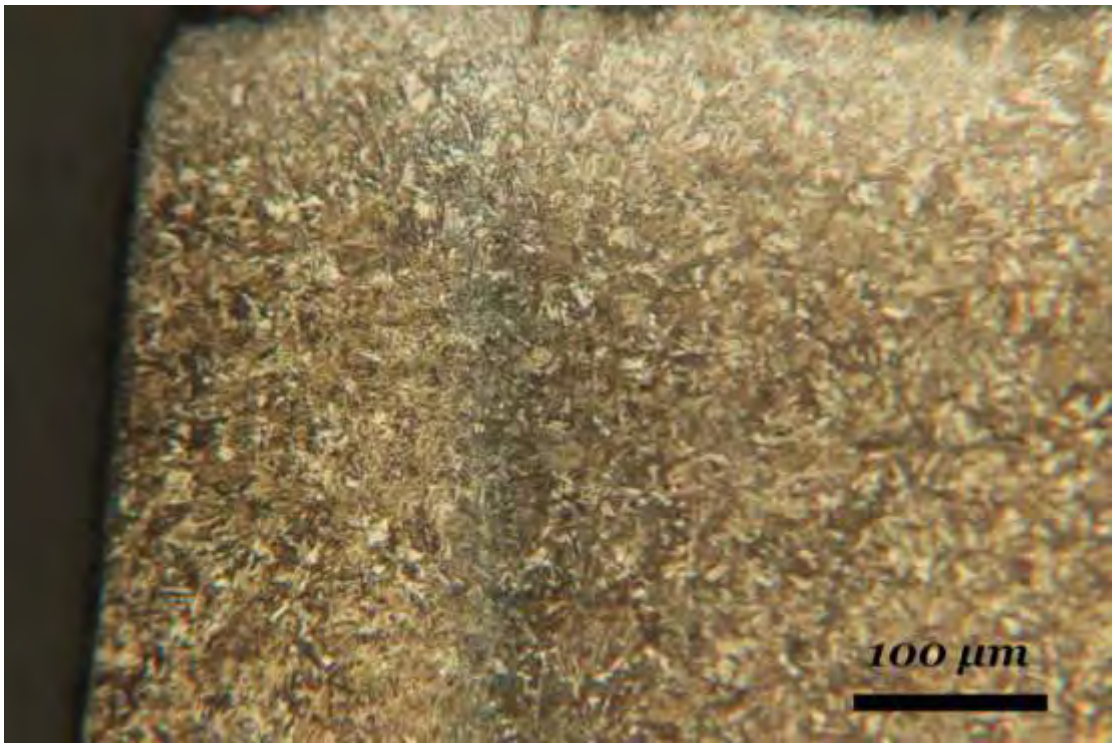

Figure 4.14 (x200) – B2 SPECIMEN'S HAZ, NEAR THE TOP PLATE'S SURFACE

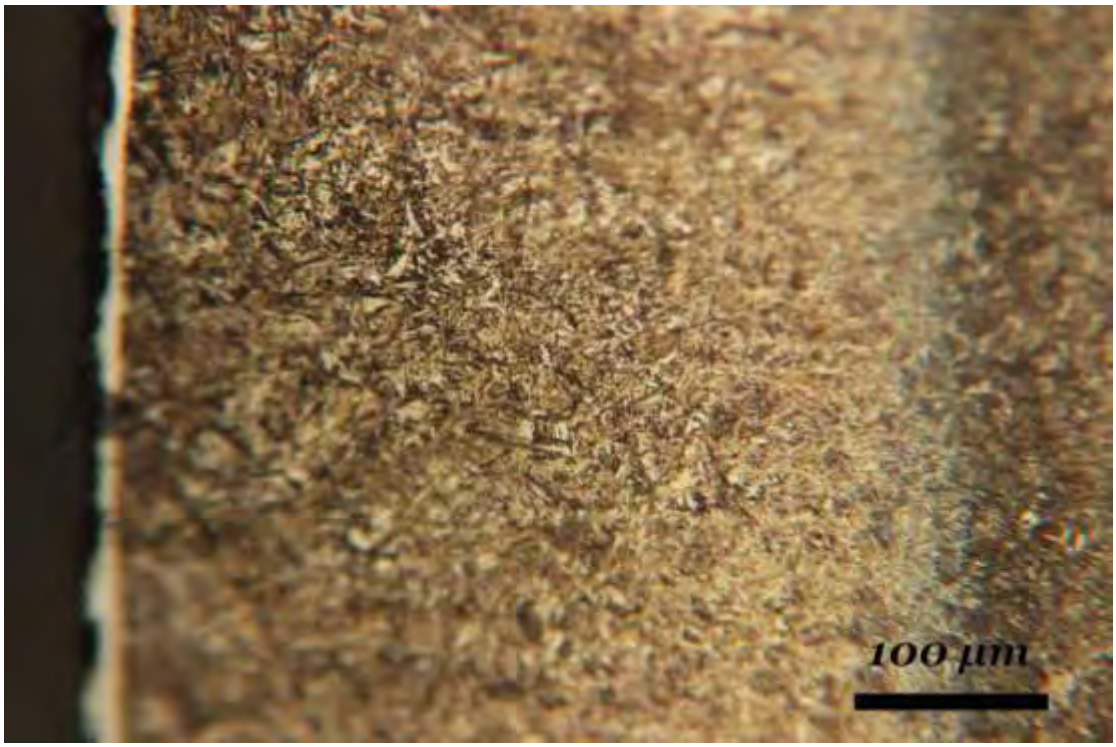

Figure 4.15 (x200) – B2 SPECIMEN'S HAZ, NEAR THE BOTTOM PLATE'S SURFACE

SPECIMEN B3

Figures 4.15 and 4.16 show the microstructure of B3 specimen's HAZ near the top and near the bottom respectively. There HAZ appeared narrower at the top of the specimen in comparison to the bottom.

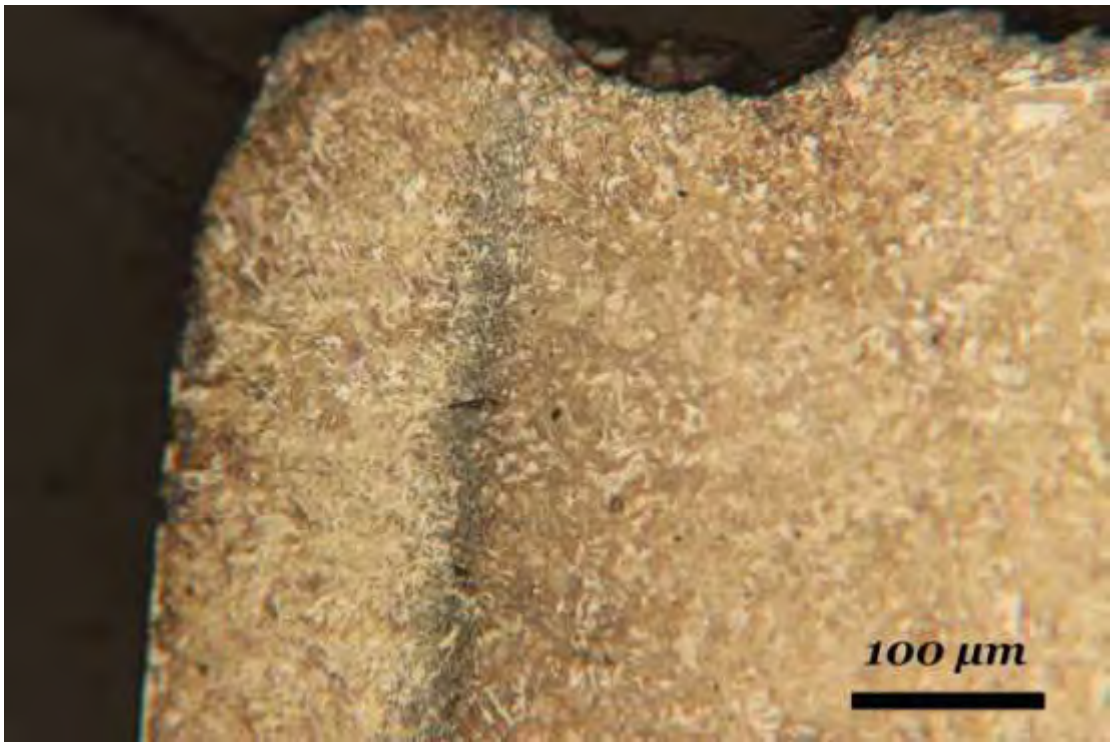

Figure 4.16 (x200) – B3 SPECIMEN'S HAZ, NEAR THE TOP PLATE'S SURFACE

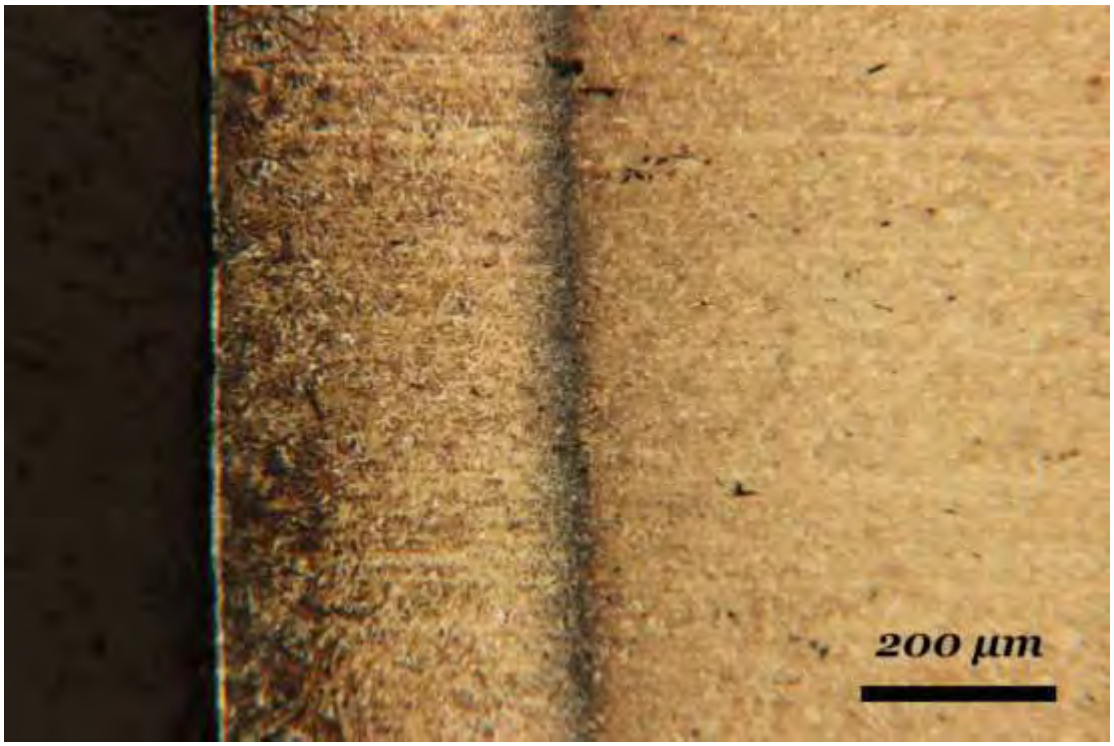

Figure 4.17 (x100) – B1 SPECIMEN'S HAZ, NEAR THE BOTTOM PLATE'S SURFACE

SPECIMEN B4

Figures 4.17 and 4.18 show the microstructure of B4 specimen's HAZ near the top and near the bottom respectively. There HAZ appeared narrower at the top of the specimen in comparison to the bottom.

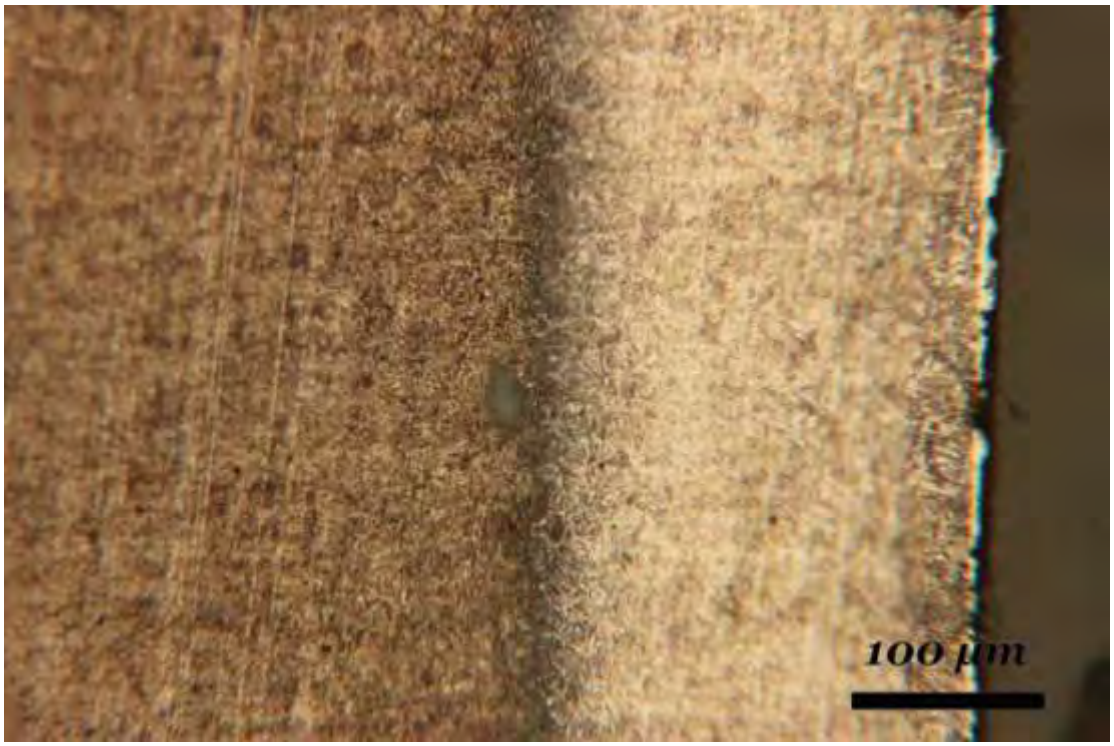

Figure 4.18 (x200) – B4 SPECIMEN'S HAZ, NEAR THE TOP PLATE'S SURFACE

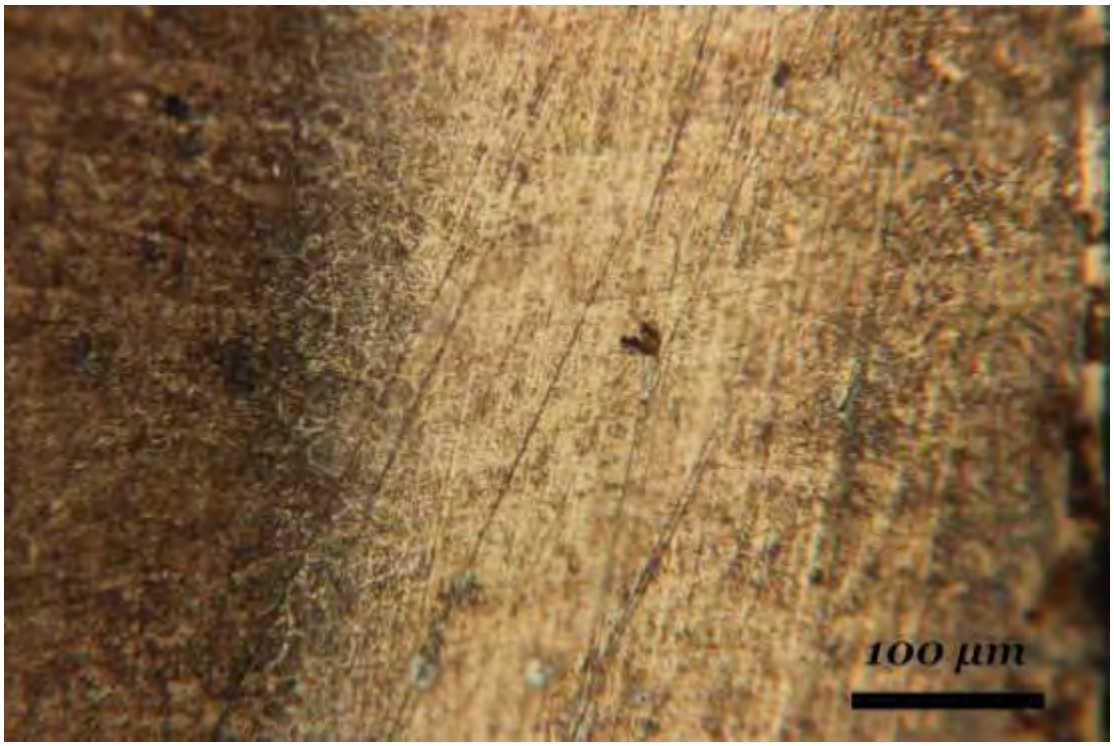

Figure 4.19 (x200) – B4 SPECIMEN'S HAZ, NEAR THE BOTTOM PLATE'S SURFACE

4.2.3 GROUP C

Figure 4.19 shows the unaffected material of Group C specimens. The microstructure consists of tempered martensite.

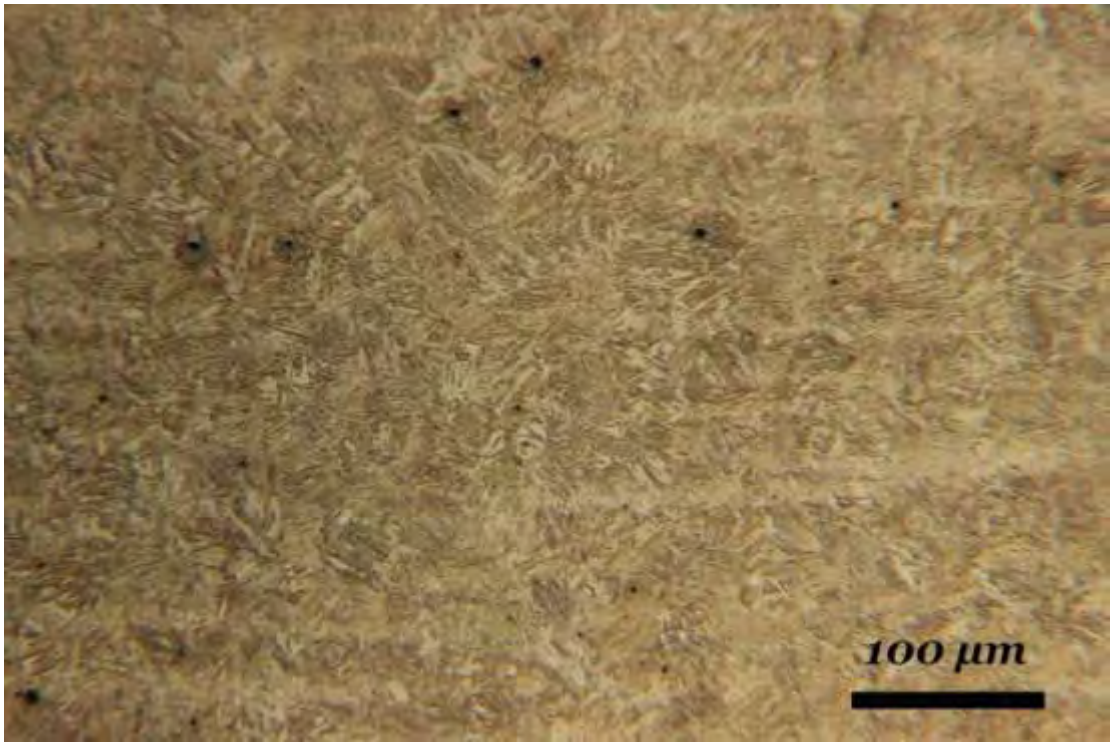

Figure 4.20 (x200) - C GROUP'S UNAFFECTED MATERIAL,

SPECIMEN C1

Figures 4.20 and 4.21 show the microstructure of C1 specimen's HAZ near the top and near the bottom respectively. There HAZ appeared narrower at the top of the specimen in comparison to the bottom.

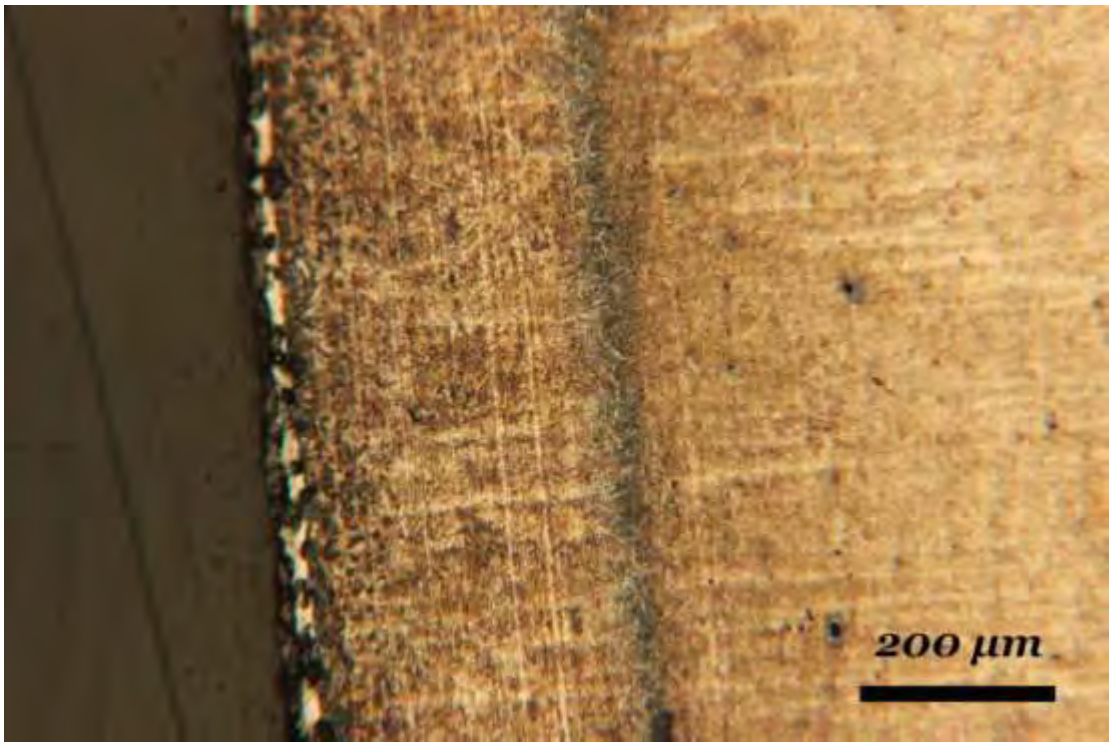

Figure 4.21 (x100) – C1 SPECIMEN'S HAZ, NEAR THE TOP PLATE'S SURFACE

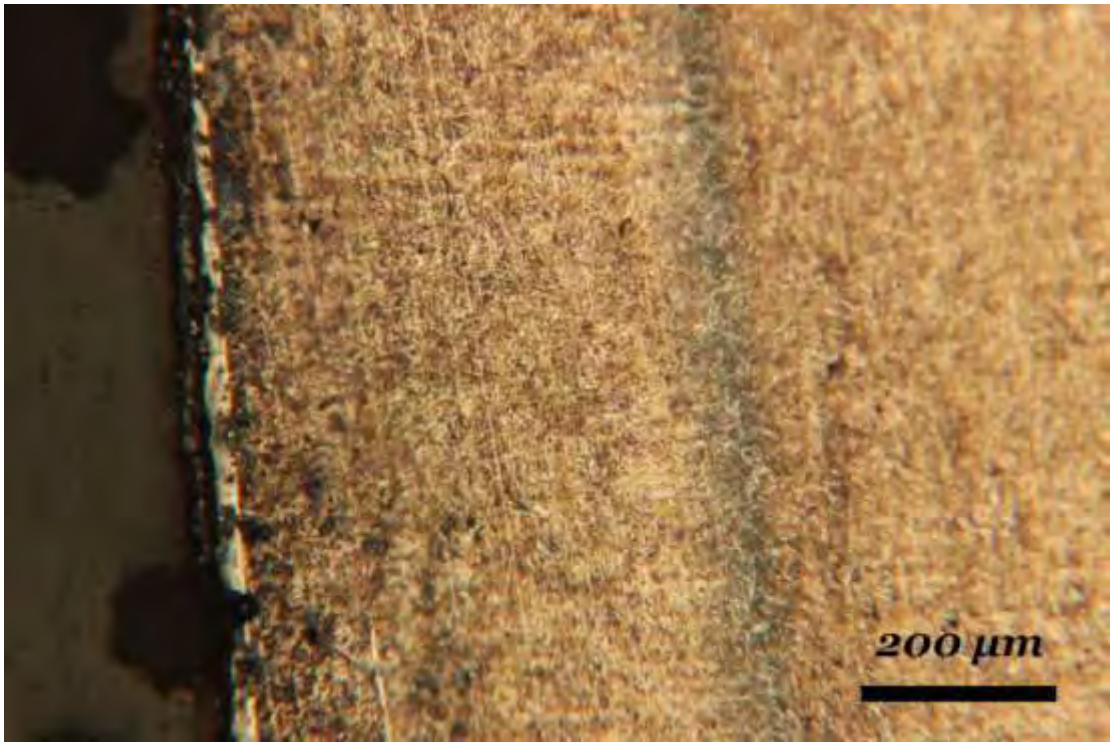

Figure 4.22 (x100) - C1 SPECIMEN'S HAZ, NEAR THE BOTTOM PLATE'S SURFACE

SPECIMEN C2

Figures 4.22 and 4.23 show the microstructure of C2 specimen's HAZ near the top and near the bottom respectively. There HAZ appeared narrower at the top of the specimen in comparison to the bottom.

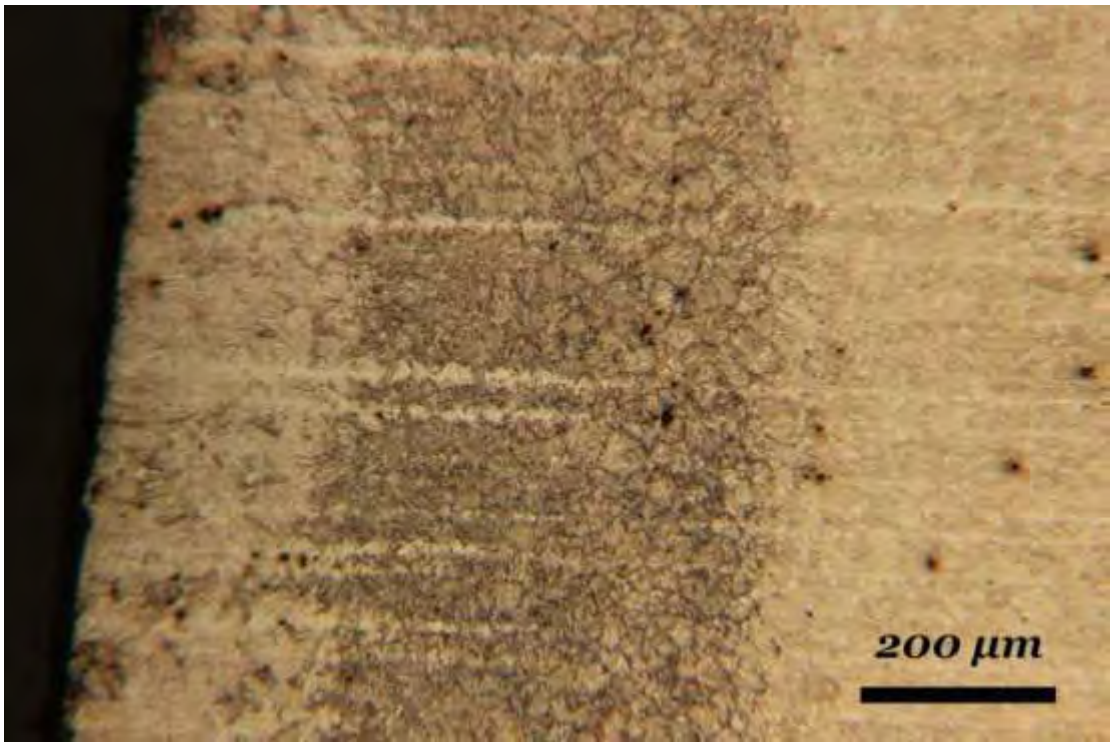

Figure 4.23 (x100) – C2 SPECIMEN'S HAZ, NEAR THE TOP PLATE'S SURFACE

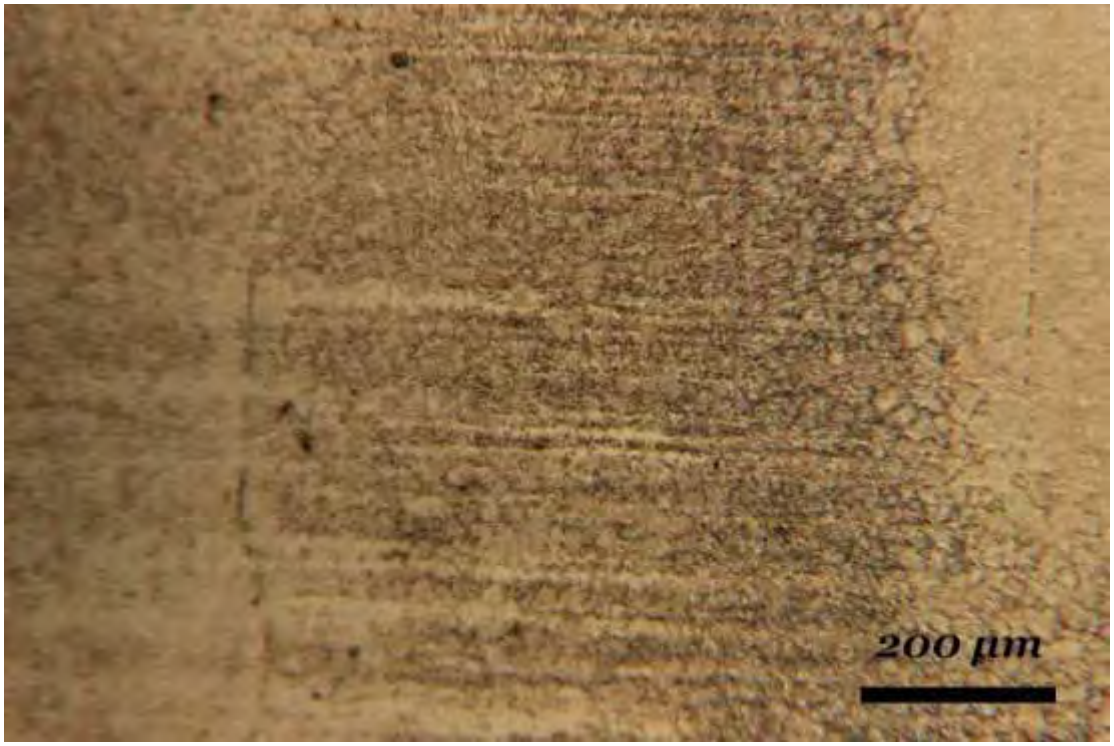

Figure 4.24 (x100) - C2 SPECIMEN'S HAZ, NEAR THE BOTTOM PLATE'S SURFACE

SPECIMEN C3

Figures 4.24 and 4.25 show the microstructure of C3 specimen's HAZ near the top and near the bottom respectively. There HAZ appeared narrower at the top of the specimen in comparison to the bottom.

Figure 4.25 (x100) – C3 SPECIMEN'S HAZ, NEAR THE TOP PLATE'S SURFACE

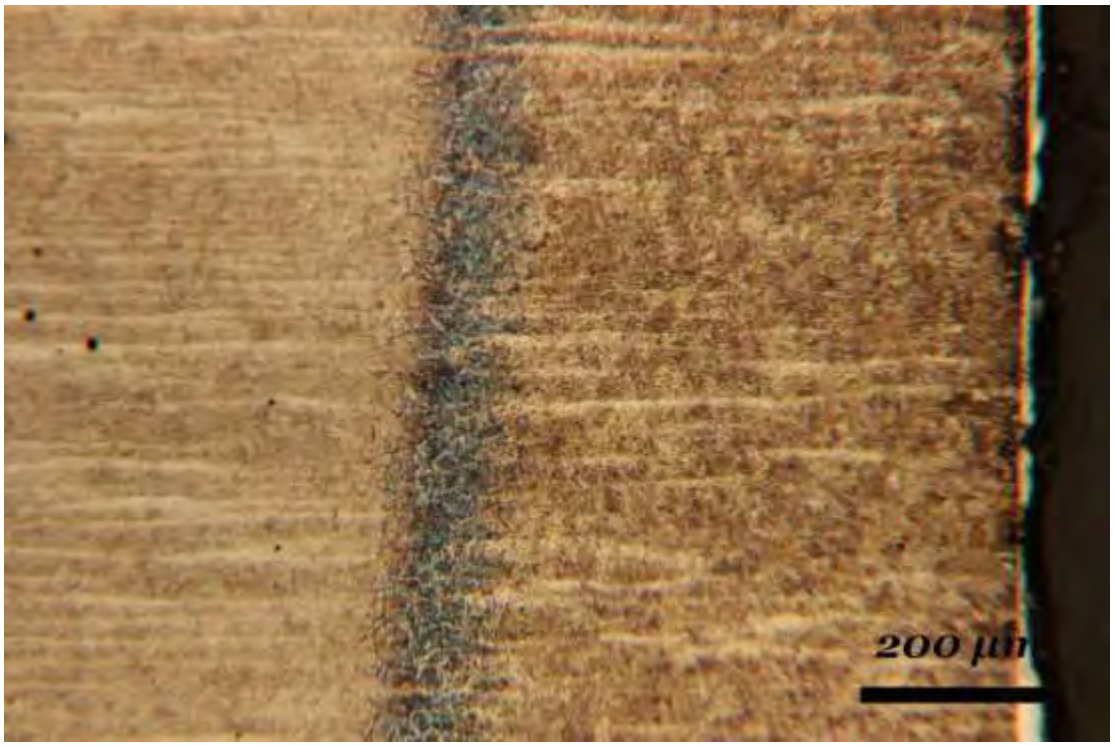

Figure 4.26 (x100) – C3 SPECIMEN'S HAZ, NEAR THE BOTTOM PLATE'S SURFACE

SPECIMEN C4

Figures 4.26 and 4.27 show the microstructure of C4 specimen's HAZ near the top and near the bottom respectively. There HAZ appeared narrower at the top of the specimen in comparison to the bottom.

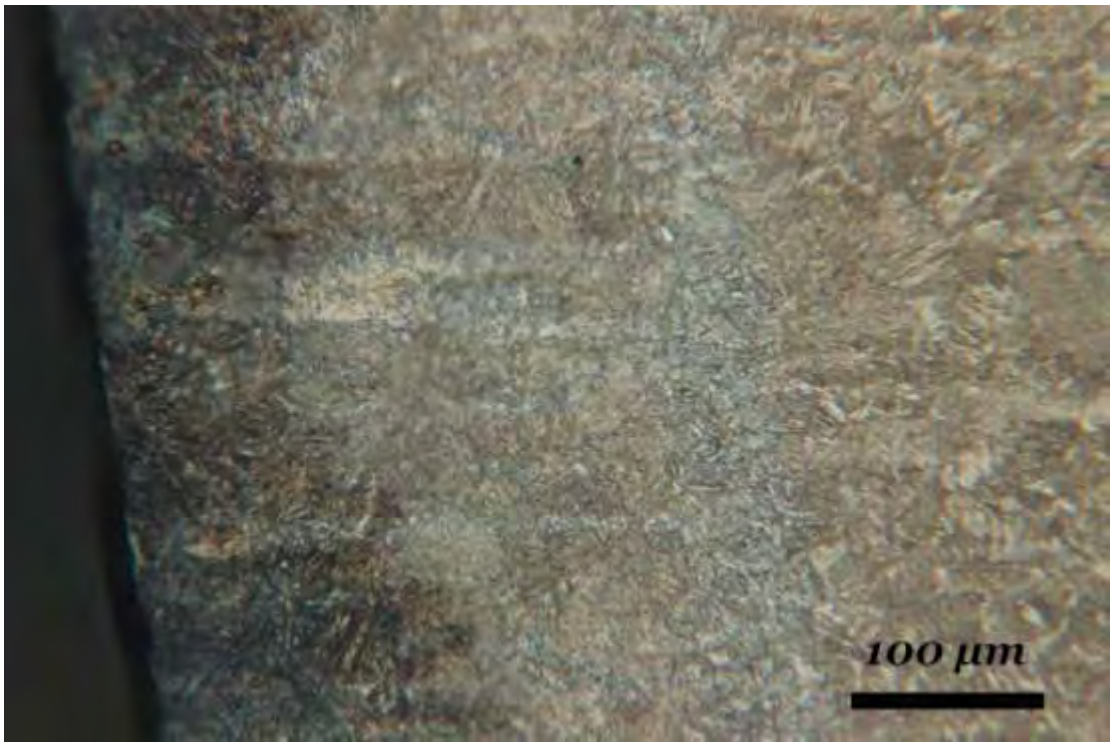

Figure 4.27 (x200) – C4 SPECIMEN'S HAZ, NEAR THE TOP PLATE'S SURFACE

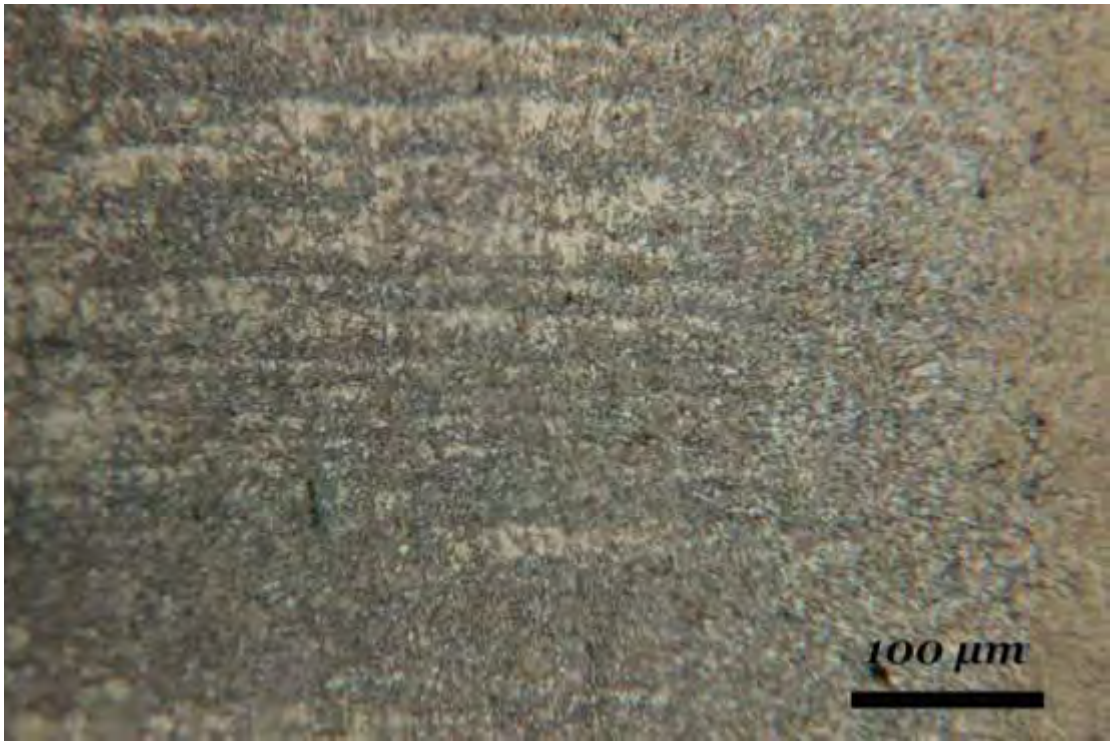

Figure 4.28 (x200) – C4 SPECIMEN'S HAZ, NEAR THE BOTTOM PLATE'S SURFACE

4.2.4 METALLOGRAPHY IN HIGHER MAGNIFICATIONS

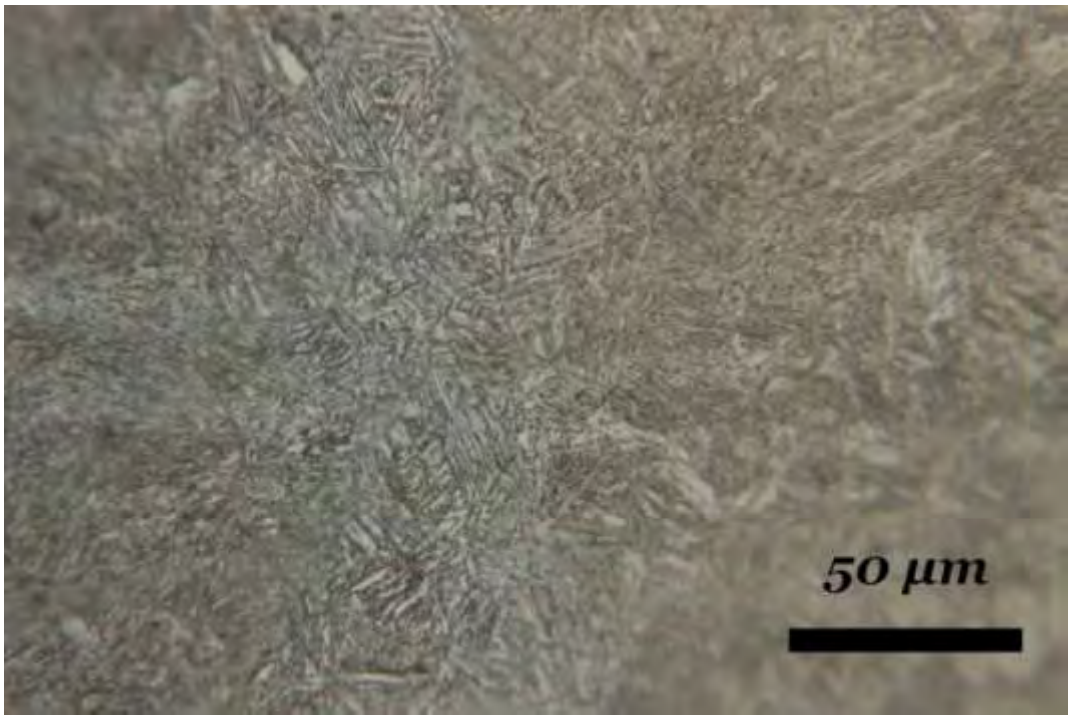

Figure 4.29 (x500) - HAZ OF C4 SPECIMEN, BAINITIC MICROSTRUCTURE

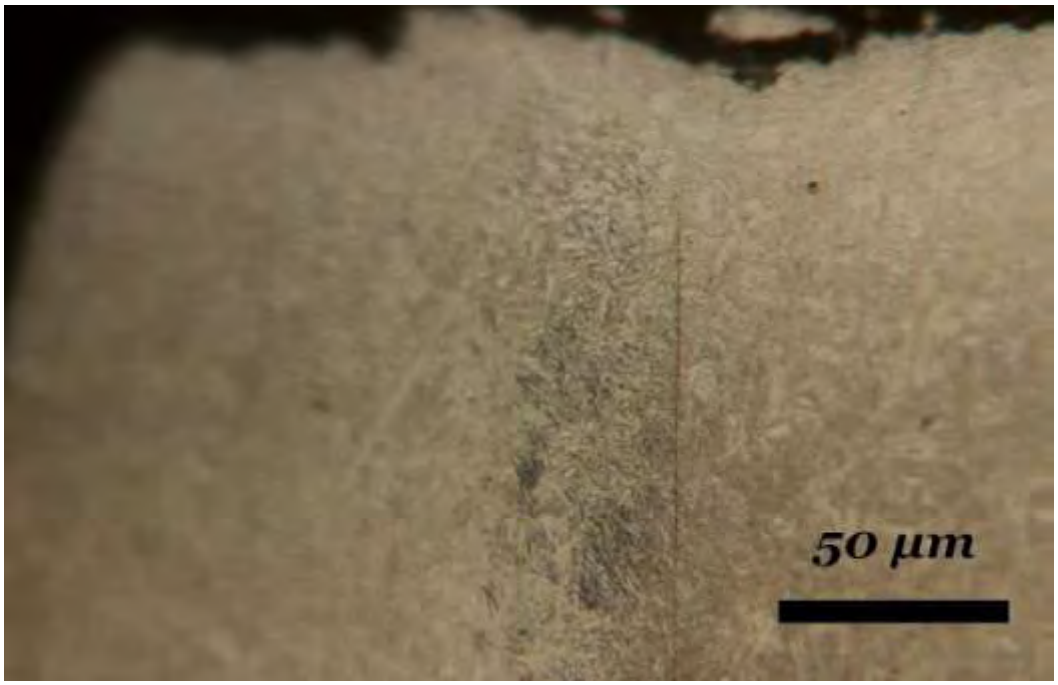

Figure 4.30 (x500) – HAZ OF SPECIMEN A2 NEAR THE TOP SURFACE

Figures 4.29 and 4.30 show the bainitic microstructure at the HAZ of specimens C4 and A2 respectively.

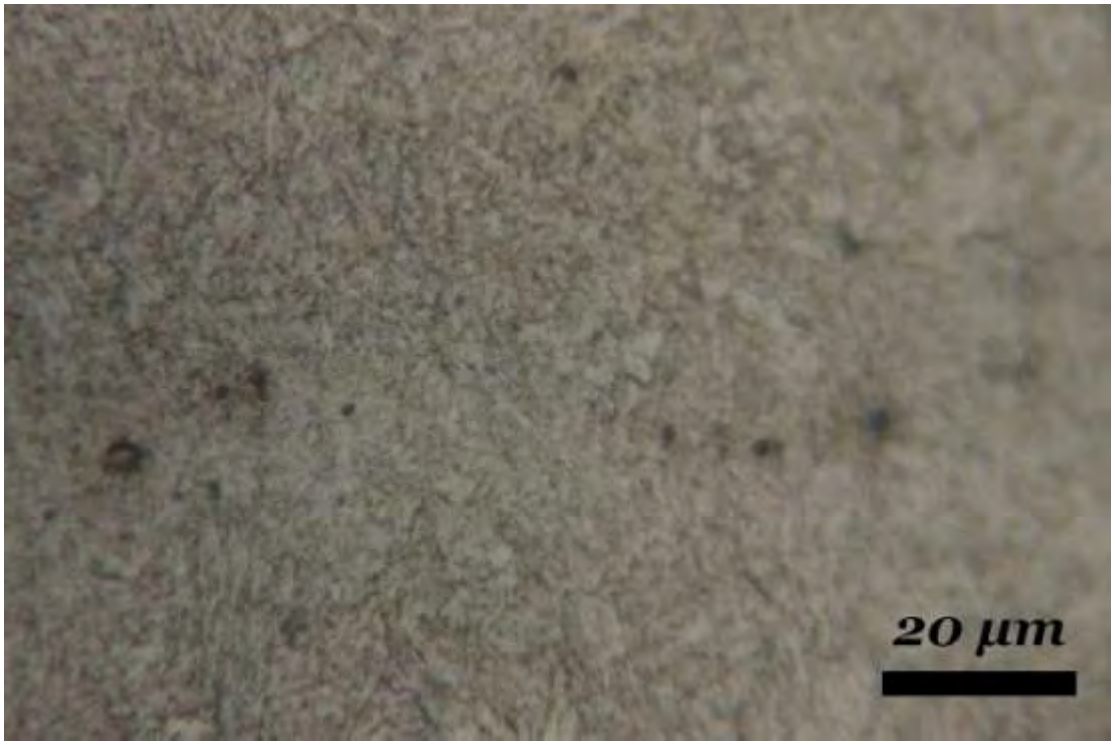

Figure 4.31 (x1000) – BULK MATERIAL NEAR HAZ OF C4 SPECIMEN, FINE GRAINED MARTENSITE

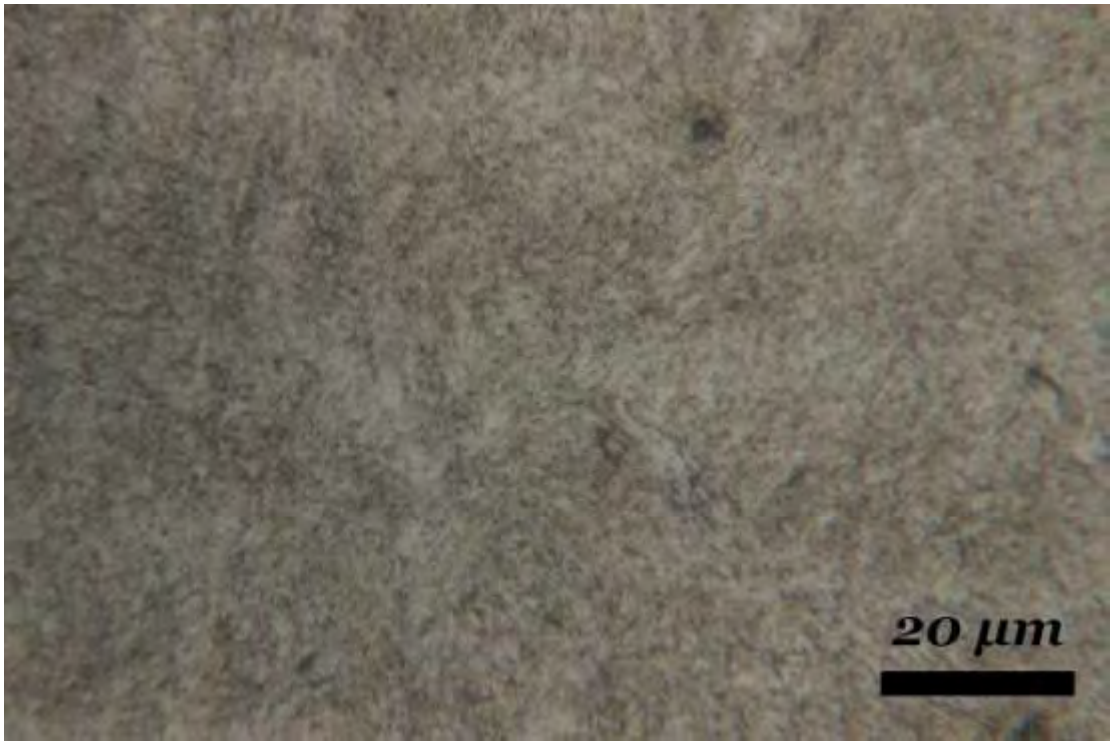

Figure 4.32 (x1000) – CENTER OF C4 SPECIMEN – FINE GRAINED MARTENSITE

Figures 4.31 and 4.32, show the difference in grain size of the martensite at the regions near the HAZ and the center of the specimen C4.

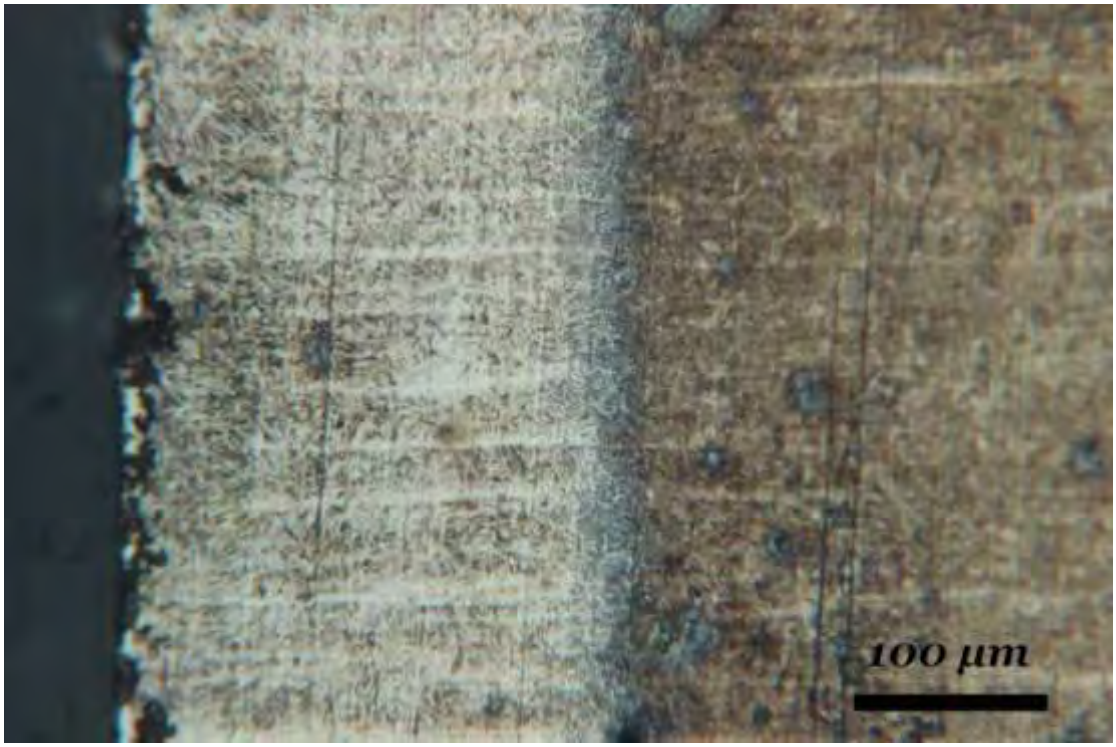

Figure 4.33- A2 HAZ 200x

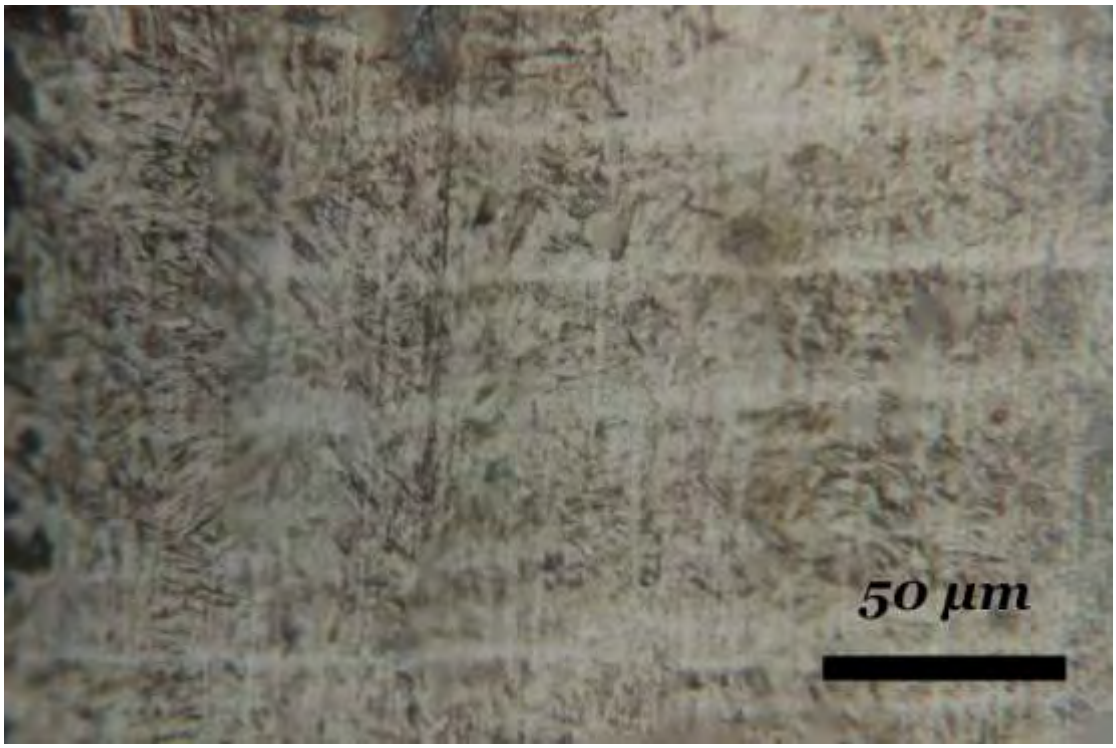

Figure 4.34 – A2 CUT TO BAINITE 500X

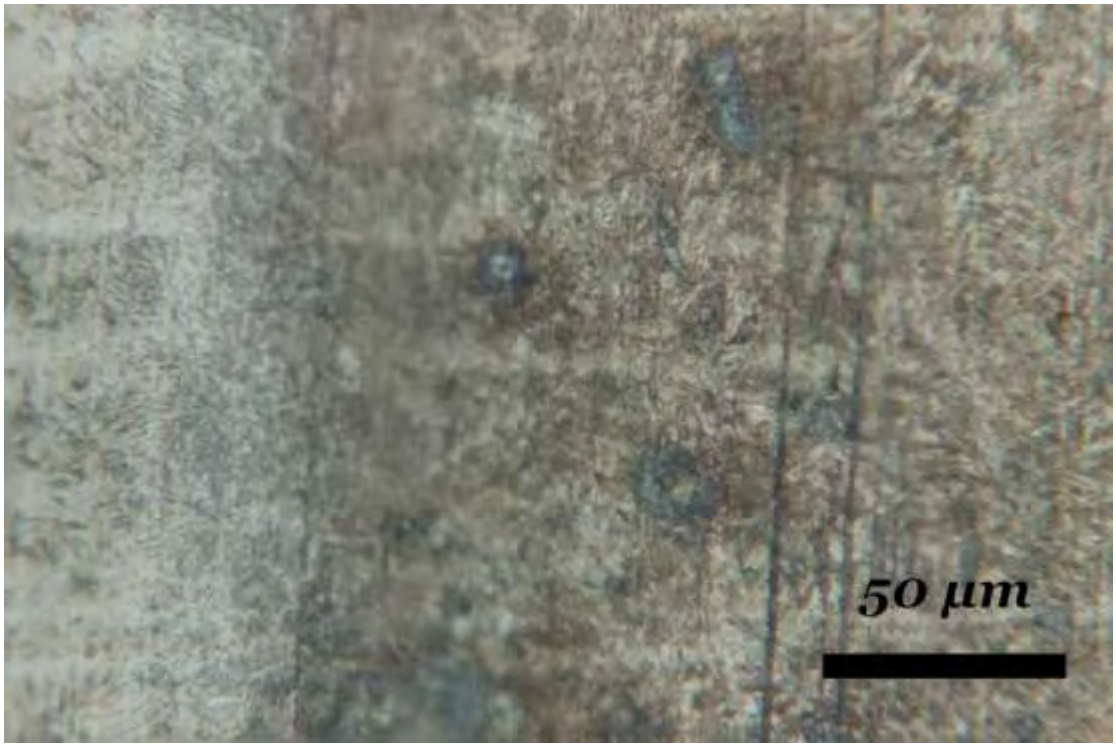

Figure 4.35 – A2 AFTER HAZ 500X

Figures 4.33 to 4.35 show the microstructure changes at the cross section of the specimen A2.

Figure 4.33 shows the presence of a white layer, called melted zone (MZ). The White layer is formed due to the rapid re-solidification of the molten material with thickness 5-7µm. The microhardness of the white layer in the laser cut samples is lower than the bulk material, but due to its low dimensions nanohardness measurements should be contacted to determine exactly this difference. [11] [12]

The results of the metallography match those of the free cooling simulation of Armox 500 in the air, with temperature of 20°C, at "SECONDARY PROCESSING OF UHSLA ARMOX 500 STEEL WITH HEAT BASED TECHNOLOGIES". [10]

4.3 MICROHARDNESS

Graphs 4.8 to 4.13 show the effect of cutting parameters on hardness, at specimens of the same thickness.

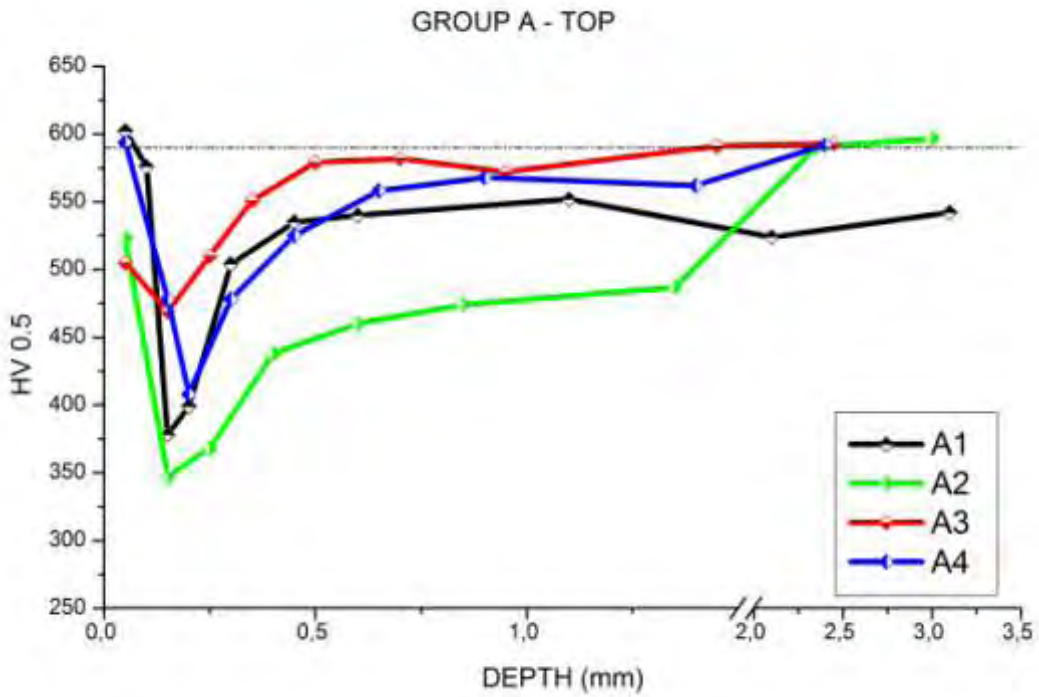

Graph 4.8 - MICROHARDNESS ON THE CROSS SECTION OF GROUP A SPECIMENS, NEAR THE TOP SURFACE

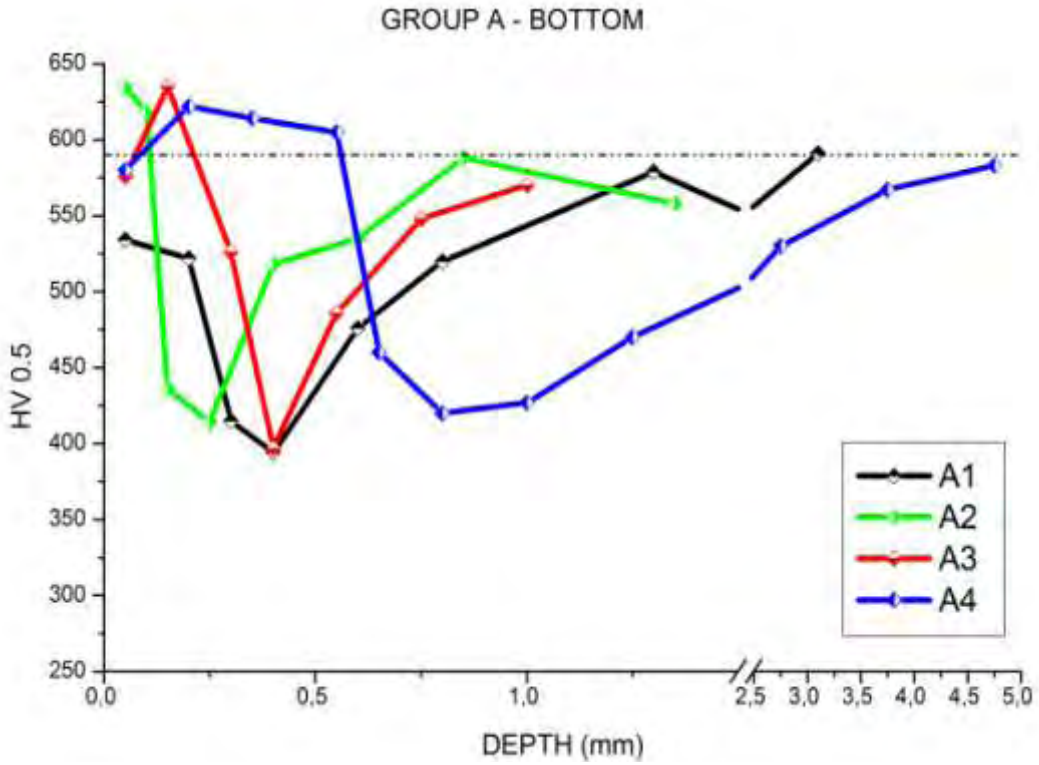

Graph 4.9 - MICROHARDNESS ON THE CROSS SECTION OF GROUP A SPECIMENS, NEAR THE BOTTOM SURFACE

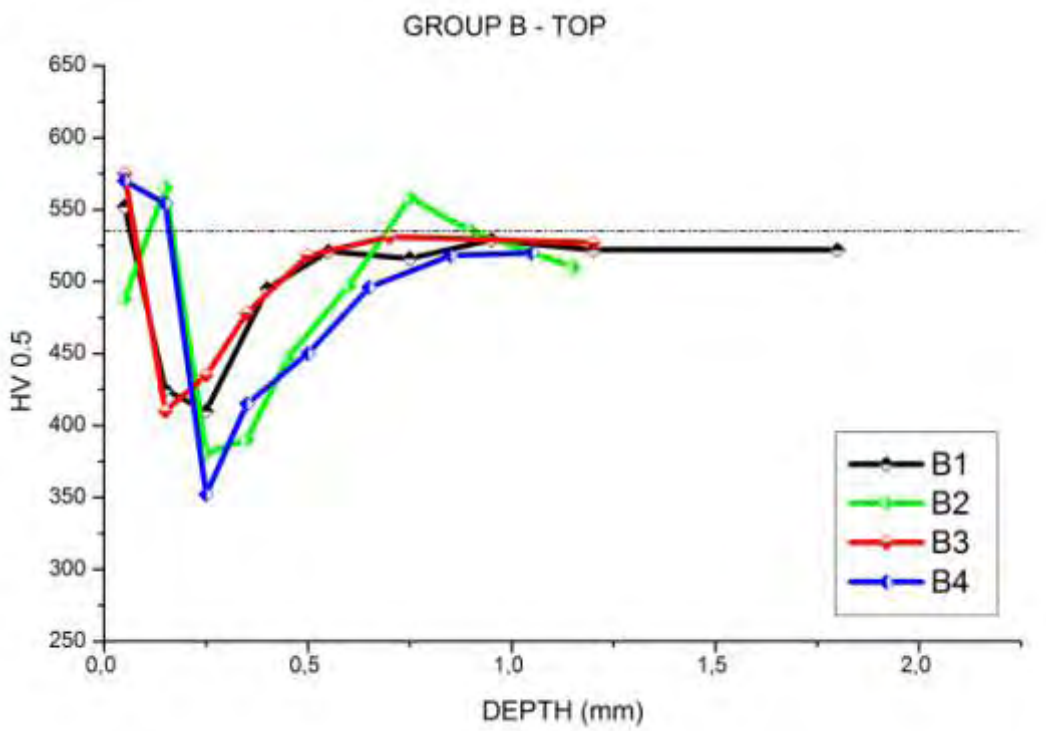

Graph 4.10 - MICROHARDNESS ON THE CROSS SECTION OF GROUP B SPECIMENS, NEAR THE TOP SURFACE

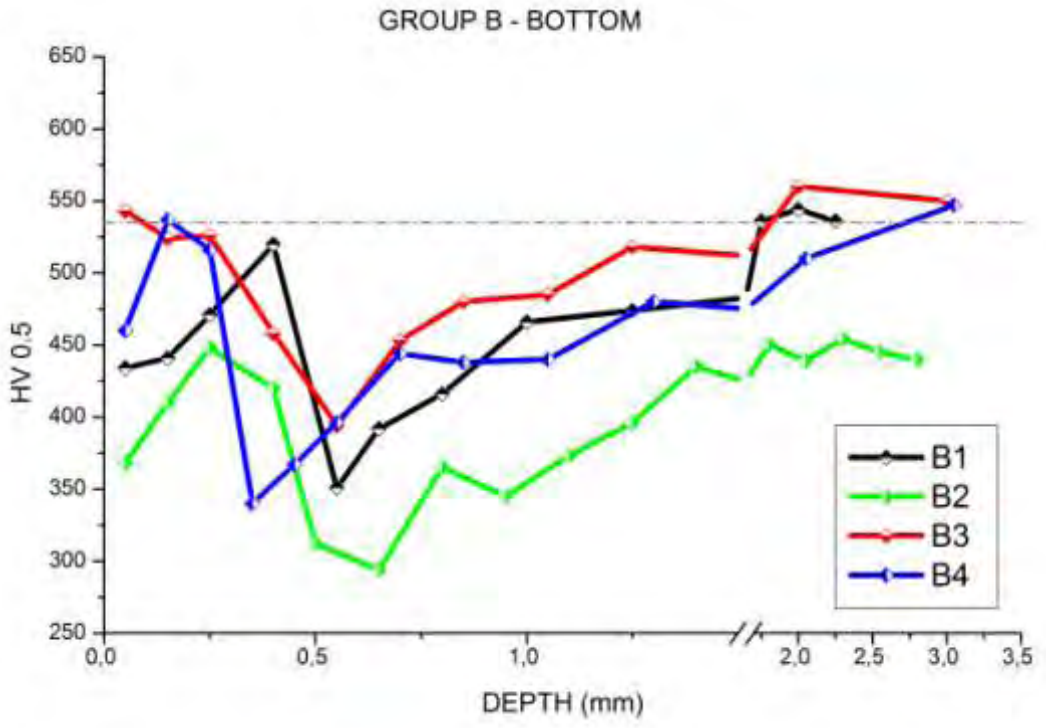

Graph 4.11 - MICROHARDNESS ON THE CROSS SECTION OF GROUP B SPECIMENS, NEAR THE BOTTOM SURFACE

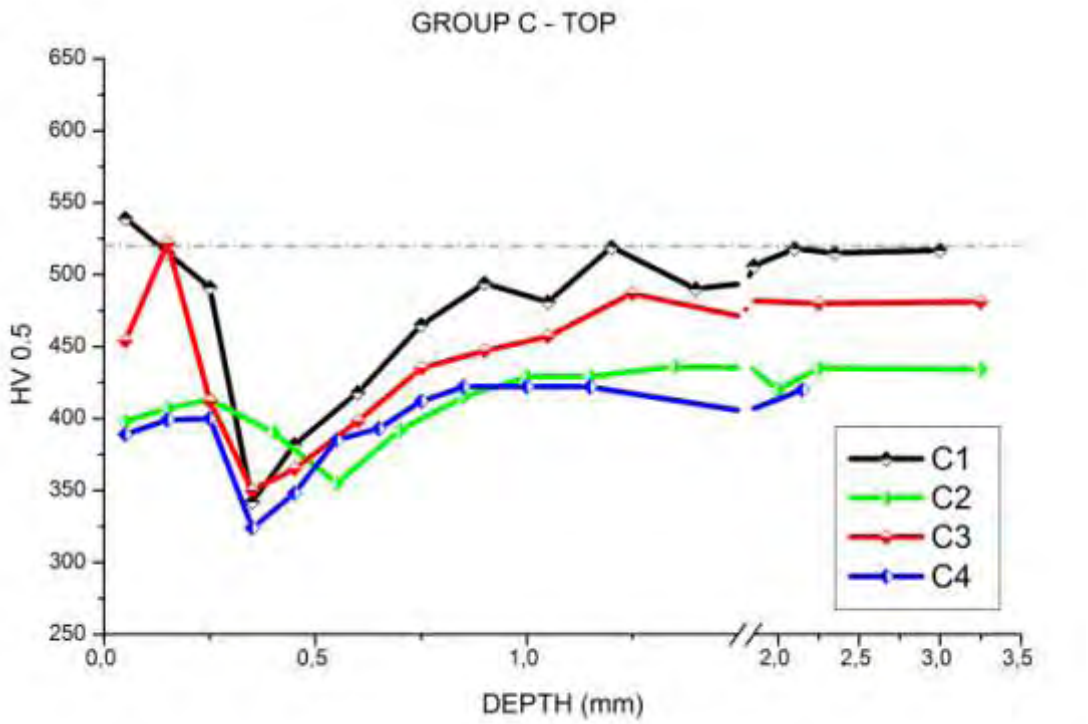

Graph 4.12 - MICROHARDNESS ON THE CROSS SECTION OF GROUP C SPECIMENS, NEAR THE TOP SURFACE

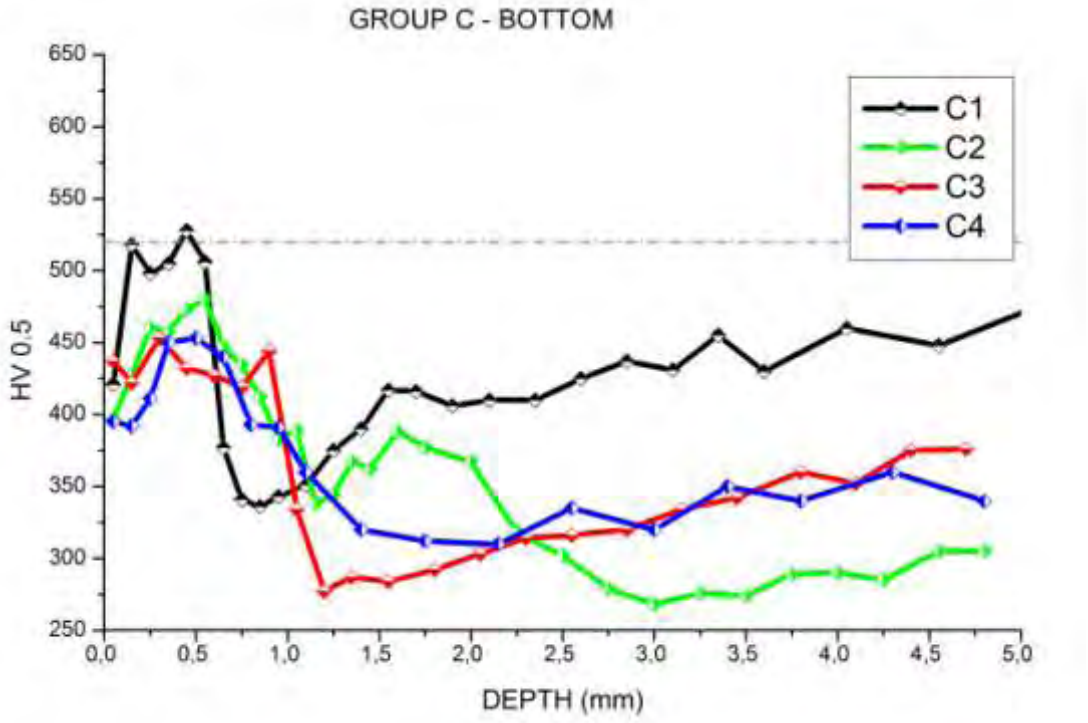

Graph 4.13 - MICROHARDNESS ON THE CROSS SECTION OF GROUP C SPECIMENS, NEAR THE BOTTOM SURFACE

Graphs 4.14 to 4.21 show the hardness differences at specimens of different thickness from the same group of cutting parameters.

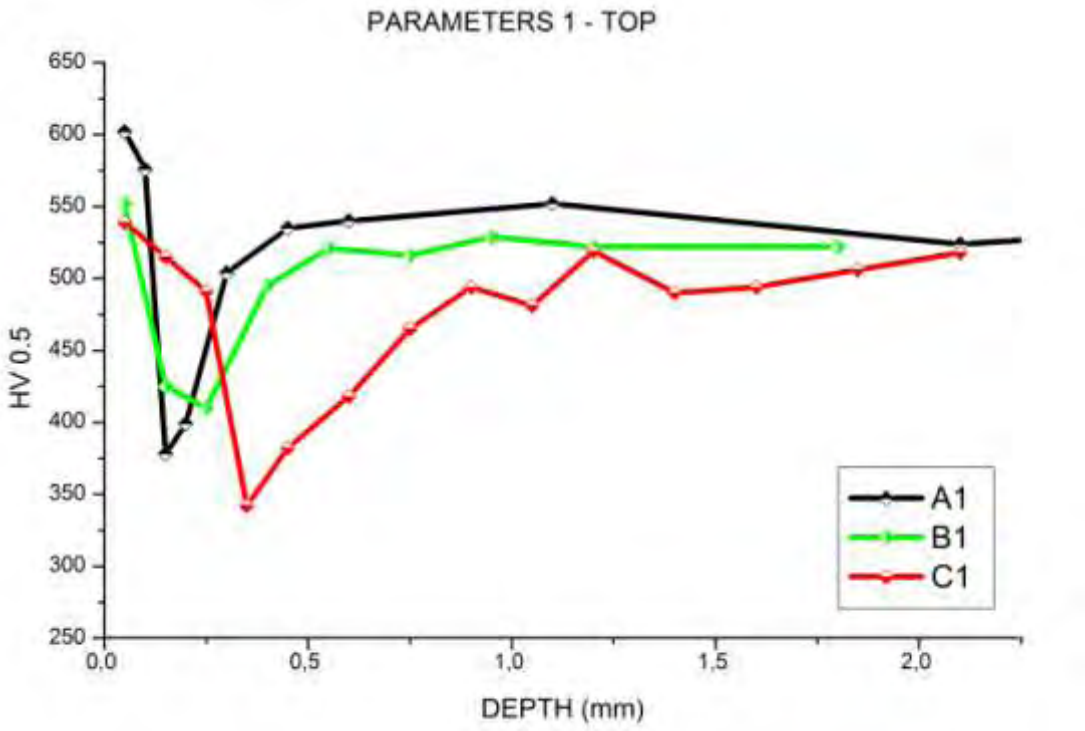

Graph 4.14 - MICROHARDNESS ON THE CROSS SECTION OF SPECIMENS CUT WITH PARAMETERS 1, NEAR THE TOP SURFACE

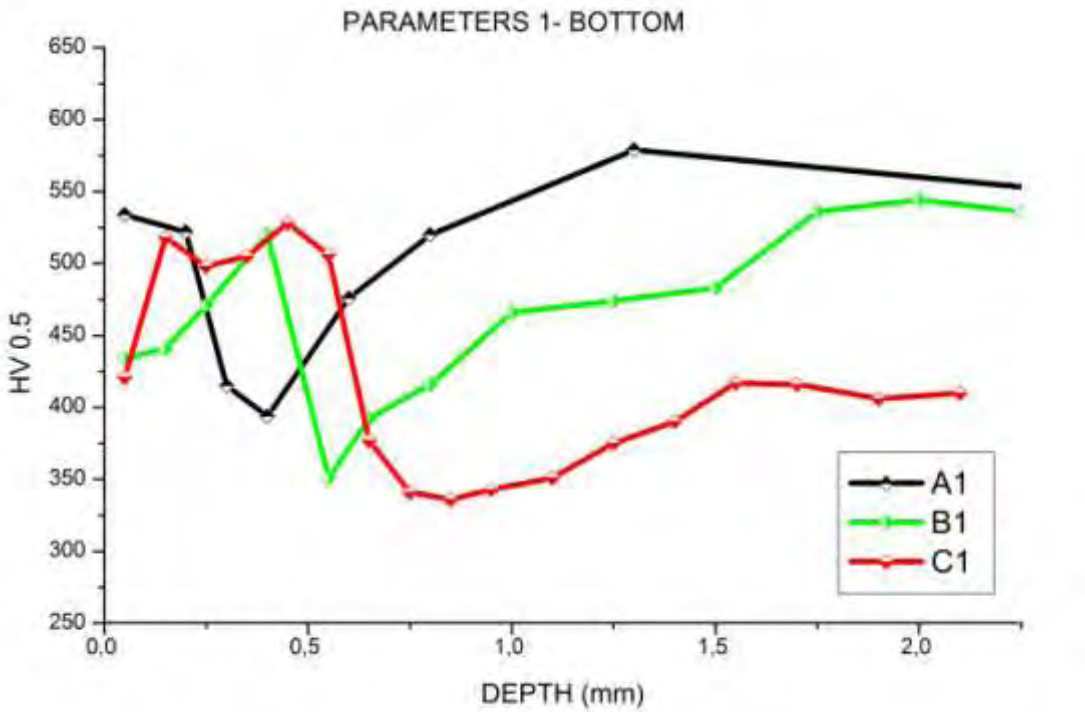

Graph 4.15 - MICROHARDNESS ON THE CROSS SECTION OF SPECIMENS CUT WITH PARAMETERS 1, NEAR THE BOTTOM SURFACE

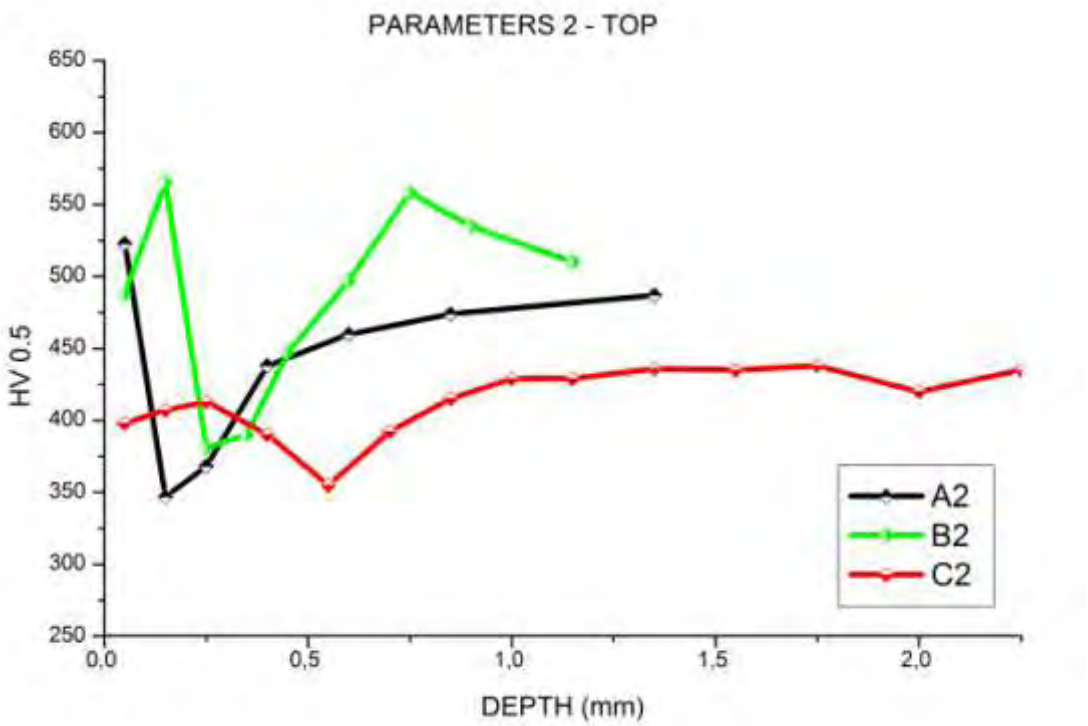

Graph 4.16 - MICROHARDNESS ON THE CROSS SECTION OF SPECIMENS CUT WITH PARAMETERS 2, NEAR THE TOP SURFACE

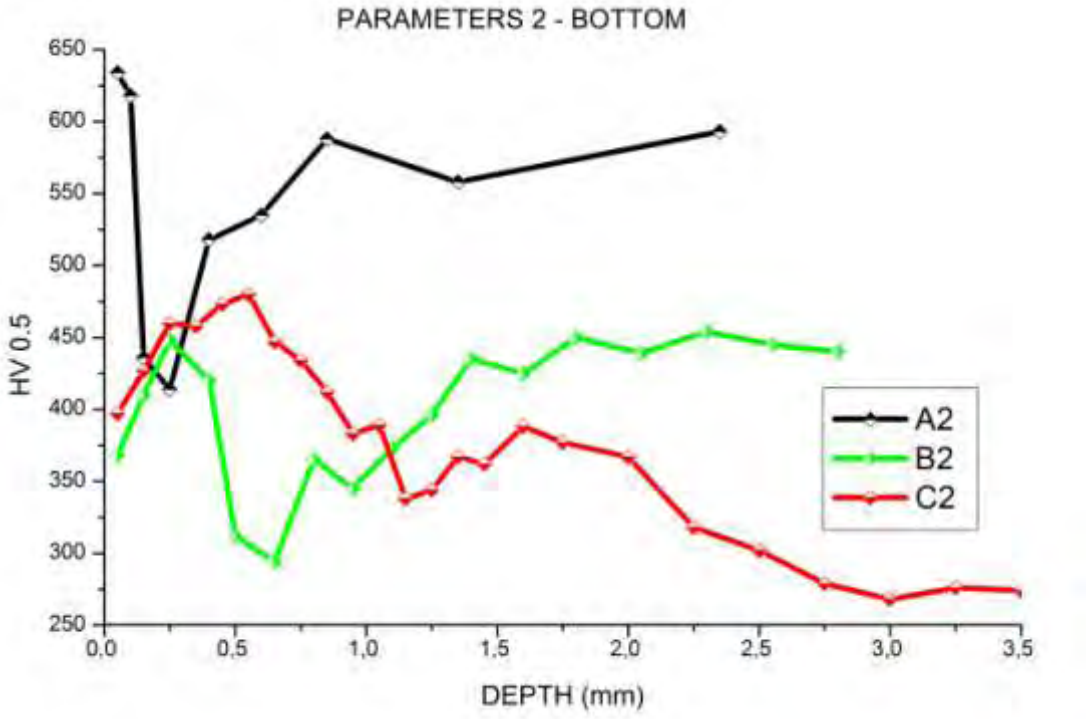

Graph 4.17 - MICROHARDNESS ON THE CROSS SECTION OF SPECIMENS CUT WITH PARAMETERS 2, NEAR THE BOTTOM SURFACE

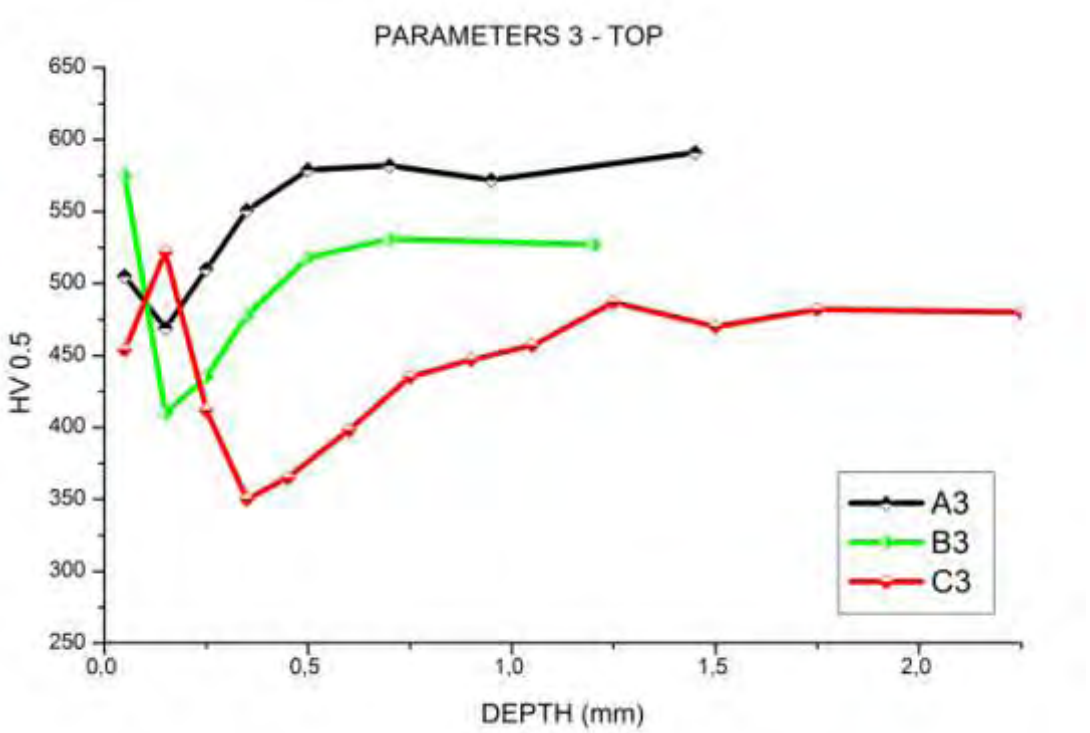

Graph 4.18 - MICROHARDNESS ON THE CROSS SECTION OF SPECIMENS CUT WITH PARAMETERS 3, NEAR THE TOP SURFACE

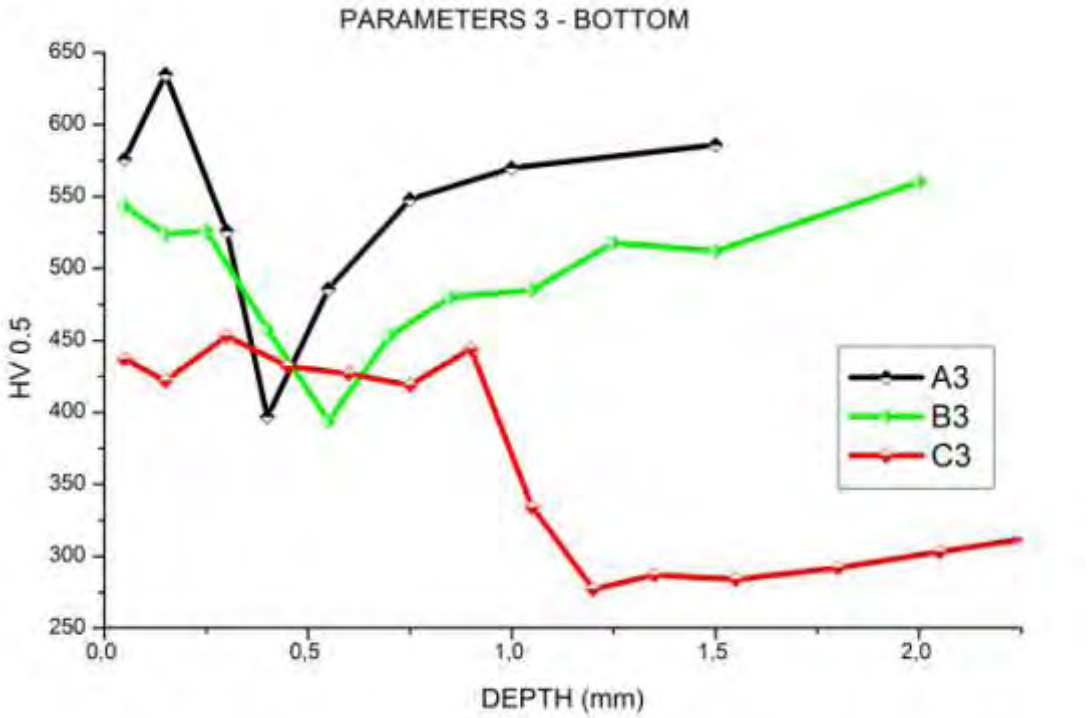

Graph 4.19 - MICROHARDNESS ON THE CROSS SECTION OF SPECIMENS CUT WITH PARAMETERS 3, NEAR THE BOTTOM SURFACE

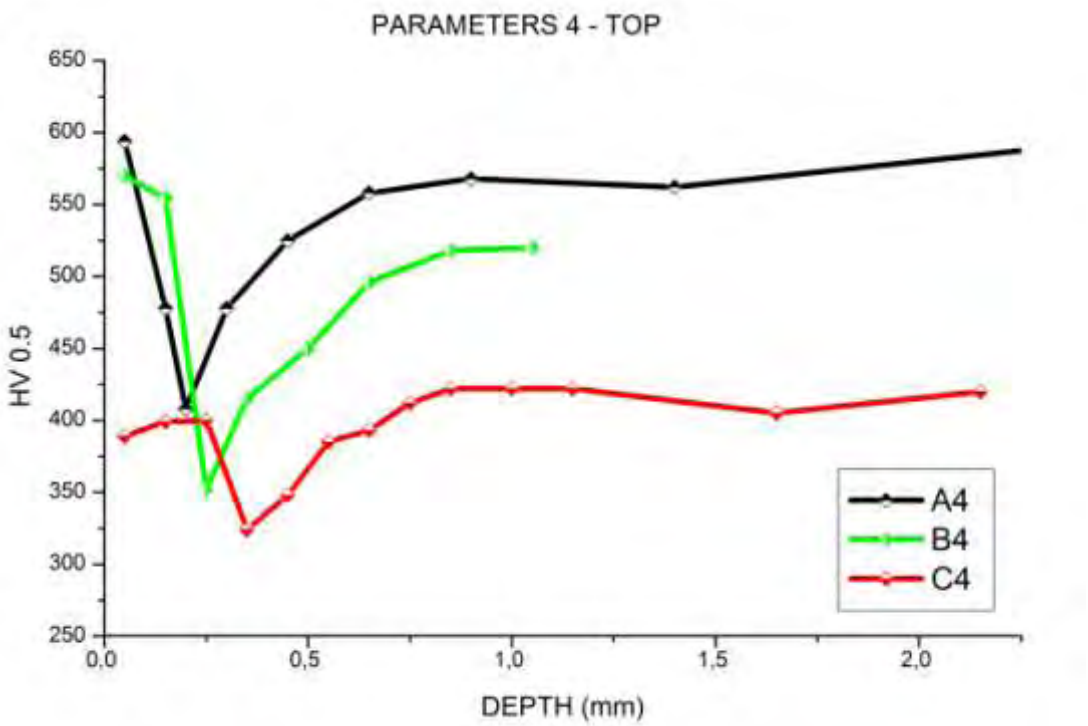

Graph 4.20 - MICROHARDNESS ON THE CROSS SECTION OF SPECIMENS CUT WITH PARAMETERS 4, NEAR THE TOP SURFACE

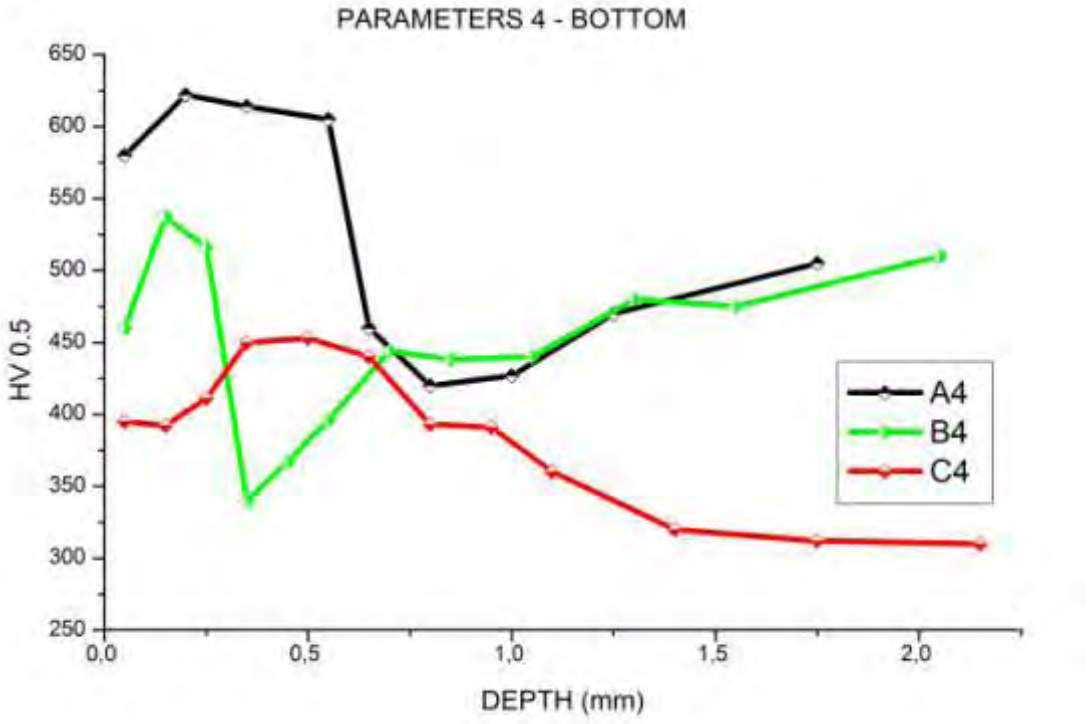

Graph 4.21 - MICROHARDNESS ON THE CROSS SECTION OF SPECIMENS CUT WITH PARAMETERS 4, NEAR THE BOTTOM SURFACE

Table 4.2 summarizes the critical points of the microhardness measurements. For each specimen the value of minimum hardness and its position are listed, as well as the depth of the heat affected zone. For each group, the lowest values of hardness and HAZ depth are marked with red background.

Table 4.2 – CRITICAL POINTS OF SPECIMENS MICROHARDNESS

CRITICAL POINTS									
	TOP					BOTTOM			
SPECIMEN	unaffected material hardness (HV0,5)	min Hardness (HV0,5)	% degradation	pos.(mm) of min Hardness	pos.(mm) of bulk hardness	min Hardness (HV0,5)	% degradation	pos. (mm) of min Hardness	pos. (mm) of bulk hardness
A1	590 (± 20)	378	35,9	0,15	-	394	33,2	0,4	1,25
A2		347	41,2	0,15	2,2	414	29,8	0,25	2,35
A3		469	20,5	0,15	0,45	397	32,7	0,4	1,5
A4		408	30,8	0,2	2,4	420	28,8	0,8	5,25
B1	530 (± 20)	410	22,6	0,25	0,5	351	33,8	0,55	1,75
B2		381	28,1	0,25	0,65	294	44,5	0,65	-
B3		410	22,6	0,15	0,45	394	25,7	0,55	1,2
B4		352	33,6	0,25	0,8	340	35,8	0,35	2,05
C1	520 (± 20)	342	34,2	0,35	1,1	336	35,4	0,85	-
C2		355	31,7	0,55	-	268	48,5	3	-
C3		350	32,7	0,35	-	277	46,7	1,2	-
C4		324	37,7	0,35	-	310	40,4	2,15	-

5 DISCUSSION

5.1 ROUGHNESS

From the roughness measurements it is observed that, comparatively to the first specimen, reduction in speed leads to rapid increase of roughness both near the top and bottom surface. The increase is in the range of 250%-520%. (Comparison of 1st and 2nd specimen of each group)

Also an increase of roughness was observed at the specimens at which the focal point was moved, but in this case the increase was in the range of 10%-20%.(Comparison of 1st and 3rd specimen of each group)

Furthermore, the movement of the focal point improves the roughness results, 15%-20%, at the specimens with the cutting speed reduced. (Comparison of 2nd and 4th specimen of each group)

At the first specimen of 5mm width (Group A) better roughness is observed near the top surface. The reduction of cutting speed led to the opposite results, surface with better roughness near the bottom of the plate. (Comparison of A2, A4 with A1, A3 specimens)

In addition, a completely reversed situation is going on with specimens of 10mm width (Group B), at which roughness is better near the top surface when the focal point is moved. (Comparison of B3, B4 with B1, B2 specimens)

For the specimens of 20mm width (Group C), with the reduced cutting speed, the roughness was so high that measurement was not possible with the available equipment. Additional photos of these specimens are shown in figures 5.1 and 5.2.

Figure 5.2 – CUT FACE OF SPECIMEN C2

Figure 5.1 – CUT FACE OF SPECIMEN C4

Finally, it is observed that when the width of the plate is increased the resulting roughness is worse, as expected.

5.2 METALLOGRAPHY

The microstructure of the basic material consists of very fine-grained martensite.

The microstructure in the heat affected zone is different in comparison to the microstructure of the base material. As shown on figures 4.37 to 4.39 the microstructure of the heat affected zone from the cut face to the no heat-affected material consists of:

A coarse-grained martensitic zone that becomes finest gradually farther from the cut face. This structure is a result of very rapid cooling after heat up to the austenitization temperatures where the cooling speed decreases in relation to the distance from surface.

A zone in which, the cooling rate is even lower and bainitic structure is formed.

Finally, a transition zone between HAZ and core material, consisting of tempered martensite (heated up below A1) where no phase transformation is present and the morphology of martensite is changed from coarse to fine coarse (base material).

The final microstructure of the HAZ matches the results of the simulation that Igor BARÉNYI, Ondrej HÍREŠ, Peter LIPTÁK have done [8], which predicted the presence of martensite and bainite after free cooling of Armox 500 steel from 1000°C in the air with a temperature of 20°C. The results of this simulation are shown in figure 5.3 and table 5.1.

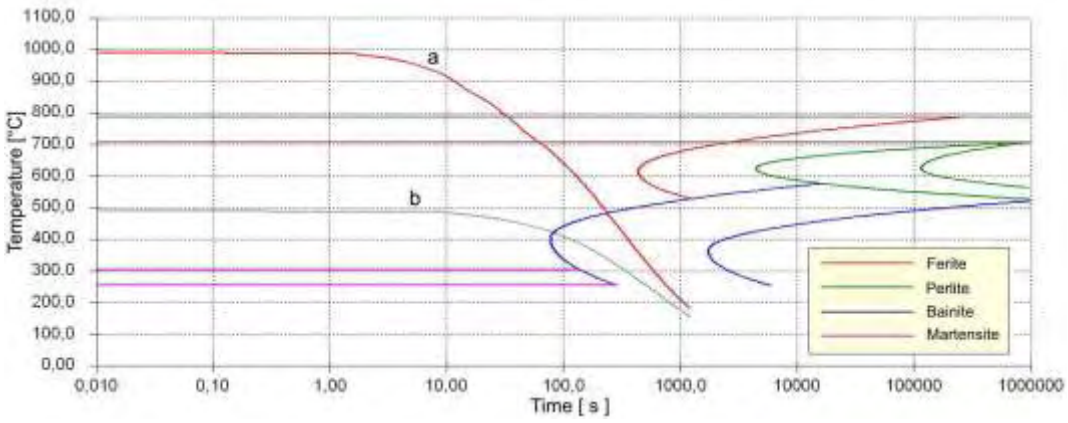

Figure 5.3 - CCT diagram of ARMOX 500T cooling, a) starting temperature 1000°C, b) starting temperature 500° [8]

Table 5.1 – ARMOX 500T PROPERTIES CALCULATED BY COOLING SIMULATION [8]

ARMOX 500T properties calculated by simulaton		Starting Temperature		Delivered conditions
		500°C	1000°C	
Critical temperatures [°C]	A_{c3}	786		-
	A_{c1}	707		-
Structural components [%]	Bainite	81	84.5	-
	Martensite	19	15.5	-
Mechanical properties	R_m [MPa]	1335	1312	1750
	$R_{p0.2}$ [MPa]	1070	1049	1250
	HV/HB	441/418	435/413	610/540

5.3 MICROHARDNESS

The results from the microhardness measurements are provided below per steel thickness:

- t=5mm

The microhardness values show that, reduction in cutting speed lead to rapid decrease of hardness and increase of the affected area, near the top surface. The exact opposite happens near the bottom surface. At the third specimen, for which the focal point was moved lower in the thickness, the results were slightly improved at both top and bottom areas, compared to the first specimen. Finally, the fourth specimen gave results similar to the first one, at the near the top surface, but at the near the bottom surface there is great increase of the affected area, where the hardness is low.

- t=10mm

The results for the near the top surface of specimens B1 and B3 are similar, with those of B3 being slightly better. Similarity at the results exist also for the other two specimens, which were cut with reduced speed, B2 and B4, but are worse than those of the two others. That is not the case for the bottom surface, where reduction of cutting speed led to a rapid reduction of hardness and increase of the affected area. In this case, with the speed reduced, moving the focal point improves considerable the results. The best scenario of the four comes from the third specimen, which only had the focal point moved and gives the better results.

- t=20mm

From the hardness measurements graphs, of the group C specimens, it is noticed that although they have the same tendency with those of the two other groups, hardness does not reach the expected range of values. This happened due to the

small width to thickness ratio of the cut specimens, which affected the temperature and cooling rate even at the center of the specimens, enough to affect their properties. However, some observations can be done. Both at the near the top and near the bottom surfaces, the first cutting parameters provided the best results. At the rest of the specimens the only difference is that of the third specimen, having slightly better results at the near the top surface than the two others.

Moreover, while moving from the cut face to the center of the specimens at the cross sections, the microhardness starts from a low value, at area of coarse grained martensite and then raises, at the area of fine grained martensite before it fall again and reaches its minimum, at the area with bainitic structure. As we move further from the bainitic structure it raises again in respective to the microstructure becoming from coarse grained to fine grained martensitic. This can be seen in figures 5.4 and 5.5.

The phenomenon at the near the cut face, may not be clear at the specimens with relatively small HAZ, where very small area between the cut face and the bainitic microstructure occurs and not enough microhardness measurements could be done. Such an example is shown in figure 5.5.

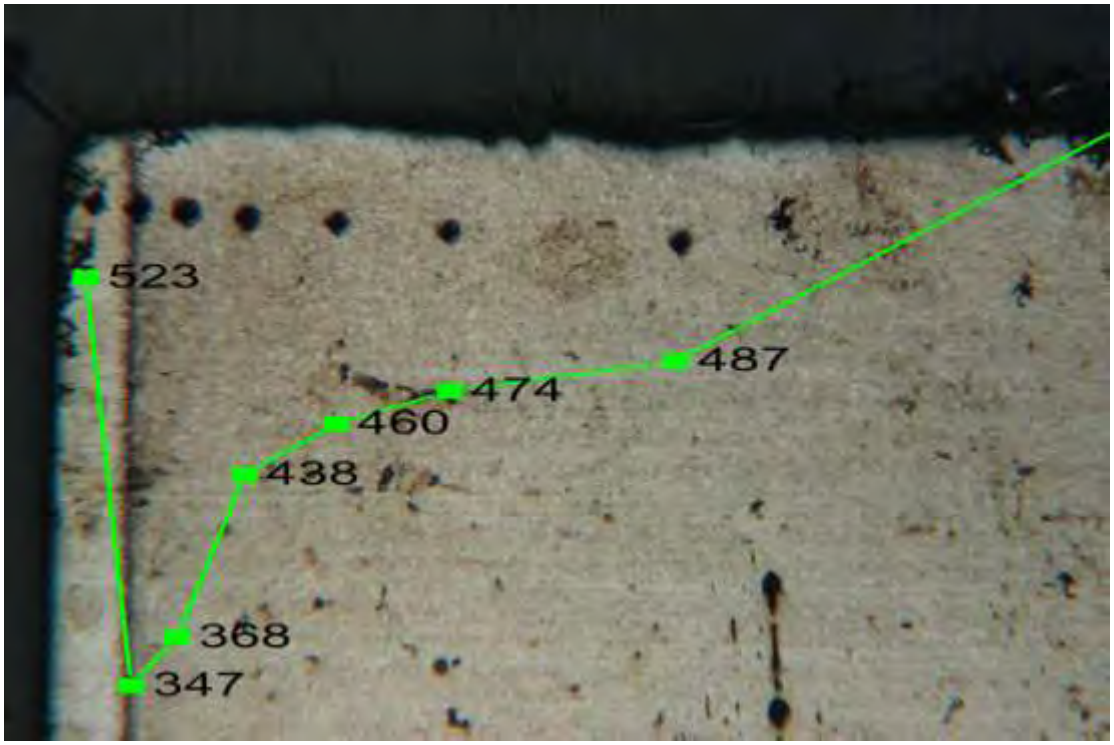

Figure 5.4 (x50) – MICROHARDNESS GRAPH AND MICROSTRUCTURE OF A2 SPECIMEN NEAR THE TOP SURFACE

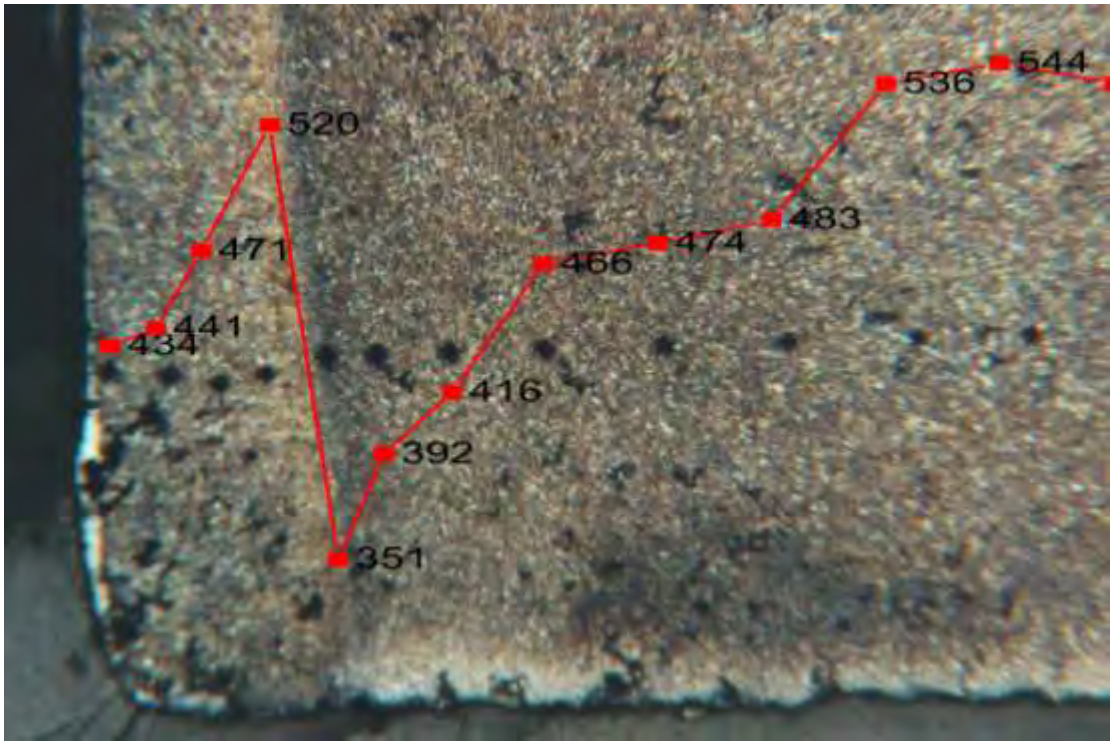

Figure 5.5 (x50) – MICROHARDNESS GRAPH AND MICROSTRUCTURE OF B1 SPECIMEN NEAR THE BOTTOM SURFACE

Finally from table 4.2 it is observed that the degradation of microhardness in the HAZ varies from 20% to 50% depending on the cutting parameters.

6 CONCLUSIONS

From the results presented above the following conclusions can be drawn:

- The heat input rate affects the roughness of the cutting surface. The higher heat input rates increase significantly the roughness. The lowest roughness values (Ra) were determined for each thickness as follows:

  t=5mm, HIR=0.09 J/mm, focal point: 0mm

  t=10mm, HIR=0.15 J/mm, focal point: +0,5mm

  t=20mm, HIR=0.33 J/mm, focal point: +4,5 mm

- The minimum width of the HAZ was measured (lower surface):

  t=5mm, HIR=0.09 J/mm, focal point: 0mm

  t=10mm, HIR=0.15 J/mm, focal point: -3,5mm

  t=20mm, microhardness does not reach the expected range of values, however the best results were found for HIR=0.33 J/mm, focal point: +4,5mm

- The minimum microhardness values were determined:

  t=5mm, HIR=0.09 J/mm, focal point: 0mm

  t=10mm, HIR=0.3 J/mm, focal point: +0,5mm

  t=20mm, HIR=0.65 J/mm, focal point: +4,5mm

The HAZ consists of four zones:

- A white layer (5-9μm) which was formed due to the rapid re-solidification of the molten material. The micrhardness of the white layer in the laser cut samples is lower than the bulk material, but due to its low dimensions nanohardenss measurements should be contacted to determine exactly this difference.
- A coarse-grained martensitic zone that becomes finest gradually farther from the cut face. This structure is a result of very rapid cooling after heat up to

the austenitization temperatures where the cooling rate decreases in relation to the distance from surface.

- A zone in which, the cooling rate is even lower and bainitic structure was formed.
- Finally, a transition zone between HAZ and core material, consists of tempered martensite (heated up below A1). The morphology of martensite is changed from coarse to fine coarse (base material).

The results are in good agreement with the literature. Based on the above results the optimum laser cutting conditions are:

- t=5mm, HIR=0.09 J/mm, focal point: -2mm
- t=10mm, HIR=0.15 J/mm, focal point: -3,5mm
- t=20mm, HIR=0.33 J/mm, focal point: +4,5mm

REFERENCES

[1] MAHMOUD Y. DEMERI, ADVANCED HIGH-STRENGTH STEELS: SCIENCE, TECHNOLOGY, AND APPLICATIONS

[2] HAO QU, ADVANCED HIGH STRENGTH STEEL THROUGH PARAEQUILIBRIUM CARBON PARTITIONING AND AUSTENITE STABILIZATION, DEPARTMENT OF MATERIALS SCIENCE AND ENGINEERING CASE WESTERN RESERVE UNIVERSITY, JANUARY 2011

[3] PRADIPTA KUMAR JENA∗, PONGURU SENTHIL P., SIVA KUMAR K., EFFECT OF TEMPERING TIME ON THE BALLISTIC PERFORMANCE OF A HIGH STRENGTH ARMOUR STEEL, AVAILABLE ONLINE AT www.sciencedirect.com, JOURNAL OF APPLIED RESEARCH AND TECHNOLOGY, 14 (2016) 47–53

[4] IGOR BARÉNYI MICROSTRUCTURE CHANGES IN CUT FACE OBTAINED BY PLASMA AND LASER CUTTING OF SELECTED HIGH STRENGTH STEELS, U.P.B. SCI. BULL., SERIES D, VOL. 78, ISS. 1, 2016 ISSN 1454-2358

[5] ESAB KNOWLEDGE CENTER
http://www.esabna.com/us/en/education/blog/index.cfm

[6] M. PIRINENA, YU. MARTIKAINENA, S.YU. IVANOVB AND V.A. KARKHINB, COMPARATIVE ANALYSIS OF THE MICROSTRUCTURE OF THE HEAT-AFFECTED ZONE METAL IN WELDING OF HIGH-STRENGTH STEELS, ISSN: 0950-7116 (PRINT) 1754-2138 (ONLINE) JOURNAL HOMEPAGE: http://www.tandfonline.com/loi/twld20

[7] IGOR BARÉNYI, DEGRADATION OF MECHANICAL PROPERTIES OF SELECTED UHSS STEELS IN HAZ AFTER THEIR WELDING, UNIVERSITY REVIEW, VOL. 8, 2014, NO. 3-4, P. 99-103 99

[8] IGOR BARÉNYI, ONDREJ HÍREŠ, PETER LIPTÁK, CHANGES IN MECHANICAL PROPERTIES OF ARMOURED UHSLA STEEL ARMOX 500 AFTER OVER TEMPERING, ISSN 2081-5891 4, 4 (14), 2013, 7-14

[9] SIMULATION OF ARMOX STEELS MECHANICAL PROPERTIES DEGRADATION IN HAZ AFTER SELECTED THERMAL CUTTING PROCESSES, IGOR BARÉNYI, UNIVERSITY REVIEW, VOL. 8, 2014, NO. 3-4, P. 18-22

[10] SECONDARY PROCESSING OF UHSLA ARMOX 500 STEEL WITH HEAT BASED TECHNOLOGIES, IGOR BARÉNYI

[11] IMED MIRAOUI, MOHAMED BOUJELBENE, AND MOUNA ZAIED, ADVANCES IN MATERIALS SCIENCE AND ENGINEERING, VOLUME 2016 (2016), HIGH-POWER LASER CUTTING OF STEEL PLATES: HEAT AFFECTED ZONE ANALYSIS

[12] C.H. FUA , J.F. LIUA , Y.B. GUOA *, Q.Z. ZHAO, A COMPARATIVE STUDY ON WHITE LAYER PROPERTIES BY LASER CUTTING VS. ELECTRICAL DISCHARGE MACHINING OF NITINOL SHAPE MEMORY ALLOY, PROCEDIA CIRP 42 (2016) 246 – 251]